Nada är en gemensam institution mellan
Kungliga Tekniska högskolan och Stockholms universitet.

Optimal Control of Partial Differential Equations in Optimal Design

JESPER CARLSSON

Avhandling som med tillstånd av Kungliga Tekniska högskolan
framlägges till offentlig granskning för avläggande av teknologie doktorsexamen
fredagen den 7 november 2008 kl 10.00
i sal F3, Lindstedtsvägen 26,
Kungliga Tekniska högskolan, Stockholm.

TRITA-CSC-A 2008:15
ISSN-1653-5723
ISRN-KTH/CSC/A--08/15--SE
ISBN-978-91-7415-149-7

TRITA-CSC-A 2008:15
ISSN-1653-5723
ISRN-KTH/CSC/A--08/15--SE
ISBN-978-91-7415-149-7

KTH
School of Computer Science and Communication
SE-100 44 Stockholm
SWEDEN

Akademisk avhandling som med tillstånd av Kungl Tekniska högskolan framlägges till offentlig granskning för avläggande av teknologie doktorsexamen i numerisk analys fredagen den 7 november 2008 klockan 10.00 i sal F3, Kungl Tekniska högskolan, Lindstedtsvägen 26, Stockholm.

Tryck: Universitetsservice US AB

Abstract

This thesis concerns the approximation of optimally controlled partial differential equations for inverse problems in optimal design. Important examples of such problems are optimal material design and parameter reconstruction. In optimal material design the goal is to construct a material that meets some optimality criterion, e.g. to design a beam, with fixed weight, that is as stiff as possible. Parameter reconstrucion concerns, for example, the problem to find the interior structure of a material from surface displacement measurements resulting from applied external forces.

Optimal control problems, particularly for partial differential equations, are often ill-posed and need to be regularized to obtain good approximations. We here use the theory of the corresponding Hamilton-Jacobi-Bellman equations to construct regularizations and derive error estimates for optimal design problems. The constructed Pontryagin method is a simple and general method where the first, analytical, step is to regularize the Hamiltonian. Next its Hamiltonian system is computed efficiently with the Newton method using a sparse Jacobian. An error estimate for the difference between exact and approximate objective functions is derived, depending only on the difference of the Hamiltonian and its finite dimensional regularization along the solution path and its L^2 projection, i.e. not on the difference of the exact and approximate solutions to the Hamiltonian systems.

Another treated issue is the relevance of input data for parameter reconstruction problems, where the goal is to determine a spacially distributed coefficient of a partial differential equation from partial observations of the solution. It is here shown that the choice of input data, that generates the partial observations, affects the reconstruction, and that it is possible to formulate meaningful optimality criteria for the input data that enhances the quality of the reconstructed coefficient.

In the thesis we present solutions to various applications in optimal material design and reconstuction.

Sammanfattning

Denna avhandling handlar om approximation av optimalt styrda partiella differentialekvationer för inversa problem inom optimal design. Viktiga exempel på sådana problem är optimal materialdesign och parameterskattning. Inom materialdesign är målet att konstruera ett material som uppfyller vissa optimalitetsvillkor, t.ex. att konstruera en så styv balk som möjligt under en given vikt, medan ett exempel på parameterskattning är att hitta den inre strukturen hos ett material genom att applicera ytkrafter och mäta de resulterande förskjutningarna.

Problem inom optimal styrning, speciellt för styrning av partiella differentialekvationer, är ofta illa ställa och måste regulariseras för att kunna lösas numeriskt. Teorin för Hamilton-Jacobi-Bellmans ekvationer används här för att konstruera regulariseringar och ge feluppskattningar till problem inom optimal design. Den konstruerade Pontryaginmetoden är en enkel och generell metod där det första analytiska steget är att regularisera Hamiltonianen. I nästa steg löses det Hamiltonska systemet effektivt med Newtons metod och en gles Jacobian. Vi härleder även en feluppskattning för skillnaden mellan den exakta och den approximerade målfunktionen. Denna uppskattning beror endast på skillnaden mellan den sanna och den regulariserade, ändligt dimensionella, Hamiltonianen, båda utvärderade längst lösningsbanan och dess L^2-projektion. Felet beror alltså ej på skillnaden mellan den exakta och den approximativa lösningen till det Hamiltonska systemet.

Ett annat fall som behandlas är frågan hur indata ska väljas för parameterskattningsproblem. För sådana problem är målet vanligen att bestämma en rumsligt beroende koefficient till en partiell differentialekvation, givet ofullständiga mätningar av lösningen. Här visas att valet av indata, som genererar de ofullständiga mätningarna, påverkar parameterskattningen, och att det är möjligt att formulera meningsfulla optimalitetsvillkor för indata som ökar kvaliteten på parameterskattningen.

I avhandlingen presenteras lösningar för diverse tillämpningar inom optimal materialdesign och parameterskattning.

Preface

This thesis consists of an introduction and four papers.

Paper 1: Jesper Carlsson, Mattias Sandberg and Anders Szepessy. Symplectic Pontryagin Approximations for Optimal Design, *to appear in ESAIM - Mathematical Modelling and Numerical Analysis*, 2008.

The author of this thesis contributed to the ideas presented, performed the numerical computations and wrote sections 3, 4, and parts of section 2, of the manuscript.

Paper 2: Jesper Carlsson. Pontryagin Approximations for Optimal Design of Elastic Structures, *preprint*, 2006.

Paper 3: Jesper Carlsson. Symplectic Reconstruction of Data for Heat and Wave Equations, *preprint*, 2008.

Paper 4: Jesper Carlsson. Inverse Reconstruction from Optimal Input Data, *preprint*, 2008.

Acknowledgments

I wish to thank my supervisor, professor Anders Szepessy, for his support and guidance throughout this work. I am also grateful to Mattias Sandberg, Erik von Schwerin and Raul Tempone for the fruitful discussions and cooperation we have had over the years. Finally, I also wish to thank all my colleagues at NADA.

Financial support from VR is gratefully acknowledged.

Contents

Chapter 1

Introduction

This thesis deals with the problem on how to solve ill-posed inverse problems with optimal control techniques. The purpose of *optimal control* is to control a dynamical system to achieve a desired goal in an optimal way. Optimal control is of great importance in many areas of science such as finance, economics, aeronautics, chemistry, physics and mechanics. In fact, almost any discipline that deals with dynamical systems also have applications where it is of interest to control that dynamical system. Another area where optimal control is of interest is *inverse problems*, *cf.* [3, 13, 24, 13]. The goal is then to determine input data to an equation from its solution, *i.e.* if the solution y to the *forward problem* is given by

$$y = A(x),$$

where x is the input, and A is a (non-linear) operator, then the inverse problem to find x is simply

$$x = A^{-1}(y).$$

In the finite dimensional case for a linear operator, *e.g.* $A(x) = Ax$ where A is an invertible matrix, the inverse problem is just to solve a linear system. For the infinite dimensional case, however, the inverse problem may be *ill-posed*, *i.e.* one or more of the following properties for well-posedness is not satisfied:

1. There exists a solution x.

2. The solution is unique.

3. The solution depends continuously on the input y.

A simple example of an ill-posed inverse problem is to find $x^* : [0, T] \to \mathbb{R}$ for

$$y^*(t) = \int_0^T x^*(t) \, \mathrm{d}t := A(x^*), \tag{1.1}$$

where $y^* : [0,T] \to \mathbb{R}$ is non-differentiable. For the corresponding discretized problem, with A^{-1} being the difference operator, the sensitivity to data is reflected by the condition number which grows as the step size goes to zero.

To formulate an optimal control problem for the inverse problem (1.1) it is necessary to introduce an objective functional, *e.g.* the least-squares functional

$$\int_0^T \big(y(t) - y^*(t)\big)^2 \, \mathrm{d}t. \tag{1.2}$$

The optimal control problem is then to find $x, y : [0,T] \to \mathbb{R}$ that satisfies

$$\begin{aligned} \frac{\mathrm{d}y(t)}{\mathrm{d}t} &= x(t), \quad t \in (0,T], \\ x(0) &= 0. \end{aligned}$$

and minimizes (1.2). Since the optimal control problem still is ill posed it is necessary to modify it to allow a solution and to lessen the dependence on data. One way is to *regularize* it by adding an extra penalty on the control x, *e.g.* to replace (1.2) with

$$\int_0^T \big(y(t) - y^*(t)\big)^2 + \delta x^2(t) \, \mathrm{d}t,$$

see [19].

In this thesis *optimal design* problems are considered, *i.e.* inverse problems for partial differential equations, *cf.* [19, 20] . Optimal design also includes control problems without time dynamics, *e.g.* control of stationary partial differential equations, and can in the general form be written as the mimimization of a functional

$$F(u,\sigma) : V(U) \times W(U) \to \mathbb{R},$$

where U is a domain (possibly in both time and space), and the state u and the control σ belongs to Hilbert spaces V and W, and satisfies a partial differential constraint

$$G(u,\sigma) = 0 \text{ in } U.$$

Usually the control is also restriced to only attain values in some admissible set in W. In the following chapter, the special case of optimal design problems where the control is only able to attain discrete values, *e.g.* $\sigma : U \to \{\sigma_-, \sigma_+\}$, is discussed. The theory for this case can easily be extended to the more general cases $\sigma : U \to [\sigma_-, \sigma_+]$ or $\sigma : U \to \mathbb{R}$.

Chapter 2

Optimal Design

Optimal design has with the increase of computational capacity and commercial software for solving partial differential equations become an important industrial field, with applications in virtually all fields of science. Two important applications are optimal design of material structures, and inverse optimal reconstruction of physical properties from experimental data, see e.g. [5] and [6], respectively.

Mathematically, optimal design can be described as the particular inverse problem of controlling one or more a partial differential equations to meet some design criteria in an optimal way. For example, consider the general problem to find a bounded open set $D \subset \Omega \subset \mathbb{R}^d$ such that

$$\inf_{D \in \mathcal{D}_{ad}} \left\{ \int_D F(u) \, \mathrm{d}x \;\middle|\; G(u) = 0 \text{ in } D \right\}, \tag{2.1}$$

where the design criteria is described by the functional $F : \mathbb{R}^n \to \mathbb{R}$, the state variable $u : \Omega \to \mathbb{R}^n$ satisfies the partial differential equation $G(u) = 0$ in D, and $\mathcal{D}_{ad}$ describes a set of admissible designs. Typically, the partial differential operator G here describes a physical state, while the design criteria consists of some energy to minimize or, for a reconstruction problem, an error functional relating the solution u to measurements.

The above problem (2.1) is usually referred to as an optimal shape problem [20] and is in general ill-posed in the sense that small perturbations of data lead to large changes in the solution [13, 24]. Also, for a too large set of admissible designs $\mathcal{D}_{ad}$, the infimum in (2.1) may not even be attained.

An alternative way to write the optimal shape problem (2.1) is as a parameter design problem

$$\inf_{\chi \in \chi_{ad}} \left\{ \int_\Omega \chi F(u) \, \mathrm{d}x \;\middle|\; \chi G(u) = 0 \text{ in } \Omega \right\}, \tag{2.2}$$

where the domain Ω is fixed and the infimum is taken is over all characteristic functions $\chi : \Omega \to \{0, 1\}$ in the admissible set χ_{ad}.

Example 2.1 (Optimal design in conductivity)**.** *Consider the problem of minimizing the power loss in an electric conductor, by placing a given amount C of conducting material in a given domain $\Omega \subset \mathbb{R}^d$, for a given surface current $q : \Gamma \to \mathbb{R}$, $\Gamma \subseteq \partial\Omega$. In the shape optimization setting this can be formulated as finding the conducting domain $D \subset \Omega$, $\Gamma \subseteq \partial D$, such that*

$$\inf_{D\in\mathcal{D}_{ad}} \left\{ \int_D |\nabla\varphi|^2 \ \mathrm{d}x \ \middle| \ -\operatorname{div}(\nabla\varphi)\big|_D = 0,\ \frac{\partial\varphi}{\partial n}\big|_{\partial D\setminus\Gamma} = 0,\ \frac{\partial\varphi}{\partial n}\big|_{\Gamma} = q, \right\}, \tag{2.3}$$

where $\partial/\partial n$ denotes the normal derivative on the boundary,

$$\varphi \in V \equiv \left\{ v \in H^1(D) : \int_D v \ \mathrm{d}x = 0 \right\},$$

is the electric potential, and where

$$\mathcal{D}_{ad} \equiv \left\{ D \subset \Omega : \Gamma \subseteq \partial D, \int_D \ \mathrm{d}x = C \right\}.$$

A corresponding parameter design problem can be formulated as to find the characteristic conductivity function $\sigma : \Omega \to \{0, 1\}$ such that

$$\inf_{\sigma} \left\{ \int_\Omega \sigma|\nabla\varphi|^2 \ \mathrm{d}x \ \middle| \ -\operatorname{div}(\sigma\nabla\varphi)\big|_\Omega = 0,\ \sigma\frac{\partial\varphi}{\partial n}\big|_{\partial\Omega} = q,\ \int_\Omega \sigma \ \mathrm{d}x = C \right\}. \tag{2.4}$$

This parameter design problem is studied in detail in [10].

Remark 2.1 (Two materials)**.** *For two materials, with objective functionals F^1 and F^2, and state equations G^1 and G^2, an optimal shape problem is*

$$\inf_{D\in\mathcal{D}_{ad}} \left\{ \int_D F^1(u) \ \mathrm{d}x + \int_{\Omega\setminus D} F^2(u) \ \mathrm{d}x \ \middle| \ G^1(u) = 0 \text{ in } D,\ G^2(u) = 0 \text{ in } \Omega \setminus D \right\},$$

with the corresponding parameter design problem

$$\inf_{\chi\in\chi_{ad}} \left\{ \int_\Omega \chi F^1(u) + (1-\chi)F^2(u) \ \mathrm{d}x \ \middle| \ \chi G^1(u) + (1-\chi)G^2(u) = 0 \text{ in } \Omega \right\}.$$

Example 2.2 (Time dependent reconstruction)**.** *An example of a time dependent optimal design problem is to reconstruct a time independent wave coefficient $\sigma^* : \Omega \to \{\sigma_-, \sigma_+\}$ of the wave equation from boundary measurements $\varphi^* : \partial\Omega\times[0, T] \to \mathbb{R}$. This can be formulated as*

$$\inf_{\sigma} \int_0^T \int_{\partial\Omega} (\varphi - \varphi^*)^2 \ \mathrm{d}s \ \mathrm{d}t,$$

such that

$$\begin{aligned} \varphi_{tt} &= \operatorname{div}(\sigma\nabla\varphi) && \text{in } \Omega\times(0,T],\\ \sigma\frac{\partial\varphi}{\partial n} &= q && \text{on } \partial\Omega\times(0,T],\\ \varphi &= \varphi_0, && \text{on } \Omega\times\{0\},\\ \varphi_t &= \tilde{\varphi}_0, && \text{on } \Omega\times\{0\}, \end{aligned}$$

for given Neumann boundary values $q : \partial\Omega\times(0,T]\to\mathbb{R}$ *and initial data* φ_0 *and* $\tilde{\varphi}_0$.

Remark 2.2 (Continuous material)**.** *In Example 2.1 and 2.2 it is possible to allow the sought coefficient* σ *to have intermediate values,* e.g. $\sigma : \Omega\to[\sigma_-,\sigma_+]$ *for Example 2.2. For some optimal design problems allowing intermediate values leads to a well posed problem while,* e.g. *the problem in Example 2.2 remains ill posed.*

2.1 Existence of Solutions

Without any restrictions on the class of admissible designs, optimal design problems often do not admit any solutions. A simple example is the problem to find the set $D\subset\Omega\in\mathbb{R}^2$ that minimizes $1/l(D)$, where $l(D)$ is the length of the boundary ∂D. This unconstrained minimization problem clearly has no minimizer although the minimum tends to zero, and to attain a minimizer we must add extra constraints on for example the shape of the domain D, or the boundary ∂D.

To understand why the set of admissible designs is so important we review some conditions on the existence of minimizers, see [20]: To assure existence of a solution D with a corresponding state variable u to the minimization problem (2.1), a necessary condition is that there exists a minimizing sequence D_m to (2.1) such that $\bar{D}_m\to\bar{D}$, in the Hausdorff sense. This does not imply that the corresponding characteristic functions $\chi_{D_m}:\Omega\to L^\infty(\Omega)$ converges pointwise or even weakly * to a characteristic function χ_D (see Definition 2.1 for weak * convergence). However, there always exists a minimizing sequence such that the characteristic functions χ_{D_m} converges in the weak * sense to a limit *not* belonging to the class of characteristic functions. For the problem (2.1) this means that even if the state variables u_m, corresponding to the minimizing sequence of shapes D_m, satisfies the constraint $G(u_m)=0$, the limit u may not be a solution to the original partial differential constraint $G(u)=0$.

Definition 2.1. *By weak * convergence of* $\chi_m\in L^\infty(\Omega)$ *to* $\chi\in L^\infty(\Omega)$ *we mean that*

$$\lim_{m\to\infty}\int_\Omega \chi_m(x)\phi(x)\ \ \mathrm{d}x=\int_\Omega\chi(x)\phi(x)\ \ \mathrm{d}x,$$

for all test functions $\phi\in L^1(\Omega)$. *The notation 'weak *' is here used since* $L^1(\Omega)$ *is not the dual space of* $L^\infty(\Omega)$.

To find a minimizing sequence of characteristic functions that converges to a characteristic function, we can either alter the original optimal design problem by adding penalty terms in the design criterion, or change the set of admissible designs, for example by adding conditions on the smoothness of the boundary, e.g. only allowing Lipschitz boundaries. One problem is that this restriction usually gives a minimum different from the infimum of the original problem, i.e. the problem has been altered significantly. Another approach is to extend the admissible set χ_{ad} in (2.2) to include not only characteristic functions, e.g. by introducing composites of laminated materials as in the homogenization method [1]. Such composites describes periodic material micro-structures and can for certain laminations give a minimum that coincides with the true infimum. It is worth to mention that even if a solution exists, optimal design problems may be ill-posed in the sense that small perturbations of data lead to large changes in the solution.

In Chapter 3, a different approach more connected with optimal control and calculus of variations, is used for finding a regularization. For some problems we can derive sufficient conditions for a minimizer [8, 10].

Remark 2.3. *For the particular example of minimizing energy in Example 2.1, there exists a unique minimizer without any restriction on the shape [20]. On the other hand, changing the 'inf' for a 'sup' needs regularization to admit a solution. This particular maximization problem has is addressed in [10], and can be regularized by convexification or homogenization [1, 15, 16, 17, 18].*

2.2 Solution Methods

Roughly, the computational methods solving for optimal design problems can be divided into two classes: Methods with optimality conditions derived from (2.1), and methods based on approximation of the characteristic function χ in (2.2).

In the first class we find the classical method of shape derivatives, which derives the optimal variation of the boundary. Topological derivatives, or the bubble method, is a similar method that derives optimality conditions for the creation of holes in the domain, i.e not only moves the boundary but also changes the topology. The shape optimization methods commonly use a finite element or finite difference discretization of the domain D to solve the partial differential equation $G(u) = 0$ and update both D and the discretization from the optimality conditions. Alternatively, a fixed mesh and a mapping onto the domain D can be used. Another method that uses the shape derivative, the topological derivative, or a combination of both is the level-set method. A level-set function is then used to indicate the boundary, and boundary movement and creation of holes is done by solving a transport equation for the level-set function on the whole domain Ω.

The second class of computational methods is based on the formulation (2.2) and relaxes the class of admissible designs to allow a global minimum, either by smooth approximation of χ, or as in the homogenization method, by a special class of admissible controls χ_{ad} based on periodic micro-structures. Since these methods

uses a discretization of the whole region Ω it is here often necessary to use a weak material to mimic void, i.e. $\chi > 0$. Also, to produce sharp boundaries between, in this case, the weak and the solid phase, some penalization procedure is often added. This may seem counter productive, but the hope is to first reach a global minimum to the relaxed problem, followed by a penalization which removes existence of a global minimum but forces the solution to a nearby local minimum.

In this presentation, we only deal with the continuous problem, and do not discuss any of the many optimization methods dealing with the discretized versions of (2.1) and (2.2). An introduction to discrete methods concerning optimal design of material structures can be found in [5].

Shape and Topological Derivative

Consider the problem (2.1) and define the objective functional

$$J(D) \equiv \int_D F(u) \, \mathrm{d}x,$$

where $u : D \to V$ is the solution, belonging to some Hilbert space V, to the partial differential equation $G(u) = 0$ in (2.1)

For a small perturbation $\theta : \mathbb{R}^d \to \mathbb{R}^d$ of the domain $D \subset \mathbb{R}^d$ into $D + \theta = \{x + \theta(x), x \in D\}$ the shape derivative in the direction θ can be defined as

$$\delta J(D; \theta) = \int_{\partial D} L\big(u(s), \lambda(s)\big) \; \theta(s) \cdot n \;\; \mathrm{d}s, \tag{2.5}$$

where n denotes the outward boundary normal. The functional L is here a certain problem dependent functional which is described for an example below, see Example 2.3. The variable $\lambda : D \to V$ is here the solution to a corresponding adjoint problem. One way to define the adjoint problem is from the Lagrangian

$$\mathcal{L}(D, u, \lambda) \equiv J(D, u) + \langle \lambda, G(u) \rangle,$$

where $\langle v, w \rangle$ is the duality pairing on V, which reduces to the L^2 inner product if $v, w \in L^2(D)$. The Gâteaux derivative with respect to λ gives the original constraint $G(u) = 0$, in the distribution sense, while the Gâteaux derivative with respect to u gives the dual problem for λ. The shape derivative (2.5) gives the sensitivity of the value function J with respect to change in the domain, and indicates how to move the boundary $\partial\Omega$, or the individual mesh points in the discretization of D.

Example 2.3. *Consider a simplified version of the conductivity optimization problem* (2.3)*, given in Example 2.1, where the objective functional now is*

$$J(D) = \int_D |\nabla \varphi|^2 \;\; \mathrm{d}x + \eta \int_D \;\; \mathrm{d}x,$$

and the state variable φ solves

$$-\mathrm{div}(\nabla\varphi)\big|_D = 0, \quad \frac{\partial\varphi}{\partial n}\big|_{\partial D\setminus\Gamma} = 0, \quad \frac{\partial\varphi}{\partial n}\big|_{\Gamma} = q.$$

The shape derivative is then given by

$$\delta J(D;\theta) = \int_{\partial D} (\nabla u \cdot \nabla\lambda)\ \theta\cdot n\ \ \mathrm{d}s + \eta \int_{\partial D} \theta\cdot n\ \ \mathrm{d}s$$

where the dual solution is given by $\lambda = \varphi$, see [20].

Unfortunately, the shape derivative does not deal with changes in the topology, e.g. nucleation of holes in the domain. A method which does consider topological changes is the method of topological derivatives, see e.g. [11]. The topological derivative is an extension of the shape derivative, and derives an expression for the change in the value function with respect to the creation of a small hole inside the domain.

Level-Set Methods

The level-set method, conveniently connects the two problems (2.1) and (2.2) by parameterizing the boundary between the phases using a level-set function $\psi : \Omega \times [0,T] \to \mathbb{R}$, given by

$$\begin{cases} \psi(x,\cdot) & > & 0, & x \in \Omega - D, \\ \psi(x,\cdot) & = & 0, & x \in \partial D, \\ \psi(x,\cdot) & < & 0, & x \in D, \end{cases}$$

where the normal n of ∂D is given by $\nabla\psi/|\nabla\psi|$ and the curvature by $\mathrm{div}(\nabla\psi/|\nabla\psi|)$. The time is here an artificial variable used to evolve the shape towards its optimum, by the dynamics of the Hamilton-Jacobi equation

$$\partial_t\psi + V|\nabla\psi| = 0 \text{ in } \Omega \tag{2.6}$$

where $V : \Omega \times [0,T] \to \mathbb{R}$ denotes the normal velocity of ∂D. Here, the normal velocity can be chosen according to the shape or topological derivatives, see [2, 7], and the time T corresponds to the length of the gradient step. In practice, the T is chosen such that the normal and curvature of the level-set function does not become too distorted. From the solution $\psi(\cdot,T)$, a reinitialization where the partial differential equation in (2.2) is solved, gives new initial data $\psi(\cdot,0)$ for solving (2.6) again. The level-set method requires using a weak phase to mimic void when solving the partial differential equation in (2.2), and extra computational work is introduced from introducing the additional function ψ. Also, a fixed discretization of the whole domain Ω is used for both (2.6) and the partial differential equation constraint in (2.2).

Homogenization

The previous methods all tried to find an optimal domain $D \in \Omega$, which may not exist for certain problems, unless some restriction is put on the shape of the boundary ∂D. The homogenization method, on the other hand, looks for optimal designs in the class of periodic micro-structures. Such structures do not in general form sharp boundaries, but instead share the property that there exists a minimum which coincides in average with the infimum of the original problem, as mentioned in Section 2.1.

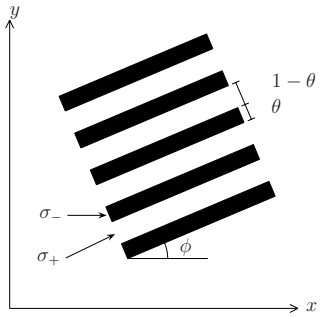

Figure 2.1: The rank-1 laminate used in (2.8)

To exemplify, we state the problem briefly mentioned in Remark 2.3: Find the conductivity function $\sigma : \Omega \to \{\sigma_-, 1\}$ that maximizes the power loss in an electric conductor, i.e.

$$\sup_{\sigma} \left\{ \int_\Omega \sigma |\nabla \varphi|^2 \ \mathrm{d}x \ \middle| \ -\operatorname{div}(\sigma \nabla \varphi)\big|_\Omega = 0, \ \sigma \frac{\partial \varphi}{\partial n}\big|_{\partial\Omega} = q, \ \int_\Omega \sigma \ \mathrm{d}x = C \right\}, \quad (2.7)$$

for $\sigma : \Omega \to \{\sigma_-, 1\}$. Note that we have here filled the void with a weak phase $\sigma_- > 0$. This maximization problem lacks maximizers, but can be relaxed to allow the existence a maximizer by simply using $\sigma : \Omega \to [\sigma_-, 1]$ instead of $\sigma : \Omega \to \{\sigma_-, 1\}$. A more clever approach is to use the homogenization method for laminated materials. We then look at the problem

$$\max_{\theta,\phi} \left\{ \int_\Omega \sigma^* |\nabla \varphi|^2 \ \mathrm{d}x \ \middle| \ -\operatorname{div}\big(\sigma^* \nabla \varphi\big)\big|_\Omega = 0, \ \sigma^* \frac{\partial \varphi}{\partial n}\big|_{\partial\Omega} = q, \ \int_\Omega \theta \ \mathrm{d}x = C \right\}. \quad (2.8)$$

with $\theta : \Omega \to [0, 1]$, $\phi : \Omega \to [0, \pi]$ and the rank-1 laminate tensor

$$\sigma^*(\theta, \phi) = \begin{pmatrix} \cos\phi & \sin\phi \\ -\sin\phi & \cos\phi \end{pmatrix} \begin{pmatrix} \lambda_\theta^+ & 0 \\ 0 & \lambda_\theta^- \end{pmatrix} \begin{pmatrix} \cos\phi & -\sin\phi \\ \sin\phi & \cos\phi \end{pmatrix},$$

with

$$\lambda_\theta^- = \left(\frac{\theta}{\sigma_-} + \frac{1-\theta}{\sigma_+} \right)^{-1}, \quad \lambda_\theta^+ = \theta\sigma_- + (1-\theta)\sigma_+.$$

The tensor σ^* is obtained from rotation and mixing of the two tensor valued controls $\sigma_- I$ and $\sigma_+ I$ in proportions θ and $1-\theta$ and direction ϕ, see Figure 2.1. We have thus enlarged the set of admissible controls by introducing two new parameters θ, ϕ describing a laminated material. The effective conductivities in the principal directions of the material is λ_θ^+ and λ_θ^-, while $(\lambda_\theta^+)^{-1}$ and $(\lambda_\theta^-)^{-1}$ correspond to the total resistances for resistors connected in parallel and in series, respectively. The homogenization method has the advantage that a maximizer (θ, ϕ) is found and that that the value of (2.8) coincides with (2.7). This particular problem uses a rank-1 laminate, but higher rank laminates, sufficient to find minimizers (or maximizers) for many important optimal design problems, can be found [1].

Chapter 3

Optimal Control and the Pontryagin Method

In the previous chapter we saw that optimal design problems often need to be regularized to obtain good approximations, and that regularization may also be necessary to assure the mere existence of a solution. In this chapter we present a method for optimal design using a regularization derived from the Hamilton-Jacobi-Bellman equations for the corresponding optimal control problem. We first describe the method for control of a system of ordinary differential equations, and then apply the methodology to control partial differential equations.

3.1 Dynamic Programming

Consider an optimal control problem for a controlled ordinary differential equation

$$\inf_{\alpha\in\mathcal{A}}\left\{g\big(X(T)\big)+\int_0^T h\big(X(s),\alpha(s)\big)\,\mathrm{d}s \;\middle|\; X'(t)=f\big(X(t),\alpha(t)\big),\ X(0)=X_0\right\}, \quad (3.1)$$

with given data $g:\mathbb{R}^n\to\mathbb{R}$, $h:\mathbb{R}^n\times B\to\mathbb{R}$, $f:\mathbb{R}^n\times B\to\mathbb{R}^n$, $X_0\in\mathbb{R}^n$, the state variable $X:[0,T]\to\mathbb{R}^n$ and a set of controls $\mathcal{A}=\{\alpha:[0,T]\to B\subset\mathbb{R}^m\}$. Optimal control problems like (3.1) can be solved by dynamic programming or by the Lagrange principle, *cf.* [14]. From the dynamic programming approach a value function $u:\mathbb{R}^n\times[0,T]\to\mathbb{R}$, defined by

$$u(x,t)\equiv\inf_{X(t)=x,\alpha\in\mathcal{A}}\left\{g\big(X(T)\big)+\int_t^T h\big(X(s),\alpha(s)\big)\ \mathrm{d}s\right\}, \quad (3.2)$$

is the unique viscosity solution (see Definition 3.1 and [14, 12]) of the nonlinear Hamilton-Jacobi-Bellman partial differential equation

$$\begin{aligned}\partial_t u(x,t)+H\big(\partial_x u(x,t),x\big)&=0, \qquad (x,t)\in\mathbb{R}^n\times(0,T),\\ u(x,T)&=g(x), \qquad x\in\mathbb{R}^n,\end{aligned} \quad (3.3)$$

where the Hamiltonian function $H : \mathbb{R}^n \times \mathbb{R}^n \to \mathbb{R}$ is defined by

$$H(\lambda, x) \equiv \min_{\alpha \in B} \big\{ \lambda \cdot f(x, \alpha) + h(x, \alpha) \big\}. \tag{3.4}$$

The value function (3.2) indicates the least cost from starting at a point (x, t) and following an optimal path $X(s)$ and control $\alpha(s)$ for the remaining time $s \in [t, T]$, and the infimum of (3.1) is given by the solution to (3.3) in the point $(X_0, 0)$. Although we can here find a global minimum, the Hamilton-Jacobi equation can in practice not be solved numerically for high dimensional problems where $n \gg 1$.

Definition 3.1. *(Viscosity solution) A bounded uniformly continuous function u is a viscosity solution to* (3.3)*, if $u(\cdot, T) = g(\cdot)$, and for each $v \in C^\infty(\mathbb{R}^n \times (0, T))$*

- *$\partial_t v(x,t) + H\big(\partial_x v(x,t), x\big) \geq 0$ when $u - v$ has a local maximum in (x, t), and*
- *$\partial_t v(x,t) + H\big(\partial_x v(x,t), x\big) \leq 0$ when $u - v$ has a local minimum in (x, t).*

The viscosity solution u is also unique, see [14, 12].

3.2 The Pontryagin Principle

To derive information on the optimal path $X(t)$ and the corresponding optimal control $\alpha(t)$, we consider the Pontryagin (Minimum) Principle, see [21], which states the following necessary condition for an optimal control to (3.1): Assuming that f, g, h are differentiable, then given an optimal path $X(t)$ with an optimal control $\alpha(t)$, there exists a path $\lambda(t)$ such that

$$\begin{aligned} X'(t) &= f\big(X(t), \alpha(t)\big), \\ X(0) &= X_0, \\ -\lambda_i'(t) &= \partial_{x_i} f\big(X(t), \alpha(t)\big) \cdot \lambda(t) + \partial_{x_i} h\big(X(t), \alpha(t)\big), \\ \lambda(T) &= g'\big(X(T)\big), \end{aligned} \tag{3.5}$$

and

$$\lambda(t) \cdot f\big(X(t), \alpha(t)\big) + h\big(X(t), \alpha(t)\big) \leq \lambda(t) \cdot f\big(X(t), a\big) + h\big(X(t), a\big), \quad a \in B,$$

or equivalently

$$\alpha(t) \in \operatorname{argmin}_{a \in B} \big\{ \lambda(t) \cdot f\big(X(t), a\big) + h\big(X(t), a\big) \big\}. \tag{3.6}$$

Also, assuming that the Hamiltonian H defined in (3.4) is differentiable, the Pontryagin Principle (3.5) and (3.6), equals the Lagrange principle, i.e. an optimal path $X(t)$ satisfies the Hamiltonian boundary value system

$$\begin{aligned} X'(t) &= \partial_\lambda H\big(\lambda(t), X(t)\big), \quad X(0) = X_0, \\ -\lambda'(t) &= \partial_x H\big(\lambda(t), X(t)\big), \quad \lambda(T) = g'(X(T)), \end{aligned} \tag{3.7}$$

cf. [4], which in fact is the method of characteristics for the Hamilton-Jacobi equation (3.3) provided $\lambda(t) \equiv \partial_x u(X(t),t)$ exists. The Lagrange principle has the advantage that high dimensional problems, $n \gg 1$ can be solved computationally and the drawback is that in practice only local minima can be found computationally. When using (3.7) to solve the minimization problem (3.1) it is assumed that the Hamiltonian is explicitly known and differentiable. In general, Hamiltonians are only Lipschitz continuous for smooth f, g and h.

Many optimal control problems lead to non-smooth optimal controls, which occur by two reasons: the Hamiltonian is in general only Lipschitz continuous, even though f, g, h are smooth, and backward optimal paths $X(t)$ may collide. To be able to use the computational advantage of solving the Hamiltonian boundary value system (3.7) a regularized problem with a $\mathcal{C}^2(\mathbb{R}^n \times \mathbb{R}^n)$ λ-concave approximation H_δ of the Hamiltonian H, is introduced in [22]. This approximation not only gives meaning to (3.7), but is well defined in the sense that the corresponding approximated value function u_δ is close to the original value function u, see [22]. In [22], error analysis yields the estimate

$$\|u_\delta - u\|_{L^\infty(\mathbb{R}^n \times \mathbb{R}_+)} = \mathcal{O}(\delta), \tag{3.8}$$

for the real and approximate value functions u and u_δ, and with a regularization parameter δ, such that $\|H_\delta - H\|_{L^\infty(\mathbb{R}^n \times \mathbb{R}^n)} = \mathcal{O}(\delta)$. This error estimate is not explicitly dependent on the dimension n, which makes the regularization suitable for optimal control of discretized partial differential equations. Observe that $\|u_\delta - u\|_{L^\infty(\mathbb{R}^n \times \mathbb{R}_+)} \to 0$ does not necessarily imply convergence of the optimal paths $X(t)$ or the controls $\alpha(t)$.

3.3 Pontryagin Approximations for Optimal Design

In [10], the above analysis for optimal control of ordinary differential equations is extended to control of a time dependent partial differential equation

$$\begin{aligned} \partial_t \varphi(x,t) &= f\big(\varphi(x,t), \alpha(x,t)\big), \quad (x,t) \in \Omega \times (0,T) \\ \varphi(x,0) &= \varphi_0, \qquad\qquad\qquad\quad x \in \Omega \end{aligned}$$

where f is a partial differential operator, $\Omega \subset \mathbb{R}^n$, and $\varphi(\cdot,t)$ belongs to some Hilbert space V on Ω. The minimization problem corresponding to (3.1) then becomes

$$\begin{aligned} \inf_{\alpha:\Omega\times[0,T]\to B} \Big\{ g\big(\varphi(\cdot,T)\big) + \int_0^T h\big(\varphi(\cdot,t), \alpha(\cdot,t)\big)\, \mathrm{d}t \;\Big|\; \\ \partial_t \varphi = f\big(\varphi(\cdot,t), \alpha(\cdot,t)\big),\ \varphi(\cdot,0) = \varphi_0 \Big\}, \end{aligned} \tag{3.9}$$

The Hamiltonian $H : V \times V \to \mathbb{R}$ is defined as

$$H(\lambda, \varphi) \equiv \min_{\alpha:\Omega\to B} \{\langle \lambda, f(\varphi,\alpha)\rangle + h(\varphi,\alpha)\}, \tag{3.10}$$

and the value function $u : V \times [0,T] \to \mathbb{R}$,

$$u(\phi,\tau) \equiv \inf_{\alpha:\Omega\times[0,T]\to B} \Big\{ g\big(\varphi(\cdot,T)\big) + \int_\tau^T h\big(\varphi(\cdot,t),\alpha(\cdot,t)\big)\ \mathrm{d}t \ \Big| \\ \partial_t\varphi = f\big(\varphi(\cdot,t),\alpha(\cdot,t)\big),\ \varphi(\cdot,\tau)=\phi\in V \Big\}$$

solves the Hamilton-Jacobi-Bellman equation

$$\partial_t u(\phi,t) + H\big(\partial_\phi u(\phi,t),\phi\big) = 0, \quad u(\cdot,T) = g, \tag{3.11}$$

Here, ∂ now denotes Gâteaux derivatives (except for ∂_t), and $\langle v, w\rangle$ is the duality pairing on V, which reduces to the $L^2(\Omega)$ inner product if $v, w \in L^2(\Omega)$. The Lagrange principle gives the Hamiltonian system

$$\begin{aligned} \partial_t\varphi &= \partial_\lambda H(\lambda,\varphi), \qquad \varphi(\cdot,0)=\phi \\ \partial_t\lambda &= -\partial_\varphi H(\lambda,\varphi), \quad \lambda(\cdot,T) = \partial_\varphi g\big(\varphi(\cdot,T)\big). \end{aligned} \tag{3.12}$$

In [8, 10], the time-independent version of Equation (3.12) is solved for φ, λ defined on a finite element subspace $\bar{V} \subset V$ and using a $\mathcal{C}^2$ regularized approximate Hamiltonian $\bar{H}_\delta$, and in [9, 23] the time dependent problem is solved.

As an example of a time-independent optimal control problem for partial differential equations we review problem (2.4) in Example 2.1, which using Gauss theorem and a prescribed multiplier $\eta \in \mathbb{R}$ corresponding to the volume constraint C, can be written as

$$\inf_{\sigma:\Omega\to\{0,1\}} \Big\{ \int_{\partial\Omega} q\varphi\ \mathrm{d}s + \eta\int_\Omega \sigma\ \mathrm{d}x \ \Big|\ -\operatorname{div}(\sigma\nabla\varphi)\big|_\Omega = 0,\ \sigma\frac{\partial\varphi}{\partial n}\big|_{\partial\Omega} = q \Big\}. \tag{3.13}$$

In this case, the Hamiltonian becomes

$$\begin{aligned} H(\lambda,\varphi) &= \min_{\sigma:\Omega\to\{0,1\}} \Big\{ \int_\Omega \sigma(\underbrace{\eta - \nabla\varphi\cdot\nabla\lambda}_{v})\ \mathrm{d}x + \int_{\partial\Omega} q(\varphi+\lambda)\ \mathrm{d}s \Big\} \\ &= \int_\Omega \underbrace{\min_{\sigma\in\{0,1\}}\{\sigma v\}}_{\mathfrak{h}(v)}\ \mathrm{d}x + \int_{\partial\Omega} q(\varphi+\lambda)\ \mathrm{d}s. \end{aligned}$$

By replacing $\mathfrak{h}$ with a smooth function $\mathfrak{h}_\delta$ (see Figure 3.1) the time-independent version of the Hamiltonian system (3.12) can by symmetry $\varphi = \lambda$ be reduced to the non-linear partial differential equation

$$\begin{cases} -\operatorname{div}\Big(\mathfrak{h}_\delta'(\eta - |\nabla\varphi|^2)\nabla\varphi\Big) = 0, & \text{in } \Omega \\ \qquad\qquad \mathfrak{h}_\delta'(\eta - |\nabla\varphi|^2)\dfrac{\partial\varphi}{\partial n} = q, & \text{on } \partial\Omega \end{cases}$$

The regularization is here similar to adding a standard Tikhonov penalty, c.f. [13], on the L^2-norm of σ in problem (3.13), which combined with allowing intermediate conductivities $\sigma : \Omega \to [0, 1]$ gives the problem

$$\inf_{\sigma:\Omega\to[0,1]} \left\{ \int_{\partial\Omega} q\varphi \ \mathrm{d}s + \eta \int_\Omega \sigma \ \mathrm{d}x + \delta \int_\Omega \sigma^2 \ \mathrm{d}x \ \middle| \ -\mathrm{div}(\sigma\nabla\varphi)\big|_\Omega = 0, \ \sigma\frac{\partial\varphi}{\partial n}\big|_{\partial\Omega} = q \right\},$$

with a regularization parameter $\delta > 0$. The Hamiltonian then becomes

$$\begin{aligned} H(\lambda,\varphi) &= \min_{\sigma:\Omega\to[0,1]} \left\{ \int_\Omega \sigma(\underbrace{\eta - \nabla\varphi\cdot\nabla\lambda}_{v} + \delta\sigma) \ \mathrm{d}x + \int_{\partial\Omega} q(\varphi+\lambda) \ \mathrm{d}s \right\} \\ &= \int_\Omega \sigma^*(v) \ v \ \mathrm{d}x + \int_{\partial\Omega} q(\varphi+\lambda) \ \mathrm{d}s, \end{aligned}$$

with the optimal control

$$\sigma^*(v) = \begin{cases} 1, & v < -2\delta, \\ \dfrac{-v}{2\delta}, & -2\delta \le v \le 0, \\ 0, & 0 < v, \end{cases}$$

see, Figure 3.1.

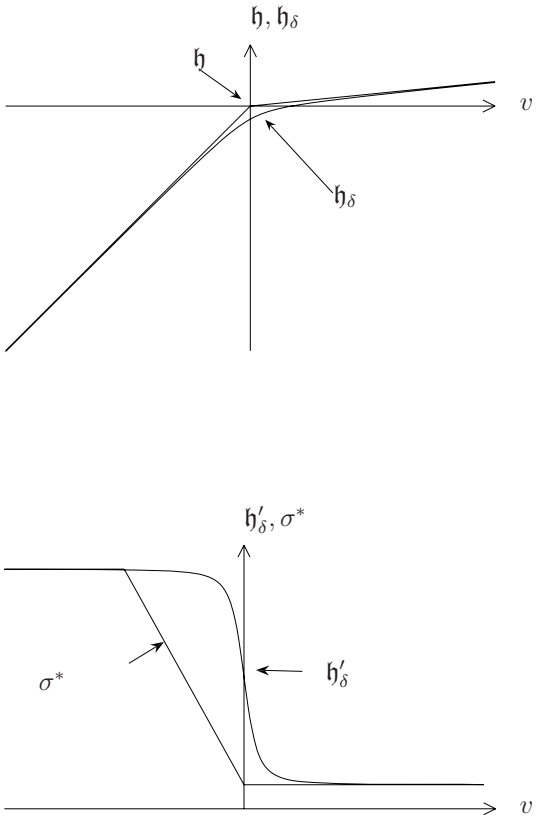

Figure 3.1: Top: The function $\mathfrak{h}$ and its regularization $\mathfrak{h}_\delta$ with respect to v. Bottom: The approximation $\mathfrak{h}'_\delta$ compared to a control σ^* obtained from adding a Tikhonov type penalty $\delta \int_\Omega \sigma^2 \, \mathrm{d}x$ to (3.13) with $\sigma : \Omega \to [\sigma_-, \sigma_+]$.

Chapter 4

Summary of Papers

Paper 1: Pontryagin Approximations for Optimal Design

In this paper the Pontryagin method presented in Chapter 3 is used to solve three different typical optimal design problems; one scalar concave maximization problem in conductivity, one scalar non-concave maximization problem in elasticity, and one inverse reconstruction problem in impedance tomography. An error estimate for the difference in the true and approximated value functions, using only the difference of the true and approximated Hamiltonians along the same paths, is also derived. This estimate gives an error estimate which in practice can be bounded in terms of the regularization parameter and the finite element mesh size, such that the value functions converge even though the optimal paths do not.

Paper 2: Pontryagin Approximations for Optimal Design of Elastic Structures

Here, the derived Pontryagin method is tested for two problems in optimal design of elastic structures: to distribute a limited amount of material in a structure to minimize its compliance, and to detect interior material distributions from surface measurements. The problem to construct a structure with minimal compliance, or maximum stiffness, is severely ill posed and needs to be regularized. It is well known that common regularizations for inverse problems gives infeasible optimal designs for minimal compliance problems, and this is also the case for the regularized Pontryagin method. To achieve physically feasible stuctures, a different approach is used, where the unregularized Pontryagin method is combined with a restriction on how much material is allowed to change in each iteration. This type of restriction acts as a regularization and gives meaningful designs that agree with other topology optimization methods.

Paper 3: Symplectic Reconstruction of Data for Heat and Wave Equations

This paper deals with the inverse problem of estimating a spacially dependent coefficient of a time dependent partial differential equation from observations of the solution at the boundary. The asumption that the coefficient is independent of time causes some extra difficulties in the Pontryagin method and different remedies are here investigated.

Paper 4: Inverse Reconstruction from Optimal Input Data

Here, the spacially dependent wave speed coefficient of the acoustic wave equation is sought given observations of the solution on the boundary. The reconstruction of the coefficient is highly dependent on input data, *e.g.* if Neumann boundary values serve as input data it is in general not possible to determine the coefficient for all possible input data. This paper shows that it is possible to formulate meaningful optimality criteria for finding optimal input data that enhances quality of the reconstructed coefficient, which is also verified by numerical experiments. An interesting property of the gradient method used to find optimal input data is that it depends on not only the observed solution to the forward problem, but also on observed solutions to a dual problem.

Bibliography

[1] Grégoire Allaire. *Shape optimization by the homogenization method*, volume 146 of *Applied Mathematical Sciences*. Springer-Verlag, Nw York, 2002.

[2] Grégoire Allaire, François Jouve, and Anca-Maria Toader. Structural optimization using sensitivity analysis and a level-set method. *J. Comput. Phys.*, 194(1):363–393, 2004.

[3] H. T. Banks and K. Kunisch. *Estimation techniques for distributed parameter systems*, volume 1 of *Systems & Control: Foundations & Applications*. Birkhäuser Boston Inc., Boston, MA, 1989.

[4] Emmanuel Nicholas Barron and Robert Jensen. The Pontryagin maximum principle from dynamic programming and viscosity solutions to first-order partial differential equations. *Trans. Amer. Math. Soc.*, 298(2):635–641, 1986.

[5] M. P. Bendsøe and O. Sigmund. *Topology optimization*. Springer-Verlag, Berlin, 2003. Theory, methods and applications.

[6] Liliana Borcea. Electrical impedance tomography. *Inverse Problems*, 18(6):R99–R136, 2002.

[7] Martin Burger and Stanley J. Osher. A survey on level set methods for inverse problems and optimal design. *European J. Appl. Math.*, 16(2):263–301, 2005.

[8] Jesper Carlsson. Pontryagin approximations for optimal design of elastic structures. *preprint*, 2006.

[9] Jesper Carlsson. Symplectic reconstruction of data for heat and wave equations. *preprint*, 2008.

[10] Jesper Carlsson, Mattias Sandberg, and Anders Szepessy. Symplectic Pontryagin approximations for optimal design. *preprint*, 2006.

[11] Jean Céa, Stéphane Garreau, Philippe Guillaume, and Mohamed Masmoudi. The shape and topological optimizations connection. *Comput. Methods Appl. Mech. Engrg.*, 188(4):713–726, 2000. IV WCCM, Part II (Buenos Aires, 1998).

[12] M. G. Crandall, L. C. Evans, and P.-L. Lions. Some properties of viscosity solutions of Hamilton-Jacobi equations. *Trans. Amer. Math. Soc.*, 282(2):487–502, 1984.

[13] Heinz W. Engl, Martin Hanke, and Andreas Neubauer. *Regularization of inverse problems*, volume 375 of *Mathematics and its Applications*. Kluwer Academic Publishers Group, Dordrecht, 1996.

[14] Lawrence C. Evans. *Partial differential equations*, volume 19 of *Graduate Studies in Mathematics*. American Mathematical Society, Providence, RI, 1998.

[15] Jonathan Goodman, Robert V. Kohn, and Luis Reyna. Numerical study of a relaxed variational problem from optimal design. *Comput. Methods Appl. Mech. Engrg.*, 57(1):107–127, 1986.

[16] Robert V. Kohn and Gilbert Strang. Optimal design and relaxation of variational problems. I. *Comm. Pure Appl. Math.*, 39(1):113–137, 1986.

[17] Robert V. Kohn and Gilbert Strang. Optimal design and relaxation of variational problems. II. *Comm. Pure Appl. Math.*, 39(2):139–182, 1986.

[18] Robert V. Kohn and Gilbert Strang. Optimal design and relaxation of variational problems. III. *Comm. Pure Appl. Math.*, 39(3):353–377, 1986.

[19] J.-L. Lions. *Optimal control of systems governed by partial differential equations.* Translated from the French by S. K. Mitter. Die Grundlehren der mathematischen Wissenschaften, Band 170. Springer-Verlag, New York, 1971.

[20] Olivier Pironneau. *Optimal shape design for elliptic systems*. Springer Series in Computational Physics. Springer-Verlag, New York, 1984.

[21] L. S. Pontryagin, V. G. Boltyanskii, R. V. Gamkrelidze, and E. F. Mishchenko. *The mathematical theory of optimal processes*. Translated from the Russian by K. N. Trirogoff; edited by L. W. Neustadt. Interscience Publishers John Wiley & Sons, Inc. New York-London, 1962.

[22] M. Sandberg and A. Szepessy. Convergence rates of symplectic Pontryagin approximations in optimal control theory. *M2AN*, 40(1), 2006.

[23] Mattias Sandberg. Convergence rates for numerical approximations of an optimally controlled Ginzburg-Landau equation. *preprint*, 2006.

[24] Curtis R. Vogel. *Computational methods for inverse problems*, volume 23 of *Frontiers in Applied Mathematics*. Society for Industrial and Applied Mathematics (SIAM), Philadelphia, PA, 2002. With a foreword by H. T. Banks.

Paper 1

SYMPLECTIC PONTRYAGIN APPROXIMATIONS FOR OPTIMAL DESIGN

JESPER CARLSSON, MATTIAS SANDBERG, AND ANDERS SZEPESSY

Abstract. The powerful Hamilton-Jacobi theory is used for constructing regularizations and error estimates for optimal design problems. The constructed Pontryagin method is a simple and general method for optimal design and reconstruction: the first, analytical, step is to regularize the Hamiltonian; next the solution to its stationary Hamiltonian system, a nonlinear partial differential equation, is computed with the Newton method. The method is efficient for designs where the Hamiltonian function can be explicitly formulated and when the Jacobian is sparse, but becomes impractical otherwise (*e.g.* for non local control constraints). An error estimate for the difference between exact and approximate objective functions is derived, depending only on the difference of the Hamiltonian and its finite dimensional regularization along the solution path and its L^2 projection, *i.e.* not on the difference of the exact and approximate solutions to the Hamiltonian systems.

Contents

1. Introduction to Optimal Design

As the computational capacity increases it becomes possible to solve more demanding construction problems. For instance, instead of only computing the deformation of a given construction, it is possible to computationally design an optimal construction with minimal deformation for a given load. In a mathematical setting

2000 *Mathematics Subject Classification.* Primary: 65N21; Secondary: 49L25.

Key words and phrases. Topology Optimization, Inverse Problems, Hamilton-Jacobi, Regularization, Error Estimates, Impedance Tomography, Convexification, Homogenization.

Support by the Swedish Research Council grants 2002-6285 and 2002-4961, and the European network HYKE, funded by the EC as contract HPRN-CT-2002-00282, is acknowledged.

optimal design is a particular inverse problem where the goal is to determine input functions in a partial differential equation that meet the design criteria in an optimal way; for instance, to distribute a fixed amount of material in space to construct a bridge with minimal deformation, for a given load, means to solve the elasticity equations and determine a material configuration. The start of this computational work is presented in [30] and has now become an activity with large international optimal design conferences and several books [4],[1],[30]. Inverse problems are often ill posed, *e.g.* small perturbations of data lead to large changes in the solution. To computationally solve inverse problems therefore requires some regularization, *cf.* [19],[36],[4],[1],[30]. The standard Tikhonov method [35] requires to choose a penalty, usually a norm and a parameter, with the purpose to regularize the computational method. Although there is good understanding how to choose the penalty for some problems, *e.g.* in tomography [29], with norms related to the required regularity of solutions and parameters related to the error in data, there is no complete theory for how to regularize general nonlinear problems.

The objective of this work is to show how the powerful theory of viscosity solutions, for time dependent optimal control problems in the dynamic programming setting, can be used as a theoretical tool to find a regularization criterion and estimate its approximation error; based on this regularization we then construct a simple and general computational method also for some highly nonlinear time independent optimal design problems, extending the work [33] on time dependent problems. Our method [32] reduces to solve a Hamiltonian system, where the Hamiltonian is a C^2-regularized version of the original Hamiltonian. This Hamiltonian system is a nonlinear partial differential equation, where the Newton method with a sparse Jacobian becomes efficient and simple to use, *e.g.* in standard PDE software. The idea is to start by computing solutions to the Hamiltonian system with a highly regularized Hamiltonian. When this is done a less regularized Hamiltonian is chosen, and the previously computed solutions serve as a starting position for the Newton method with the new Hamiltonian. This procedure of successively decreasing the regularization is repeated as far as possible. As it is sufficient to use a one-parameter family of regularized Hamiltonians, it is only needed to tune this one parameter. In the ideal situation, however, this parameter may successively be decreased to zero. Therefore only one parameter needs to be set at the start of the first Newton iteration. This is an advantage compared to methods based on regularizations using penalization of terms involving the control variable, and (sometimes many) differentials of it; in such methods there are often several parameters.

A clear limitation of our method is the requirement to obtain an explicit formula for the regularized Hamiltonian. The optimal design and reconstruction problems presented in this paper need local constraints on the control and have explicit formulas. Non local constraints on the control or Lagrangians depending on derivatives of the control typically do not admit explicit formulas, and then our method may become impractical; in other words, we use an advantage of those particular problems having explicit formulas of the Hamiltonian. When penalty terms with derivatives are present, these derivatives must be considered as control variables. Another limitation is that the solution to the Hamiltonian system gives the primal and dual variables, but not the control function directly. As will be shown in the examples considered in this paper, it is however often possible to obtain an approximate control using the approximate primal and dual solutions.

We present a natural regularization to meet the (minimal) requirement that there is a regularized discrete solution, which is accurately approximating the optimal objective function (but not necessary the optimal control function). This

regularization is derived from viscosity solutions theory for time dependent problems. Future work may use better insight also on the more demanding task to be able to iteratively compute solutions (instead of as above only approximate them) - *e.g.* in the time independent setting - to find further improved regularizations.

We derive an error estimate for the difference between exact and approximate objective functions, depending only on the difference of the Hamiltonian and its finite dimensional regularization along the solution path and its L^2 projection, *i.e.* not on the difference of the exact and approximate solutions to the Hamiltonian systems. This error estimate is of the right form to be a good starting point for new studies on adaptive methods for optimal control problems: the difference of the Hamiltonians yields an error density which measures errors both from discretization and the regularization. Our experiments show that the estimate is relatively sharp.

One way to characterize so called symplectic time discretizations for Hamiltonian systems is that these approximations are exact solutions to another Hamiltonian system, *cf.* [23]. In this sense, our approximation in space and regularization shares this symplectic property. An equivalent definition of symplectic time discretization methods for Hamiltonian systems derived from optimal control problems is that the first variation of the discrete value function agrees with the discretization of the Lagrange multiplier, see [32] where symplectic time discretizations are analyzed for optimal control problems with the the similar use of viscosity solution theory as here. This property that the first variation of the discrete value function agrees with the discretization of the Lagrange multiplier only makes sense for time dependent problems, which is one reason our analysis starts by extending the original time independent optimal control problem to an artificial time dependent dynamic programming formulation.

We study three different examples where the nonlinear PDEs are of different character: scalar concave maximization, scalar non-concave maximization and an elliptic system for reconstruction. The homogenization method is a theoretically powerful way to regularize some optimal design problems [1], based on a change of control variables related to composite micro structure. This regularization changes the differential operator part of the Lagrangian. Section 3.2 suggests a simple alternative regularization based on the material constraint part of the Lagrangian: the constraint on material volume $\int_\Omega \sigma dx = C$, which usually is included in the Lagrangian by a term $\eta \int_\Omega \sigma dx$, is now instead represented by $\eta' \int_\Omega \sigma^{-1} dx$ which turns out to give the same regularized Hamiltonian as the homogenization method for a scalar problem.

2. Symplectic Pontryagin Approximations in Optimal Control

Consider a differential equation constrained minimization problem with solution φ in some Hilbert space V on a domain Ω and control $\sigma \in \mathcal{A} := \{\sigma : \Omega \to B\}$:

$$\begin{aligned} & f(\varphi, \sigma) = 0 \quad \text{in distribution,} \\ & \min_{\sigma \in \mathcal{A}} h(\varphi, \sigma), \end{aligned} \tag{1}$$

and its approximation with solution $\bar{\varphi} \in \bar{V} \subset V$ and control $\bar{\sigma} \in \bar{\mathcal{A}}$:

$$\begin{aligned} & \bar{f}(\bar{\varphi}, \bar{\sigma}) = 0 \\ & \min_{\bar{\sigma} \in \bar{\mathcal{A}}} \bar{h}(\bar{\varphi}, \bar{\sigma}). \end{aligned} \tag{2}$$

Example 2.1 (Optimal conductor)**.** *Section 3.1 presents minimization of the power loss in an electric conductor, by distributing a given amount of conducting material in a domain $\Omega \subset \mathbb{R}^d$, with a surface current q. Let $\eta \in \mathbb{R}$ be a constant Lagrange*

multiplier, associated to the given amount of material, and find an optimal conduction distribution $\sigma : \Omega \to \{\sigma_-, \sigma_+\} =: B$*, where* $\sigma_\pm > 0$*, such that*

$$\min_{\sigma} \left\{ \int_{\partial\Omega} q\varphi \ \mathrm{d}s + \eta \int_\Omega \sigma \ \mathrm{d}x \ \middle| \ f(\varphi,\sigma) := \mathrm{div}(\sigma\nabla\varphi)\Big|_\Omega = 0, \ \sigma\frac{\partial\varphi}{\partial n}\Big|_{\partial\Omega} = q \right\}. \tag{3}$$

Here $\partial/\partial n$ *denotes the normal derivative,* ds *is the surface measure on* $\partial\Omega$ *and* $\varphi \in V := \{v \in \mathrm{H}^1(\Omega) : \int_\Omega v \ \mathrm{d}x = 0\}$ *is the electric potential.*

The corresponding Lagrangians

$$\begin{aligned} \mathcal{L}(\lambda,\varphi,\sigma) &:= \langle \lambda, f(\varphi,\sigma)\rangle + h(\varphi,\sigma), \\ \bar{\mathcal{L}}(\bar\lambda,\bar\varphi,\bar\sigma) &:= \langle \bar\lambda, \bar f(\bar\varphi,\bar\sigma)\rangle + \bar h(\bar\varphi,\bar\sigma), \end{aligned}$$

can be used to formulate the conditions

$$\begin{aligned} \partial_1\mathcal{L} &= f(\varphi^*,\sigma^*) = 0, \\ \partial_2\mathcal{L} &= \langle \lambda^*, \partial f(\varphi^*,\sigma^*)\rangle + \partial h(\varphi^*,\sigma^*) = 0, \\ \sigma^* &\in \operatorname*{argmin}_{\sigma\in\mathcal{A}} \{\langle \lambda^*, f(\varphi^*,\sigma)\rangle + h(\varphi^*,\sigma)\}, \end{aligned} \tag{4}$$

inspired by the corresponding time dependent condition (10). Here, $\partial_1 =: \partial$ and ∂_2 are the Gateaux derivatives with respect to the first and second arguments respectively, and $\langle v, w\rangle$ is the duality pairing on V, which reduces to the $\mathrm{L}^2(\Omega)$ inner product if $v, w \in \mathrm{L}^2(\Omega)$.

Optimal control problems are inverse problems. It is well known that inverse problems often are ill-posed; therefore they need to be regularized. We will use a formulation of (4) based on the Hamiltonian to regularize our optimal design problems. The Hamiltonians $H : V \times V \to \mathbb{R}$ and $\bar H : V \times \bar V \to \mathbb{R}$ defined as

$$\begin{aligned} H(\lambda,\varphi) &:= \min_{\sigma\in\mathcal{A}} \{\langle \lambda, f(\varphi,\sigma)\rangle + h(\varphi,\sigma)\} \\ \bar H(\lambda,\bar\varphi) &:= \min_{\bar\sigma\in\bar{\mathcal{A}}} \{\langle \lambda, \bar f(\bar\varphi,\bar\sigma)\rangle + \bar h(\bar\varphi,\bar\sigma)\} \end{aligned} \tag{5}$$

eliminate the control variables in the local equilibrium conditions

$$\begin{aligned} \partial_1 H(\lambda^*,\varphi^*) &= 0 \\ -\partial_2 H(\lambda^*,\varphi^*) &= 0, \end{aligned} \tag{6}$$

and similarly for $(\bar\lambda^*, \bar\varphi^*)$

$$\begin{aligned} \partial_1 \bar H(\bar\lambda^*,\bar\varphi^*) &= 0 \\ -\partial_2 \bar H(\bar\lambda^*,\bar\varphi^*) &= 0. \end{aligned}$$

It turns out that for our optimal design problems it is easy to find an explicit expression for the Hamiltonian; for some other constrained minimization problems the Hamiltonian can be too complicated to use computationally. The Hamiltonian is in general only Lipschitz continuous even if f, g and h are smooth and we shall see that in particular for optimal design the Hamiltonians indeed are not differentiable everywhere. We also see that the stationary Hamiltonian system (6) becomes undefined where the Hamiltonian is not differentiable. At a point where the Hamiltonian is not differentiable the optimal control depends discontinuously on (λ, φ). The Hamiltonian form has the advantage that the Newton method can be used to iteratively solve the nonlinear constrained optimization problem (1) when the Hamiltonian can be written using a simple formula so that the Hessian of H is explicitly known, while Hessian information is in general not available for direct constrained minimization based on the control variable σ. We want to understand

how to regularize and to estimate errors introduced by approximation and regularization of the optimal control problem. In particular we seek an estimate of the error

$$E := \min_{\bar\sigma\in\bar{\mathcal{A}}}\{\bar h(\bar\varphi,\bar\sigma) \mid \bar f(\bar\varphi,\bar\sigma)=0\} - \min_{\sigma\in\mathcal{A}}\{h(\varphi,\sigma) \mid f(\varphi,\sigma)=0\}.$$

The definition of λ^*, φ^* and H imply

$$\min_{\sigma\in\mathcal{A}}\{h(\varphi,\sigma) \mid f(\varphi,\sigma)=0\} = H(\lambda^*,\varphi^*) \tag{7}$$

$$\min_{\bar\sigma\in\bar{\mathcal{A}}}\{\bar h(\bar\varphi,\bar\sigma) \mid \bar f(\bar\varphi,\bar\sigma)=0\} = \bar H(\bar\lambda^*,\bar\varphi^*) \tag{8}$$

which seems to require estimates of $(\bar\varphi^*-\varphi^*, \bar\lambda^*-\lambda^*)$ to yield a bound on E. To obtain bounds on $\bar\varphi^*-\varphi^*$ is in fact a harder problem than to estimate E. The situation is similar to minimization of a non strictly convex function where convergence of the minimum value may hold without having convergence of the minimizing points. In our case the error in the objective function can be small although the difference of the controls is large, *e.g.* near a point where H is not differentiable.

We shall see that the corresponding time dependent optimal control problem is useful for understanding regularizations and error estimates; in particular we use the time dependent formulation to derive bounds on E depending only on the difference of the two Hamiltonians along the *same path*, *i.e.* depending on $H(\lambda,\bar\varphi)-\bar H(\lambda,\bar\varphi)$, so that no estimate of $\varphi^*-\bar\varphi^*$ or $\lambda^*-\bar\lambda^*$ is needed. Let us now state and compare computational methods for time dependent optimal control problems. Consider two controlled differential equations

$$\begin{aligned}\partial_t\varphi_t &= f(\varphi_t,\sigma_t),\\ \partial_t\bar\varphi_t &= \bar f(\bar\varphi_t,\bar\sigma_t),\end{aligned}$$

with solutions $\varphi : [0,T]\to V$, and $\bar\varphi : [0,T]\to\bar V$, and given initial values φ_0, $\bar\varphi_0$. Here, ∂_t denotes the partial derivative with respect to time and $\varphi_t := \varphi(t)$, $\sigma_t := \sigma(t)$. The objective is to minimize

$$\begin{aligned}&\min_{\sigma\in\mathcal{B}}\left\{\int_0^T h(\varphi_t,\sigma_t)\,\mathrm{d}t + g(\varphi_T)\;\middle|\;\partial_t\varphi_t = f(\varphi_t,\sigma_t)\right\},\quad \mathcal{B}:=\{\sigma:[0,T]\to\mathcal{A}\},\\ &\min_{\bar\sigma\in\bar{\mathcal{B}}}\left\{\int_0^T \bar h(\bar\varphi_t,\bar\sigma_t)\,\mathrm{d}t + \bar g(\bar\varphi_T)\;\middle|\;\partial_t\bar\varphi_t = \bar f(\bar\varphi_t,\bar\sigma_t)\right\},\quad \bar{\mathcal{B}}:=\{\bar\sigma:[0,T]\to\bar{\mathcal{A}}\}.\end{aligned} \tag{9}$$

These optimal control problems can be solved either directly using constrained minimization or by dynamic programming. The Lagrangian becomes

$$\mathcal{L} := \int_0^T \langle\lambda_t, f(\varphi_t,\sigma_t)-\partial_t\varphi_t\rangle + h(\varphi_t,\sigma_t)\,\mathrm{d}t + g(\varphi_T)$$

and the constrained minimization method is based on the Pontryagin method

$$\begin{aligned}\partial_t\varphi_t &= f(\varphi_t,\sigma_t)\\ \partial_t\lambda_t &= -\langle\lambda_t,\partial f(\varphi_t,\sigma_t)\rangle + \partial h(\varphi_t,\sigma_t)\\ \sigma_t &\in \operatorname*{argmin}_{\sigma\in\mathcal{A}}\{\langle\lambda_t, f(\varphi_t,\sigma)\rangle + h(\varphi_t,\sigma)\}.\end{aligned} \tag{10}$$

This can be written as a Hamiltonian system

$$\begin{aligned}\partial_t\varphi_t &= \partial_1 H(\lambda_t,\varphi_t)\\ \partial_t\lambda_t &= -\partial_2 H(\lambda_t,\varphi_t)\end{aligned} \tag{11}$$

with φ_0 given, and $\lambda_T = \partial g(\varphi_T)$.

The alternative dynamic programming method is based on the value functions $u : V \times [0,T] \to \mathbb{R}$ and $\bar{u} : \bar{V} \times [0,T] \to \mathbb{R}$,

$$
\begin{aligned}
u(\phi,\tau) &:= \inf_{\sigma\in\mathcal{B}} \left\{ \int_\tau^T h(\varphi_t,\sigma_t)\ \mathrm{d}t + g(\varphi_T) \;\middle|\; \partial_t\varphi_t = f(\varphi_t,\sigma_t),\ \varphi_\tau = \phi \in V \right\} \\
\bar{u}(\phi,\tau) &:= \inf_{\bar{\sigma}\in\bar{\mathcal{B}}} \left\{ \int_\tau^T \bar{h}(\bar{\varphi}_t,\bar{\sigma}_t)\ \mathrm{d}t + \bar{g}(\bar{\varphi}_T) \;\middle|\; \partial_t\bar{\varphi}_t = f(\bar{\varphi}_t,\bar{\sigma}_t),\ \bar{\varphi}_\tau = \phi \in \bar{V} \right\},
\end{aligned}
\tag{12}
$$

which solve the nonlinear Hamilton-Jacobi-Bellman equations

$$
\begin{aligned}
&\partial_t u(\phi,t) + H\big(\partial u(\phi,t),\phi\big) = 0, \quad u(\cdot,T) = g, \\
&\partial_t \bar{u}(\phi,t) + \bar{H}\big(\partial \bar{u}(\phi,t),\phi\big) = 0, \quad \bar{u}(\cdot,T) = \bar{g}.
\end{aligned}
\tag{13}
$$

with Hamiltonians defined as in (5).

The Hamilton-Jacobi formulation has two advantages and a severe disadvantage:

+ there is complete well posedness theory for Hamilton-Jacobi equations, based on viscosity solutions, see [15], although, in general, the value function is not everywhere differentiable, corresponding in the constrained optimization method to optimal backward paths φ^* that collide and hence the Lagrange multiplier λ^* becomes ill defined in a standard sense;
+ the Hamilton-Jacobi formulation finds a global minimum, while constrained minimization focuses on local minima;
– the drawback with dynamic programming is that the method is only computationally feasible for problems in low dimension, $\bar{\varphi}_t \in \mathbb{R}^n$, while constrained minimization is computable also for high dimensional problems where $\bar{\varphi}$ is an approximation of a solution to a partial differential equation with $n \gg 1$.

Therefore the computational option is to use constrained minimization for problems in high dimension and we will choose a discretization of the stationary Hamiltonian system (6) to solve optimal design problems. However, we shall use the Hamilton-Jacobi equation in infinite dimension to understand regularizations and to derive error estimates. The additional structure extending our optimal design problems to dynamic programming problems is hence a useful theoretical tool. Note however that not all constrained optimal control problems have such extensions. Note also that solving the Hamiltonian system (11) is the method of characteristics for the Hamilton-Jacobi equation (13), with $\lambda_t = \partial u(\varphi_t, t)$.

Example 2.2 (Artificial time dependent optimal conductor)**.** *The time dependent extension of example 2.1 is to find an optimal time dependent conductivity* $\sigma : \Omega \times [0,T] \to \{\sigma_-, \sigma_+\}$ *to minimize the power loss under constraint of the parabolic equation*

$$
\partial_t\varphi = \operatorname{div}(\sigma\nabla\varphi),
$$

where $\varphi = \varphi(x,t)$*. The Lagrangian takes the form*

$$
\mathcal{L}(\sigma,\lambda,\varphi) := \int_0^T \int_{\partial\Omega} q(\varphi+\lambda)\ \mathrm{d}s\ \mathrm{d}t + \int_0^T \int_\Omega \sigma \underbrace{(\eta - \nabla\varphi\cdot\nabla\lambda)}_{v} - \partial_t\varphi\lambda\ \mathrm{d}x\ \mathrm{d}t,
$$

with $\lambda = \lambda(x,t)$ *and the Hamiltonian*

$$
\begin{aligned}
H(\lambda,\varphi) &= \min_{\sigma:\Omega\to\{\sigma_\pm\}} \left\{ \int_\Omega \sigma v\ \mathrm{d}x + \int_{\partial\Omega} q(\varphi+\lambda)\ \mathrm{d}s \right\} \\
&= \int_\Omega \underbrace{\min_{\sigma\in\sigma_\pm}\{\sigma v\}}_{\mathfrak{h}(v)}\ \mathrm{d}x + \int_{\partial\Omega} q(\varphi+\lambda)\ \mathrm{d}s,
\end{aligned}
$$

where we have introduced the function $\mathfrak{h}(v) = \min_{\sigma\in\sigma_\pm}\{\sigma v\}$. *The value function*

$$u(\phi,\tau) = \inf_{\sigma}\left\{ \int_\tau^T \int_{\partial\Omega} q\varphi \ \mathrm{d}s + \eta \int_\Omega \sigma \ \mathrm{d}x \ \mathrm{d}t \ \middle|\ \partial_t\varphi = \operatorname{div}(\sigma\nabla\varphi),\ \varphi_\tau = \phi \right\}$$

yields the infinite dimensional Hamilton-Jacobi equation

$$\partial_t u(\phi,t) + H(\partial u(\phi,t),\phi) = 0 \quad t<T, \quad u(\cdot,T) = 0,$$

using the Gateaux derivative $\partial u(\phi,t)$ *of the functional* $u(\phi,t)$ *in* $\mathrm{L}^2(\Omega)$. *The corresponding Hamiltonian system is the parabolic system*

$$\begin{aligned}
&\int_\Omega \partial_t\varphi w + \mathfrak{h}'(\eta - \nabla\varphi\cdot\nabla\lambda)\nabla\varphi\cdot\nabla w \ \mathrm{d}x = \int_{\partial\Omega} qw \ \mathrm{d}s, \quad \varphi(\cdot,0) \text{ given},\\
&\int_\Omega -\partial_t\lambda v + \mathfrak{h}'(\eta - \nabla\varphi\cdot\nabla\lambda)\nabla\lambda\cdot\nabla v \ \mathrm{d}x = \int_{\partial\Omega} qv \ \mathrm{d}s, \quad \lambda(\cdot,T) = 0,
\end{aligned}$$

for all test functions $v, w \in V \equiv \{v\in \mathrm{H}^1(\Omega) : \int_\Omega v \ \mathrm{d}x = 0\}$.

2.1. **Derivation of Approximation Error.** We simplify by considering the case when $\bar g = g$. A similar approximation study is in [33]. Let us first derive the approximation error, $\bar u(\bar\varphi_0,0) - u(\varphi_0,0) =: \tilde E$, of the value functions (12) given solutions $\sigma,\bar\sigma$ and $\varphi,\bar\varphi$ to the time dependent optimal control problems (9)

$$\begin{aligned}
\tilde E &:= \int_0^T \bar h(\bar\varphi_t,\bar\sigma_t) \ \mathrm{d}t + g(\bar\varphi_T) - \big(\int_0^T h(\varphi_t,\sigma_t) \ \mathrm{d}t + g(\varphi_T)\big)\\
&= \int_0^T \bar h(\bar\varphi_t,\bar\sigma_t) \ \mathrm{d}t + u(\bar\varphi_T,T) - u(\varphi_0,0) \qquad (14)\\
&= \int_0^T \bar h(\bar\varphi_t,\bar\sigma_t) \ \mathrm{d}t + u(\bar\varphi_T,T) - u(\bar\varphi_0,0) + u(\bar\varphi_0,0) - u(\varphi_0,0)
\end{aligned}$$

To simplify the analysis choose the initial data for the exact path to coincide with the initial data for the approximate path, *i.e.* $\varphi_0 = \bar\varphi_0$. Also assume that u is Gateaux differentiable; the general case with only sub differentiable u is in Section 2.2. Then the right hand side simplifies to

$$\begin{aligned}
&\int_0^T \mathrm{d}u(\bar\varphi_t,t) + \int_0^T \bar h(\bar\varphi,\bar\sigma) \ \mathrm{d}t\\
&= \int_0^T \partial_t u(\bar\varphi_t,t) + \langle \partial u(\bar\varphi_t,t), \bar f(\bar\varphi_t,\bar\sigma_t)\rangle + \bar h(\bar\varphi_t,\bar\sigma_t) \ \mathrm{d}t \qquad (15)\\
&\geq \int_0^T \underbrace{-H\big(\partial u(\bar\varphi_t,t),\bar\varphi_t\big)}_{=\partial_t u(\bar\varphi_t,t)} + \bar H\big(\partial u(\bar\varphi_t,t),\bar\varphi_t\big) \ \mathrm{d}t.
\end{aligned}$$

where the inequality follows from the definition (5) of $\bar H$. Note that the Pontryagin principle

$$\langle \partial\bar u(\bar\varphi_t,t), \bar f(\bar\varphi_t,\bar\sigma_t)\rangle + \bar h(\bar\varphi_t,\bar\sigma_t) = \bar H\big(\partial\bar u(\bar\varphi_t,t),\bar\varphi_t\big),$$

is not applicable here since we have ∂u instead of $\partial\bar u$. The more general case with $\bar g \neq g$ yields the additional error term

$$(g-\bar g)(\bar\varphi_T)$$

to the right hand side in (15).

Similarly, exchange the role of the exact value function along the approximate path, $(u,\bar\varphi)$, with the approximate value function along the exact path, $(\bar u,\varphi)$, to obtain an upper bound on $\tilde E$. This requires a new step; to give meaning to $\bar u$ along

the exact path φ_t. For this purpose we introduce the projection $P : V \to \bar{V}$. We have, using $\bar{\varphi}_0 = \varphi_0 = P\varphi_0$,

$$
\begin{aligned}
-\tilde{E} &= \int_0^T h(\varphi_t, \sigma_t)\ \mathrm{d}t + g(\varphi_T) - \big(\int_0^T \bar{h}(\bar{\varphi}_t, \bar{\sigma}_t)\ \mathrm{d}t + g(\bar{\varphi}_T)\big) \\
&= \int_0^T h(\varphi_t, \sigma_t)\ \mathrm{d}t + g(\varphi_T) + \bar{u}(P\varphi_T, T) - g(P\varphi_T) - \bar{u}(\bar{\varphi}_0, 0) \qquad (16) \\
&= \int_0^T h(\varphi_t, \sigma_t)\ \mathrm{d}t + \bar{u}(P\varphi_T, T) - \bar{u}(P\varphi_0, 0) + g(\varphi_T) - g(P\varphi_T)
\end{aligned}
$$

The first three terms in the right hand side become

$$
\begin{aligned}
&\int_0^T \mathrm{d}\bar{u}(P\varphi_t, t) + \int_0^T h(\varphi_t, \sigma_t)\ \mathrm{d}t \\
&= \int_0^T \partial_t \bar{u}(P\varphi_t, t) + \langle \partial \bar{u}(P\varphi_t, t), Pf(\varphi_t, \sigma_t)\rangle + h(\varphi_t, \sigma_t)\ \mathrm{d}t \\
&= \int_0^T \partial_t \bar{u}(P\varphi_t, t) + \langle P\partial \bar{u}(P\varphi_t, t), f(\varphi_t, \sigma_t)\rangle + h(\varphi_t, \sigma_t)\ \mathrm{d}t \qquad (17) \\
&\geq \int_0^T \partial_t \bar{u}(P\varphi_t, t) + H\big(\partial \bar{u}(P\varphi_t, t), \varphi_t\big)\ \mathrm{d}t \\
&= \int_0^T -\bar{H}\big(\partial \bar{u}(P\varphi_t, t), P\varphi_t\big) + H\big(\partial \bar{u}(P\varphi_t, t), \varphi_t\big)\ \mathrm{d}t.
\end{aligned}
$$

Combining (16) and (17) we now have

$$
\begin{aligned}
\tilde{E} &\leq \int_0^T \bar{H}\big(\partial \bar{u}(P\varphi_t, t), P\varphi_t\big) - H\big(\partial \bar{u}(P\varphi_t, t), \varphi_t\big)\ \mathrm{d}t - g(\varphi_T) + g(P\varphi_T) \\
&= \int_0^T \big(\bar{H} - H\big)\big(\partial \bar{u}(P\varphi_t, t), P\varphi_t\big)\ \mathrm{d}t \qquad (18) \\
&\quad + \int_0^T H\big(\partial \bar{u}(P\varphi_t, t), P\varphi_t\big) - H\big(\partial \bar{u}(P\varphi_t, t), \varphi_t\big)\ \mathrm{d}t + g(P\varphi_T) - g(\varphi_T).
\end{aligned}
$$

Assume now that h, g and H are Lipschitz continuous in V, with respect to the variable φ. Then the projection error terms in the right hand side of (18) are

$$
\begin{aligned}
\tilde{E}_P &:= \left| \int_0^T H\big(\partial \bar{u}(P\varphi_t, t), P\varphi_t\big) - H\big(\partial \bar{u}(P\varphi_t, t), \varphi_t\big)\ \mathrm{d}t + g(P\varphi_T) - g(\varphi_T) \right| \\
&= \sup_{t\in[0,T]} \|P\varphi_t - \varphi_t\|_V \mathcal{O}(T).
\end{aligned}
$$

Combine (15) and (18) to obtain

$$
\begin{aligned}
&\int_0^T \big(\bar{H} - H\big)\big(\partial u(\bar{\varphi}_t, t), \bar{\varphi}_t\big)\ \mathrm{d}t \leq \tilde{E} \leq \\
&\leq \int_0^T \big(\bar{H} - H\big)\big(\partial \bar{u}(P\varphi_t, t), P\varphi_t\big)\ \mathrm{d}t + \tilde{E}_P.
\end{aligned} \qquad (19)
$$

Remark 2.1 (No minimizers)**.** *If there are no minimizers to* (9)*, then for every* $\varepsilon > 0$*, we can choose controls* $\sigma, \bar{\sigma}$ *with corresponding states* $\varphi, \bar{\varphi}$ *such that*

$$E_{lhs} - \varepsilon \leq \tilde{E} \leq E_{rhs} + \varepsilon$$

with E_{lhs}, E_{rhs} *being the left and right hand sides of* (19)*.*

To estimate the error in the case of time independent optimal control problems with solutions φ and $\bar{\varphi}$, we assume that the time dependent control problems with

initial data $\varphi_0 = \bar{\varphi}_0$ for some given $\bar{\varphi}_0 \in \bar{V}$ (close to some approximation of $\bar{\varphi}$) asymptotically have the same solutions as the time independent versions, *i.e.*

$$
\begin{aligned}
&\lim_{T\to\infty} \inf_{\sigma\in\mathcal{A}} \left\{ \frac{1}{T}\int_0^T h(\varphi_t,\sigma_t)\ \mathrm{d}t \;\middle|\; \partial_t\varphi_t = f(\varphi_t,\sigma_t),\ \varphi_0 = \bar{\varphi}_0 \right\} \\
&= \inf_{\sigma\in B}\{h(\varphi,\sigma) \mid f(\varphi,\sigma) = 0\} \\
&\lim_{T\to\infty} \inf_{\bar{\sigma}\in\bar{\mathcal{A}}} \left\{ \frac{1}{T}\int_0^T \bar{h}(\bar{\varphi}_t,\bar{\sigma}_t)\ \mathrm{d}t \;\middle|\; \partial_t\bar{\varphi}_t = f(\bar{\varphi}_t,\bar{\sigma}_t),\ \bar{\varphi}_0 = \varphi_0 \right\} \\
&= \inf_{\bar{\sigma}\in\bar{B}}\{\bar{h}(\bar{\varphi},\bar{\sigma}) \mid \bar{f}(\bar{\varphi},\bar{\sigma}) = 0\},
\end{aligned}
\tag{20}
$$

which implies

Theorem 2.1. *Assume that* (20) *holds, and that g is a bounded function. Then the error E satisfies*

$$E = \lim_{T\to\infty} \frac{\tilde{E}}{T},$$

where $\tilde{E}$, given in (14), (16) *and Section 2.2, only depends on the difference between the Hamiltonians H and $\bar{H}$ along a solution path and on the projection error $\|\varphi_t - P\varphi_t\|_V$, but not on the error between the paths $(\varphi - \bar{\varphi}, \lambda - \bar{\lambda})$.*

2.2. **Non Differentiable Solution to Hamilton-Jacobi Equations.** Solutions to Hamilton-Jacobi equations are in general not differentiable. Let us extend the derivation (15), (17) to a case when u is not differentiable. The theory of viscosity solutions to Hamilton-Jacobi equations gives well posedness for solutions, which are continuous but not necessarily differentiable, cf. [20, 3, 2]. This theory is now rather complete in the finite dimensional setting, cf. [16]. Let us therefore consider a case when V and $\bar{V}$ are two finite element spaces, with $\bar{V} \subset V$ so that the corresponding Hamilton-Jacobi equations are defined on finite dimensional spaces. By theory in *e.g.* [10], which covers finite dimensional optimal control systems, it follows that the value functions, u and $\bar{u}$, in all problems treated in this report, are semiconcave on, respectively, $V \times [0,T]$ and $\bar{V} \times [0,T]$. One of the requirements for semiconcavity in [10] is that the flux (here $f(\varphi,\sigma)$) and its spatial derivative ($\partial_\varphi f(\varphi,\sigma)$) must both be Lipschitz in the state variable, φ, with a constant independent of σ. This can be verified for the fluxes in the present problems using a discrete H^2 norm which is equivalent to the Euclidean norm since the spaces are finite dimensional. The other requirements for semiconcavity are easily verified. Therefore the error estimate (19) extends to the general case when $u, \bar{u}$ are viscosity solutions that are not differentiable functions as follows. If u is a non differentiable semiconcave solution to a Hamilton-Jacobi equation the definition of viscosity solution reduces to

$$
\begin{aligned}
&q + H(p,\varphi) \geq 0 \quad \text{for all } (p,q) \in D^+u(\varphi,t) \\
&u(\cdot,T) = g,
\end{aligned}
\tag{21}
$$

where $D^+u(x) := \{z \in V \times \mathbb{R} : u(y+x) - u(x) - \langle z, y\rangle \leq o(\|y\|)\}$ is the super differential of u at the point $x = (\varphi, t)$. This means that in (15) we can for each t choose a point $(p,q) \in D^+u(\bar{\varphi}_t, t)$ so that

$$\int_0^T \mathrm{d}u(\bar{\varphi}_t,t) + \int_0^T \bar{h}(\bar{\varphi}_t,t)\ \mathrm{d}t = \int_0^T q + \langle p, \bar{f}(\bar{\varphi}_t,\bar{\sigma}_t)\rangle + \bar{h}(\bar{\varphi}_t,t)\ \mathrm{d}t,$$

and by the definition (8) of $\bar{H}$ we have

$$\int_0^T q + \langle p, \bar{f}(\bar{\varphi}_t,\bar{\sigma}_t)\rangle + \bar{h}(\bar{\varphi}_t,t)\ \mathrm{d}t \geq \int_0^T \left(q + \bar{H}(p,\bar{\varphi}_t)\right)\ \mathrm{d}t.$$

Finally, by (21),

$$\int_0^T \big(q + \bar{H}(p, \bar{\varphi}_t)\big)\ \mathrm{d}t \geq \int_0^T \big(-H + \bar{H}\big)(p, \bar{\varphi}_t)\ \mathrm{d}t.$$

The analogous formulation holds for $\bar{u}$. Consequently (19) holds for some $(p, q) \in D^+u(\bar{\varphi}_t, t)$ replacing $(\partial u(\bar{\varphi}_t, t), \partial_t u(\bar{\varphi}_t, t))$ and some $(\bar{p}, \bar{q}) \in D^+\bar{u}(P\varphi_t, t)$ replacing $(\partial\bar{u}(P\varphi_t, t), \partial_t\bar{u}(P\varphi_t, t))$.

The present analysis is, however, in principle valid even when we let V be an infinite dimensional Hilbert space, although existence and semiconcavity of solutions is not derived in full generality. For instance parabolic problems with fluxes f where the terms including second order derivatives depend on the control (as here) seem to not have been studied. In [9] and [7] the case of semilinear control problems is treated. This theory is used in [33] to perform analysis similar to the one in this section when V is infinite dimensional. For theory involving more nonlinearly operators, see *e.g.* [34].

2.3. **Derivation of Regularization Error.** In the examples treated in this report the Hamiltonian, H, is nondifferentiable, as the function $\mathfrak{h}$ is nondifferentiable. Therefore it can not be expected that using the Hamiltonian system (11), even in the discretized case, would give an optimal path which could be used to determine the value of $\bar{u}$. For this reason we will consider solutions to the regularized Hamiltonian system

$$\begin{aligned} \partial_t\bar{\varphi}_t &= \partial_1\bar{H}_\delta(\bar{\lambda}_t, \bar{\varphi}_t), \\ \partial_t\bar{\lambda}_t &= -\partial_2\bar{H}_\delta(\bar{\lambda}_t, \bar{\varphi}_t), \end{aligned} \tag{22}$$

where $\bar{H} \equiv \bar{H}_\delta$ is a smooth regularization of H, which is also concave in the $\bar{\lambda}$ variable, for $\delta > 0$ and $\bar{H}_0 = H$. To find an optimal control problem corresponding to (22), we may relate to the Hamiltonian, $\bar{H}_\delta$, the Legendre transform in the $\bar{\lambda}$ variable:

$$L(\bar{\varphi}, \bar{l}) \equiv \sup_{\bar{\lambda}\in\bar{V}} \big\{ -\langle\bar{l}, \bar{\lambda}\rangle + \bar{H}_\delta(\bar{\lambda}, \bar{\varphi})\big\}. \tag{23}$$

The function L is a running cost for the following variational problem:

$$\bar{u}_\delta(\phi, t_0) = \inf\big\{ \int_{t_0}^T L(\bar{\varphi}_t, \partial_t\bar{\varphi}_t)dt + g(\bar{\varphi}_T) \,\big|\, \bar{\varphi}_{t_0} = \phi\big\}, \tag{24}$$

where the infimum is taken over all absolutely continuous functions $\varphi : [t_0, T] \to \bar{V}$. This can be formulated as the optimal control problem

$$\inf_{\bar{\sigma}\in \mathrm{L}^1([t_0,T];\bar{V})} \big\{ \int_{t_0}^T L(\bar{\varphi}_t, \bar{\sigma})dt + g(\bar{\varphi}_T) \,\big|\, \partial_t\bar{\varphi} = \bar{\sigma},\ \bar{\varphi}_{t_0} = \phi\big\}, \tag{25}$$

and its associated Hamiltonian system is (22), since the Legendre transform of L gives

$$\bar{H}_\delta(\bar{\lambda}, \bar{\varphi}) = -\sup_{\bar{\sigma}\in\bar{V}} \big\{ -\langle\bar{\lambda}, \bar{\sigma}\rangle - L(\bar{\varphi}, \bar{\sigma})\big\} = \inf_{\bar{\sigma}\in\bar{V}} \big\{\langle\bar{\lambda}, \bar{\sigma}\rangle + L(\bar{\varphi}, \bar{\sigma})\big\}. \tag{26}$$

Note that the equivalent problem with time reversed, $s = T - t$, corresponds to

$$\inf\big\{ \int_{t_0}^T \tilde{L}(\bar{\varphi}_s, \partial_s\bar{\varphi}_s)ds + g(\bar{\varphi}_0) \,\big|\, \bar{\varphi}_T = \phi\big\}$$

where

$$\tilde{L}(\bar{\varphi}, \bar{l}) := \sup_{\bar{\lambda}\in\bar{V}} \big\{\langle\bar{l}, \bar{\lambda}\rangle + \bar{H}_\delta(\bar{\lambda}, \bar{\varphi})\big\} = L(\bar{\varphi}, -\bar{l})$$

is the usual Legendre transformation of the convex function $-\bar{H}_\delta(\cdot, \bar{\varphi})$.

The problems described in sections 3.1 and 3.3 have concave Hamiltonians which are not coercive, which implies that their corresponding running costs, L, takes the value $+\infty$ for some arguments. Such running costs are treated in [14], where it is shown that the problem (24), with the aforementioned running cost, has a minimizer $\bar{\phi} : [t_0, T] \to \bar{V}$. Furthermore, such a minimizer solves the Hamiltonian system (22) together with a function $\bar{\lambda}$, granting existence of a solution to this Hamiltonian system.

The value function $\bar{u}_\delta$ is a viscosity solution to the Hamilton-Jacobi equation

$$\partial_t \bar{u}_\delta(\phi, t) + \bar{H}_\delta(\partial \bar{u}_\delta(\phi, t), \phi) = 0, \quad \bar{u}_\delta(\cdot, T) = \bar{g}(\cdot).$$

This result can easily be obtained from Theorem 6.4.5 in [10]. This theorem treats only running costs, L, with finite values, but the proof is basically unchanged by allowing the running costs of interest here. The error estimate of Theorem 2.1 is applicable both to estimate $u - \bar{u}_\delta$, with approximation of both V and H, and to $\bar{u}_0 - \bar{u}_\delta$, with approximation only of H. We may alternativly estimate the difference between $\bar{u}$ and $\bar{u}_\delta$ by using known results of the Hamilton-Jacobi equations

$$\partial_t \bar{u}_\delta(\phi, t) + \bar{H}_\delta(\partial \bar{u}_\delta(\phi, t), \phi) = 0,$$
$$\partial_t \bar{u}_0(\phi, t) + \bar{H}_0(\partial \bar{u}_0(\phi, t), \phi) = 0,$$

and the fact that $\bar{u}_0(\cdot, T) = \bar{u}_\delta(\cdot, T) = \bar{g}(\cdot)$; the comparison principle for viscosity solutions gives that

$$||\bar{u} - \bar{u}_\delta||_{\mathcal{C}(\bar{V} \times [0,T])} \leq T ||\bar{H}_0 - \bar{H}_\delta||_{\mathcal{C}(\bar{V} \times \bar{V})},$$

see [32].

The value of $\bar{u}_\delta$ for a case with constant solutions $\bar{\phi}^*$ and $\bar{\lambda}^*$ to (22) is approximately $T \cdot L(\bar{\phi}^*, 0)$ when T is large (so that we can neglect $\bar{g}(\bar{\phi}_T)$). The definition of L gives that

$$L(\bar{\phi}^*, 0) = \bar{H}_\delta(\hat{\lambda}, \bar{\phi}^*), \tag{27}$$

where $\hat{\lambda}$ is the maximizer of $\bar{H}_\delta(\cdot, \bar{\phi}^*)$. As the Hamiltonian system for constant solutions is

$$\partial_1 \bar{H}_\delta = \partial_2 \bar{H}_\delta = 0, \tag{28}$$

and $\bar{H}_\delta$ is concave in the λ argument we have that $\hat{\lambda} = \bar{\lambda}^*$. Hence the candidate for a value approximating (8) is $\bar{H}_\delta(\bar{\lambda}^*, \bar{\phi}^*)$, where $\bar{\phi}^*$ and $\bar{\lambda}^*$ are solutions to (28).

2.4. **Smoothed Hamiltonian as Tikhonov regularization.** Tikhonov regularization in optimal control consists of penalization functions containing the control variable, and sometimes derivatives of it. The Legendre transform makes it possible to relate the regularized Hamiltonian with such penalization functions. At every point $(\bar{\lambda}, \bar{\varphi})$ where the derivative $\partial_1 \bar{H}$ exists, there is an element $\bar{\sigma} \in \bar{\mathcal{A}}$ such that $\partial_1 \bar{H}(\bar{\lambda}, \bar{\varphi}) = \bar{f}(\bar{\varphi}, \bar{\sigma})$, see [8], [21]. We now make the following assumption:

$$\partial_1 \bar{H}_\delta(\bar{\lambda}, \bar{\varphi}) \in \operatorname{co} \bar{f}(\bar{\varphi}, \bar{\mathcal{A}}) \text{ for all } (\bar{\lambda}, \bar{\varphi}) \in \bar{V} \times \bar{V}, \tag{29}$$

where co denotes the convex hull. This assumption holds for all regularizations we will consider in this paper. It also holds for regularizations by convolution

$$\bar{H}_\delta(\bar{\lambda}, \bar{\varphi}) = \int_{\bar{V}} \bar{H}(\bar{\lambda} - \bar{y}, \bar{\varphi}) \eta(\bar{y}) d\bar{y},$$

where η is a mollifier with support in the closed ball with radius δ centered at the origin.

By the definition of L in (23), it follows that $L(\bar{\varphi}, \bar{l}) = +\infty$, if

$$\bar{l} \notin \overline{\{\partial_1 \bar{H}_\delta(\bar{\lambda}, \bar{\varphi}) \mid \bar{\lambda} \in \bar{V}\}}, \tag{30}$$

where the big bar denotes set closure. Since the sets $\bar{f}(\bar{\varphi}, \bar{\mathcal{A}})$ are supposed to be closed, the assumption in (29) implies that

$$\overline{\left\{\partial_1 \bar{H}_\delta(\bar{\lambda}, \bar{\varphi}) \mid \bar{\lambda} \in \bar{V}\right\}} \subset \operatorname{co} \bar{f}(\bar{\varphi}, \bar{\mathcal{A}}).$$

The infimum in (26) may therefore be reduced to an infimum over the set $\operatorname{co} \bar{f}(\bar{\varphi}, \bar{\mathcal{A}})$. Furthermore, the function $L(\bar{\varphi}, \cdot)$ is lower semicontinuous, see [31], and therefore the infimum is attained:

$$\bar{H}_\delta(\bar{\lambda}, \bar{\varphi}) = \min\left\{\langle \bar{\lambda}, \bar{l}\rangle + L(\bar{\varphi}, \bar{l}) \mid \bar{l} \in \operatorname{co}\ \bar{f}(\bar{\varphi}, \bar{\mathcal{A}})\right\}. \tag{31}$$

In order to see the relation with ordinary Tikhonov regularization, let us now assume that the sets $\bar{f}(\bar{\varphi}, \bar{\mathcal{A}})$ are convex. Then the regularized Hamiltonian satisfies

$$\bar{H}_\delta(\bar{\lambda}, \bar{\varphi}) = \min_{\bar{\sigma} \in \bar{\mathcal{A}}} \left\{\langle \bar{\lambda}, \bar{f}(\bar{\varphi}, \bar{\sigma})\rangle + \bar{h}_\delta(\bar{\varphi}, \bar{\sigma})\right\},$$

where

$$\bar{h}_\delta(\bar{\varphi}, \bar{\sigma}) = L\big(\bar{\varphi}, \bar{f}(\bar{\varphi}, \bar{\sigma})\big).$$

Comparing with the expression for the Hamiltonian without regularization, $\bar{H}$, in (5), we see that the difference $\bar{h}_\delta(\bar{\varphi}, \bar{\sigma}) - \bar{h}(\bar{\varphi}, \bar{\sigma})$ is a penalization function of Tikhonov-type for the optimal control problem. Relation (31) is inspired by such a comparison for an example in [11].

3. Three Different Conduction Designs

In the following sections we will study numerical approximation of three optimal control problems related to optimal design, using the Hamiltonian system (11) with a regularized Hamiltonian. By optimal design we mean that we seek to optimize some physical property, such as energy loss, by distributing a discrete valued control, such as an electric conductor, on a fixed domain. The problems considered are: to optimally design an electric conductor, to design an elastic domain and to reconstruct the interior of an object from measured electrical surface currents.

All three problems produce non-smooth controls due to lack of regularity in the Hamiltonian, which for the success of a discrete Pontryagin Principle needs to be regularized. However, in the time-independent setting, even a smooth Hamiltonian may result in an ill-posed minimization problem in the sense that one cannot find a minimizer as the limit of a minimizing sequence. The existence of such a minimizer essentially depends on the weak lower semicontinuity of the Hamiltonian, which in the standard theory of variational calculus is a necessary condition closely connected to quasi-convexity [18].

Ill-posed problems related to optimal design, as the one described in Section 3.2, has been studied extensively in the context of relaxation by quasi-convexification and homogenization in [1, 22, 26, 27, 28, 24].

In Section 3.3, we study the now classical problem of impedance tomography, reviewed in [5]. Since there seems to be no algorithm to directly compute the quasi-convexification of a general problem we will here show that a simple regularization, which in Section 3.1 and 3.2 much resembles a Tichonov regularization, can produce good approximations in the value functions, with the advantage that, by the Pontryagin approach, the Newton method with a sparse Hessian can be used.

3.1. **Concave Maximization.**

A concave problem of electric conduction is to distribute a given amount of conducting material in a domain $\Omega \subset \mathbb{R}^d$ in order to minimize the power production for a surface current q, satisfying $\int_{\partial\Omega} q \, \mathrm{d}s = 0$: let

C be the given amount of material and find an optimal conduction distribution $\sigma : \Omega \to \{\sigma_-, \sigma_+\}$, where $\sigma_\pm > 0$, such that

$$\min_\sigma \left\{ \int_{\partial\Omega} q\varphi \, \mathrm{d}s \;\middle|\; \operatorname{div}(\sigma\nabla\varphi) = 0 \text{ in } \Omega,\ \sigma\frac{\partial\varphi}{\partial n}\Big|_{\partial\Omega} = q,\ \int_\Omega \sigma \, \mathrm{d}x = C \right\}. \tag{32}$$

Here $\partial/\partial n$ denotes the normal derivative and ds is the surface measure on $\partial\Omega$ and $\varphi \in V \equiv \{v \in \mathrm{H}^1(\Omega) : \int_\Omega v \, \mathrm{d}x = 0\}$ is the electric potential. Note that (32) implies that the power loss satisfies

$$\int_{\partial\Omega} q\varphi \, \mathrm{d}s = -\int_\Omega \operatorname{div}(\sigma\nabla\varphi)\varphi \, \mathrm{d}x + \int_{\partial\Omega} \sigma\frac{\partial\varphi}{\partial n}\varphi \, \mathrm{d}s = \int_\Omega \sigma|\nabla\varphi|^2 \, \mathrm{d}x.$$

For simplicity, let $\eta > 0$ be a constant, associated to the given amount of material, and replace (32) with the easier problem to find an optimal conduction distribution such that

$$\min_\sigma \left\{ \int_{\partial\Omega} q\varphi \, \mathrm{d}s + \eta \int_\Omega \sigma \, \mathrm{d}x \;\middle|\; \operatorname{div}(\sigma\nabla\varphi) = 0 \text{ in } \Omega,\ \sigma\frac{\partial\varphi}{\partial n}\Big|_{\partial\Omega} = q \right\}. \tag{33}$$

Observe, that although there exists a corresponding multiplier η for each volume constraint C, the converse may not be true.

The Lagrangian takes the form

$$\int_\Omega \sigma \underbrace{(\eta - \nabla\varphi\cdot\nabla\lambda)}_{v} \, \mathrm{d}x + \int_{\partial\Omega} q(\varphi+\lambda) \, \mathrm{d}s$$

and the Hamiltonian becomes

$$\begin{aligned} H(\lambda,\varphi) &= \min_\sigma \left\{ \int_\Omega \sigma v \, \mathrm{d}x + \int_{\partial\Omega} q(\varphi+\lambda) \, \mathrm{d}s \right\} \\ &= \int_\Omega \underbrace{\min_\sigma\{\sigma v\}}_{\mathfrak{h}(v)} \, \mathrm{d}x + \int_{\partial\Omega} q(\varphi+\lambda) \, \mathrm{d}s \end{aligned} \tag{34}$$

with the concave regularization

$$\bar{H}_\delta(\lambda,\varphi) = \int_\Omega \mathfrak{h}_\delta(\eta - \nabla\varphi\cdot\nabla\lambda) \, \mathrm{d}x + \int_{\partial\Omega} q(\varphi+\lambda) \, \mathrm{d}s, \tag{35}$$

depending on a smooth approximation, $\mathfrak{h}_\delta \in \mathrm{C}^2(\mathbb{R})$, for $\delta > 0$, of the Lipschitz continuous and monotonically increasing function $\mathfrak{h}$ (with discontinuous derivative $\mathfrak{h}'$ at the origin, see Figure 2). Note that $\mathfrak{h}_0 = \mathfrak{h}$. In this case the regularization $\bar{H}_\delta$ is therefore similar to a Tichonov regularization with penalty $\delta\int_\Omega \sigma^2 \mathrm{d}x$, see Figure 1. Note that σ need not to be restricted to discrete values in (33), since

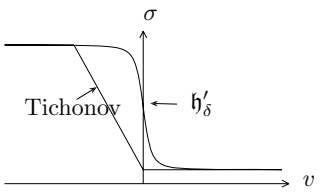

FIGURE 1. A Tichonov type penalty $\delta\int_\Omega \sigma^2 \mathrm{d}x$ compared to the approximation $\mathfrak{h}'_\delta$.

$\sigma : \Omega \to [\sigma_-, \sigma_+]$ will lead to the same Hamiltonian.

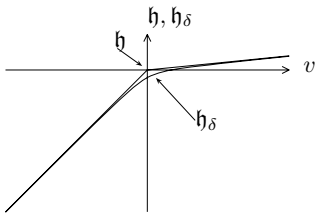

FIGURE 2. The function $\mathfrak{h}$ and its regularization $\mathfrak{h}_\delta$ with respect to v.

By symmetry in the stationary Hamiltonian system (6), the primal and dual variables are equal, $\lambda = \varphi$, and the Hamiltonian system for the electric potential reduces to finite element discretizations of the nonlinear elliptic partial differential equation

$$\operatorname{div}\big(\mathfrak{h}_\delta'(\eta - |\nabla\varphi|^2)\nabla\varphi\big) = 0 \ \text{ in } \Omega, \quad \mathfrak{h}_\delta' \frac{\partial\varphi}{\partial n}\Big|_{\partial\Omega} = q, \tag{36}$$

which can be formulated as the concave maximization problem: $\bar\varphi \in \bar V$ is the unique maximizer of

$$\bar H_\delta(\bar\varphi) = \int_\Omega \mathfrak{h}_\delta(\eta - |\nabla\bar\varphi|^2)\ \mathrm{d}x + 2\int_{\partial\Omega} q\bar\varphi\ \mathrm{d}s, \tag{37}$$

where $\bar H_\delta(\bar\varphi)$ means $\bar H_\delta(\bar\varphi, \bar\varphi)$ and $\bar V \subset V$ denotes a finite element subspace, while $\varphi \in V$ is the unique maximizer of

$$H(\varphi) = \int_\Omega \mathfrak{h}_0(\eta - |\nabla\varphi|^2)\ \mathrm{d}x + 2\int_{\partial\Omega} q\varphi\ \mathrm{d}s, \tag{38}$$

where $H(\varphi)$ means $H(\varphi, \varphi)$.

An advantage with the Pontryagin approach (36) is that the Hessian $D^2\bar H_\delta$ can be determined explicitly and is sparse, so that the Newton method can be used for iterative solution of (36). In fact, the Newton method works well to solve the finite element version of (36) by successively decreasing δ, see Section 4.1.

Since σ can be determined explicitly by the Pontryagin method an alternative approach would be to solve (36) according to the scheme

$$\sigma_{i+1} = \mathfrak{h}_\delta'(\eta - |\nabla\bar\varphi_i|^2) \tag{39}$$

where $\bar\varphi_i$ solves

$$\operatorname{div}\big(\sigma_i\nabla\bar\varphi_i(x)\big) = 0,\ x \in \Omega, \qquad \sigma_i\frac{\partial\bar\varphi_i}{\partial n}\Big|_{\partial\Omega} = q, \tag{40}$$

given an initial guess σ_0. This type of scheme, which essentially is the Jacobi method, is highly unstable with respect to the initial guess since information from the Hessian is lost. In Section 3.2, we will however use this method, with $\delta = 0$, as a post-processing method to eliminate areas of intermediate density generated by the Newton method. These iterations are allowed as long as the value of the Hamiltonian stays relatively unchanged. As pointed out in [22] convergence to a global maximum of (37) by iterating in $\sigma \equiv \mathfrak{h}_0'$ and φ separately, can not be guaranteed since it can be compared to minimizing $f(x, y) = |x - y| + \frac{1}{2}|x + y|$ by iterating in x and y separately; such iterations would terminate at $x = y$ although f is convex.

3.2. **Non-Concave Maximization.** Consider the conduction problem (33) where the objective now is changed to maximize the power production

$$\max_{\sigma}\Big\{\int_{\partial\Omega} q\varphi \,\mathrm{d}s+\eta\int_{\Omega}\sigma\,\mathrm{d}x\;\Big|\;\mathrm{div}(\sigma\nabla\varphi)=0 \text{ in } \Omega,\ \sigma\frac{\partial\varphi}{\partial n}\Big|_{\partial\Omega}=q\Big\}.$$

A problem with the same qualitative property of nonconcave maximization is to maximize the torsional rigidity of the cross section Ω of an infinitely long elastic bar

$$\max_{\sigma}\Big\{\int_{\Omega}\varphi\,\mathrm{d}x+\eta\int_{\Omega}\sigma\,\mathrm{d}x\;\Big|\;-\mathrm{div}(\sigma\nabla\varphi)=1 \text{ in } \Omega,\ \varphi\big|_{\partial\Omega}=0\Big\}, \tag{41}$$

with shear moduli σ^{-1}, see [1, 22, 24].

The maximization problem (41) has the Lagrangian

$$\int_{\Omega}(\lambda+\varphi)\,\mathrm{d}x+\int_{\Omega}\sigma\underbrace{(\eta-\nabla\varphi\cdot\nabla\lambda)}_{v}\,\mathrm{d}x$$

and the Hamiltonian

$$H(\lambda,\varphi)=\int_{\Omega}(\lambda+\varphi)\,\mathrm{d}x+\int_{\Omega}\underbrace{\max_{\sigma}\{\sigma v\}}_{\mathfrak{h}(v)}\,\mathrm{d}x$$

which, as in Section 3.1, is regularized by $\bar{H}_\delta$ with the C^2-approximation $\mathfrak{h}_\delta$ of the Lipschitz continuous function $\mathfrak{h}$. Similarly to (37) we have $\varphi=\lambda$ by symmetry and from the Hamiltonian system we arrive at finite element discretizations of the nonlinear elliptic partial differential equation

$$-\mathrm{div}\big(\mathfrak{h}'_\delta(\eta-|\nabla\varphi|^2)\nabla\varphi\big)=1\ \text{ in }\Omega,\quad \varphi\big|_{\partial\Omega}=0, \tag{42}$$

which is the Euler-Lagrange equation of the problem to find an extremal point $\varphi\in\mathrm{H}^1_0(\Omega)$ of

$$\bar{H}_\delta(\varphi)=\int_{\Omega}2\varphi\,\mathrm{d}x+\int_{\Omega}\mathfrak{h}_\delta(\eta-|\nabla\varphi|^2)\,\mathrm{d}x. \tag{43}$$

In contrast to (37), the existence of an extremal point can not be guaranteed for (43) since it lacks weak lower or upper semicontinuity as δ becomes small.

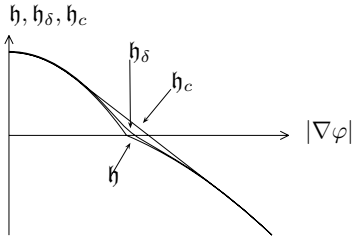

FIGURE 3. The function $\mathfrak{h}$, its regularization $\mathfrak{h}_\delta$ and its concavification $\mathfrak{h}_c$ with respect to $|\nabla\varphi|$, for the non-concave case.

Note that existence of minimizers to general functionals

$$F(\varphi)=\int_{\Omega}f(x,\varphi(x),\nabla\varphi(x))\,\mathrm{d}x. \tag{44}$$

where $\Omega\subset\mathbb{R}^d$ is a bounded open set, $\varphi:\Omega\to\mathbb{R}^n$, can be guaranteed if F fulfills appropriate growth conditions (coercivity) and is weakly lower semi-continuous on

$\mathrm{H}^1_0(\Omega)$. Weak lower semi-continuity is generally hard to verify, but for the scalar case $n = 1$, or $d = 1$, F is weakly lower semicontinuous if and only if $f(x, \varphi, \cdot)$ is convex [18]. For the vector case convexity is a sufficient but far from necessary condition and can be replaced by quasi-convexity which is both a necessary and sufficient condition, but almost as hard to verify as weak lower semi-continuity.

To achieve, in this case, a weakly upper semicontinuous functional one can replace the function $\mathfrak{h}_\delta$, for $\delta = 0$, in (43) with its concavification

$$\mathfrak{h}_c = \begin{cases} \sigma_+(\eta - |\nabla\varphi|^2), & |\nabla\varphi|^2 < \eta\frac{\sigma_-}{\sigma_+} \\ \eta(\sigma_+ + \sigma_-) - 2\sqrt{\eta\sigma_+\sigma_-}|\nabla\varphi|, & \eta\frac{\sigma_-}{\sigma_+} \le |\nabla\varphi|^2 \le \eta\frac{\sigma_+}{\sigma_-} \\ \sigma_-(\eta - |\nabla\varphi|^2), & |\nabla\varphi|^2 > \eta\frac{\sigma_+}{\sigma_-}, \end{cases} \tag{45}$$

as in [22, 24], see Figure 3. This gives a concave functional in (43) which not only has a maximizer but achieves the same supremum as the Hamiltonian H_0, and has maximizers which are exactly the weak limits of maximizing sequences for H_0. If $d > 1$ and $n > 1$, maximizers with equivalent properties are given by quasi-concavification, see [18].

Numerical experiments using a finite element discretization of (42) shows that, although existence of solutions cannot be guaranteed for small δ, the Pontryagin approach generates approximations close to the true concavified solutions in the sense that the error in the value functions is small, see Section 4.2. Of course, the sensitivity of the controls with respect to the value function may still be large.

An alternative to the above concavification (45) is to simply replace the original maximization problem in (41) by

$$\max_\sigma \left\{ \int_\Omega \varphi \, \mathrm{d}x - \gamma \int_\Omega \frac{1}{\sigma} \, \mathrm{d}x \;\middle|\; -\operatorname{div}(\sigma\nabla\varphi) = 1 \text{ in } \Omega, \; \varphi\big|_{\partial\Omega} = 0 \right\}, \tag{46}$$

with a given multiplier $\gamma \ge 0$ and $\sigma : \Omega \to \{\sigma_-, \sigma_+\}$. This formulation only differs in the choice of the given constant γ, associated to the amount of material.

From the new Hamiltonian

$$H(\varphi) = \int_\Omega 2\varphi \, \mathrm{d}x + \int_\Omega \underbrace{\max_\sigma \left\{ -\frac{\gamma}{\sigma} - \sigma|\nabla\varphi|^2 \right\}}_{\mathfrak{h}} \mathrm{d}x. \tag{47}$$

we then see that, allowing intermediate controls $\sigma : \Omega \to [\sigma_-, \sigma_+]$, the explicit maximization in σ gives the concave function

$$\mathfrak{h} = \begin{cases} -\frac{\gamma}{\sigma_+} - \sigma_+|\nabla\varphi|^2, & |\nabla\varphi| < \frac{\sqrt{\gamma}}{\sigma_+} \\ -2\sqrt{\gamma}|\nabla\varphi|, & \frac{\sqrt{\gamma}}{\sigma_+} < |\nabla\varphi| < \frac{\sqrt{\gamma}}{\sigma_-} \\ -\frac{\gamma}{\sigma_-} - \sigma_-|\nabla\varphi|^2, & \frac{\sqrt{\gamma}}{\sigma_+} < |\nabla\varphi|. \end{cases}$$

and we thus have the concave maximization problem: to find the unique maximizer $\varphi \in \mathrm{H}^1_0(\Omega)$ to (47). In fact, the formulation (46) is related to relaxation by the homogenization method [1]. Instead of just expanding the set of admissible controls for the original problem (41) to $\sigma : \Omega \to [\sigma_-, \sigma_+]$, we look at the problem

$$\max_{\theta,\phi} \left\{ \int_\Omega \varphi \, \mathrm{d}x - \eta \int_\Omega \theta \, \mathrm{d}x \;\middle|\; -\operatorname{div}\big(\sigma^*(\theta,\phi)\nabla\varphi\big) = 1 \text{ in } \Omega, \; \varphi\big|_{\partial\Omega} = 0 \right\}, \tag{48}$$

with $\theta : \Omega \to [0, 1]$, $\phi : \Omega \to [0, \pi]$ and the rank-1 laminate tensor

$$\sigma^* = \begin{pmatrix} \cos\phi & \sin\phi \\ -\sin\phi & \cos\phi \end{pmatrix} \begin{pmatrix} \lambda^+_\theta & 0 \\ 0 & \lambda^-_\theta \end{pmatrix} \begin{pmatrix} \cos\phi & -\sin\phi \\ \sin\phi & \cos\phi \end{pmatrix},$$

with

$$\lambda^-_\theta = \left(\frac{\theta}{\sigma_-} + \frac{1-\theta}{\sigma_+} \right)^{-1}, \quad \lambda^+_\theta = \theta\sigma_- + (1-\theta)\sigma_+.$$

The tensor σ^* is obtained from rotation and mixing of the two tensor valued controls $\sigma_- I$ and $\sigma_+ I$ in proportions θ and $1-\theta$ and direction ϕ, see Figure 4. We have thus enlarged the set of admissible controls by introducing two new parameters θ, ϕ describing a laminated material, where the effective conductivities in the principal directions of the material is λ_θ^+ and λ_θ^-. It is easy to see that $(\lambda_\theta^+)^{-1}$ and $(\lambda_\theta^-)^{-1}$ corresponds to the total resistances for resistors connected in parallel and in series, respectively.

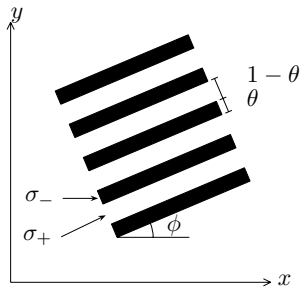

FIGURE 4. Laminate

Using symmetry, $\varphi = \lambda$, the Hamiltonian derived from (48) is

$$H(\varphi) = \int_\Omega 2\varphi \, \mathrm{d}x + \int_\Omega \max_{\theta,\phi} \Big\{ -\eta\theta - \big(\sigma^*(\theta,\phi)\nabla\varphi\big)\cdot\nabla\varphi \Big\} \, \mathrm{d}x. \tag{49}$$

Rewriting the maximization in (49) as

$$\max_{\theta,\phi} \Big\{ -\eta\theta - \big(\mathrm{diag}(\lambda_\theta^+, \lambda_\theta^-) q_\phi\big)\cdot q_\phi \Big\} \tag{50}$$

where q_ϕ is the rotation of $\nabla\varphi$, it is evident that since $\lambda_\theta^- \le \lambda_\theta^+$, aligning q_ϕ in the λ_θ^--direction or equivalently aligning the material perpendicular to $\nabla\varphi$, maximizes (50) with respect to ϕ. The maximization over ϕ thus gives

$$H(\varphi) = \int_\Omega 2\varphi \, \mathrm{d}x + \int_\Omega \max_{\sigma} \Big\{ -\frac{\eta\sigma_+\sigma_-}{\sigma_+ - \sigma_-}\Big(\frac{1}{\sigma} - \frac{1}{\sigma_+}\Big) - \sigma|\nabla\varphi|^2 \Big\} \, \mathrm{d}x, \tag{51}$$

with the change of variables $\sigma = \lambda_\theta^-$. Defining $\gamma = \eta\sigma_+\sigma_-(\sigma_+ - \sigma_-)^{-1}$, (47) and (51) have the same minimizer φ.

3.3. **Interior Reconstruction.** In the previous sections we discussed problems with symmetry, *i.e.* $\varphi = \pm\lambda$, for which convexification is a straightforward and simple approach. Although symmetry is present in many optimization problems connected to minimization of energy, there are other important problems, such as inverse problems related to reconstruction from measurements, where both φ and λ need to be determined. Even the simplest reconstruction problems are known to be highly ill-posed [19].

We will here focus on the problem to reconstruct the interior of an object from measured electrical surface currents, *i.e.* electric impedance tomography [5]: Let $\sigma^* : \Omega \to \{\sigma_-, \sigma_+\}$ denote a real valued unknown conductivity distribution, with $\sigma_\pm > 0$, in a given domain $\Omega \subset \mathbb{R}^d$. Using given surface currents q_i, $i = 1, \dots, N$ on $\partial\Omega$, satisfying $\int_{\partial\Omega} q_i \, \mathrm{d}s = 0$, and the resulting measured surface potentials φ_i^* on

$\partial\Omega$, the goal in this inverse problem is to find the optimal conductivity distribution $\sigma : \Omega \to \{\sigma_-, \sigma_+\}$ such that

$$\min_{\sigma} \Big\{ \sum_{i=1}^{N} \int_{\partial\Omega} (\varphi_i - \varphi_i^*)^2 \, \mathrm{d}s \;\Big|\; \mathrm{div}(\sigma \nabla \varphi_i) = 0 \text{ in } \Omega, \; \sigma \frac{\partial \varphi_i}{\partial n}\Big|_{\partial\Omega} = q_i \Big\}, \tag{52}$$

with $\varphi_i \in V \equiv \{v \in \mathrm{H}^1(\Omega) : \int_\Omega v \, \mathrm{d}x = 0\}$. Note, that we have here chosen the simpler case with measurements on the whole boundary; in reality often only a discrete number of contacts are allowed.

The Lagrangian becomes

$$\sum_{i=1}^{N} \int_{\partial\Omega} (\varphi_i - \varphi_i^*)^2 + \lambda_i q_i \, \mathrm{d}s + \int_\Omega \sigma \underbrace{\sum_{i=1}^{N} -\nabla\varphi_i \cdot \nabla\lambda_i}_{v} \, \mathrm{d}x$$

and the Hamiltonian

$$H(\lambda_1, \ldots, \lambda_N, \varphi_1, \ldots, \varphi_N) = \sum_{i=1}^{N} \int_{\partial\Omega} (\varphi_i - \varphi_i^*)^2 + \lambda_i q_i \, \mathrm{d}s + \int_\Omega \underbrace{\min_{\sigma}\{\sigma v\}}_{\mathfrak{h}(v)} \, \mathrm{d}x.$$

As in previous sections the Hamiltonian needs to be regularized such that

$$\bar{H}_\delta(\lambda_1, \ldots, \lambda_N, \varphi_1, \ldots, \varphi_N) = \sum_{i=1}^{N} \int_{\partial\Omega} (\varphi_i - \varphi_i^*)^2 + \lambda_i q_i \, \mathrm{d}s + \int_\Omega \mathfrak{h}_\delta(v) \, \mathrm{d}x. \tag{53}$$

which generates the coupled non-linear elliptic partial differential equations

$$\begin{aligned} &\mathrm{div}\Big(\mathfrak{h}'_\delta\Big(\sum_{k=1}^{N} -\nabla\varphi_k \cdot \nabla\lambda_k\Big)\nabla\varphi_i\Big) = 0, \text{ in } \Omega, \qquad \mathfrak{h}'_\delta \frac{\partial\varphi_i}{\partial n}\Big|_{\partial\Omega} = q_i \\ &\mathrm{div}\Big(\mathfrak{h}'_\delta\Big(\sum_{k=1}^{N} -\nabla\varphi_k \cdot \nabla\lambda_k\Big)\nabla\lambda_i\Big) = 0, \text{ in } \Omega, \qquad \mathfrak{h}'_\delta \frac{\partial\lambda_i}{\partial n}\Big|_{\partial\Omega} = 2(\varphi_i - \varphi_i^*) \end{aligned} \tag{54}$$

for $i = 1, \ldots, N$. Even though the lack of symmetry prohibits any simplification, this system is only locally coupled, and finite element discretizations can be solved by the Newton method with a sparse Hessian, see Section 4.3.

It is clear that the minimization problem (52) attains its minimum for $\sigma = \sigma^*$ and $\varphi_i = \varphi_i^*$, but it has not necessarily a unique solution. To determine uniqueness of solutions would require knowledge of the Neumann-Dirichlet map

$$\Lambda_\sigma : \sigma \frac{\partial\varphi_i}{\partial n}\Big|_{\partial\Omega} \to \varphi\big|_{\partial\Omega}$$

associating boundary voltages with currents at the boundary for a fixed σ. Perfect knowledge of the map Λ_σ can in general only be gained by measuring the resulting potentials for all possible input currents. However, if $\sigma \in \{\sigma_-, \sigma_+\}$ inside or outside a possibly multiple-connected domain $D \subset \Omega$, it is possible to uniquely determine σ with only partial knowledge of Λ_σ, i.e by using only a finite number of experiments, see [5] for references.

If the reconstruction problem (52) has a unique solution it is still ill-posed in the sense that the slightest disturbance in measurements φ_i or having a true conductivity which allows intermediate values $\sigma^* \in [\sigma_-, \sigma_+]$ would destroy all results on existence and uniqueness of solutions. This is also the case for a discrete number of contacts or for measurements on only parts of the boundary.

Alternative formulations of the impedance tomography problem related to relaxation of functionals as in Section 3.2 is found in [37] and [25]. In the latter the

reconstruction problem is formulated as

$$\min_{\sigma,\varphi_i,J_i}\left\{ I := \sum_{i=1}^{N}\int_\Omega \left|\sigma^{\frac{1}{2}}\nabla\varphi_i + \sigma^{-\frac{1}{2}}J_i\right|^2 \,\mathrm{d}x \;\middle|\; \operatorname{div}(J_i) = 0 \text{ in } \Omega,\ J_i\cdot n|_{\partial\Omega} = q_i,\ \varphi_i|_{\partial\Omega} = \varphi_i^*\right\}.$$

Here the need for regularization to guarantee existence of solutions comes from the lack of lower semicontinuity of the functional I. This formulation also allows an explicit expression for σ since expanding the squares gives

$$\min_{\sigma>0,\varphi,J}\left\{ \sigma\sum_{i=1}^{N}\int_\Omega \left|\nabla\varphi_i\right|^2 \,\mathrm{d}x + \sigma^{-1}\sum_{i=1}^{N}\int_\Omega \left|J_i\right|^2 \,\mathrm{d}x \;\middle|\; \operatorname{div}(J_i) = 0 \text{ in } \Omega,\ J_i\cdot n|_{\partial\Omega} = q_i,\ \varphi_i|_{\partial\Omega} = \varphi_i^*\right\}$$

from the constraint $\operatorname{div}(J) = 0$, which allows pointwise minimization in σ, as in our case, such that

$$\sigma = \left(\sum_{i=1}^{N}|J_i|\right)^{\frac{1}{2}}\left(\sum_{i=1}^{N}|\nabla\varphi_i|\right)^{-\frac{1}{2}}.$$

4. Numerical Examples

4.1. **Electric Conduction.** In all numerical tests for the electric conduction problem (33) we let Ω be the unit square, sometimes with holes cut out, and apply currents on contacts at the boundary. We also let $\bar{V}\subset V\equiv\{v\in \mathrm{H}^1(\Omega) : \int_\Omega v\,\mathrm{d}x = 0\}$ be the linear finite element subspace with Ω partitioned into a quasi uniform mesh with triangles of maximum diameter $h_{max} = 0.01$. The bounds on the conductivity are $\sigma_- = 10^{-3}$ and $\sigma_+ = 1$, and the regularized function $\mathfrak{h}_\delta$ is chosen to be a hyperbola with asymptotes coinciding with $\mathfrak{h}$ and with a closest distance δ from the origin, see Figure 2.

For solving the non-linear partial differential equation (36), or equivalently maximizing (37), we use the Newton method $\bar{\varphi}_{new} = \bar{\varphi}_{old} + \phi$, where the update $\phi = \sum_{i=1}^{N}\phi_i v_i$ comes from solving the system

$$\sum_{j=1}^{N} D^2_{v_i,v_j}\bar{H}_\delta(\bar{\varphi}_{old})\phi_j = -D_{v_i}\bar{H}_\delta(\bar{\varphi}_{old}),\quad i = 1,\dots,N, \tag{55}$$

with the sparse positive definite Hessian

$$D^2_{v_i,v_j}\bar{H}_\delta(\bar{\varphi}) = -2\int_\Omega \mathfrak{h}'_\delta(\eta - |\nabla\bar{\varphi}|^2)\nabla v_i\cdot\nabla v_j\,\mathrm{d}x + 4\int_\Omega \mathfrak{h}''_\delta(\eta - |\nabla\bar{\varphi}|^2)(\nabla\bar{\varphi}\cdot\nabla v_j)(\nabla\bar{\varphi}\cdot\nabla v_i)\,\mathrm{d}x,$$

and

$$D_{v_i}\bar{H}_\delta(\bar{\varphi}) = -2\int_\Omega \mathfrak{h}'_\delta(\eta - |\nabla\bar{\varphi}|^2)\nabla\bar{\varphi}\cdot\nabla v_i\,\mathrm{d}x + 2\int_{\partial\Omega} q v_i\,\mathrm{d}s.$$

Here $v_i\in\bar{V}$ denotes the nodal Lagrange element basis functions of $\bar{V}$, with $v_i(x_j) = \delta_{ij}$ and x_j denoting the corners of the triangles and δ_{ij} the Kronecker delta.

To decrease the regularization δ we use the following scheme, with the idea to decrease δ to $\alpha\delta$, $0<\alpha<1$, if the Newton method converged and increase δ to the average of δ and the last successful regularization if the iterations did not converge:

(1) Choose an initial stepsize $\alpha_{old} = 0.5$ and an initial regularization δ_{old}.

(2) If the Newton method for δ_{old} converged choose

$$\delta_{new} = \alpha_{old}\delta_{old}, \quad \alpha_{new} = \alpha_{old}$$

otherwise let

$$\delta_{new} = \frac{1}{2}\delta_{old}(1 + \frac{1}{\alpha_{old}}), \quad \alpha_{new} = \frac{2\alpha_{old}}{\alpha_{old} + 1}.$$

(3) Set δ_{old}=δ_{new}, α_{old}=α_{new} and go to (2).

Results for different regularizations can be seen in Figure 5. Figure 6 shows solutions for different multipliers η, corresponding to different volume constraints. Solutions for other geometries and boundary conditions are presented in Figure 7. The Newton method works well but requires some additional iteration steps for smaller regularizations or finer grids since the Hessian becomes ill-conditioned. It is possible that other methods using or approximating Hessian information, such as quasi-Newton methods, may be used. However, from our experience we conclude that good aproximation of the Hessian is vital for convergence. Some experiments using the non-linear multigrid method with a modification preventing large course-level corrections close to the jump in $\mathfrak{h}_\delta$ has also showed good results.

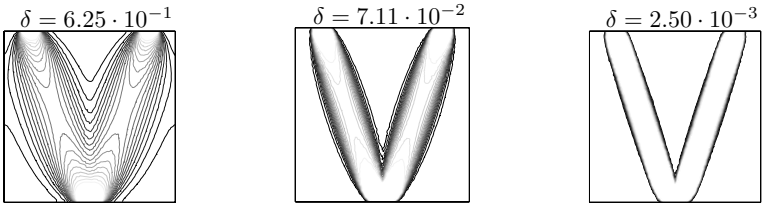

FIGURE 5. Electric conduction: Contour plots of $\mathfrak{h}'_\delta$ for different regularizations and with $\eta = 0.5$. The countours are equally spaced in the range $[\sigma_-, \sigma_+]$, with σ_+ at the contacts. Current enters the top contacts ($q = -1$) and leaves on the bottom contact ($q = 2$). All contacs are of width 0.1. The regularization was initialized to $\delta = 10$ and the pictures show the result after 5, 10 and 30 reductions of δ. For each value of δ no more than 5 Newton steps was necessary to reach a residual error of 10^{-6} in the maximum norm. For two values of δ the Newton method fails to converge, leading to a change in the update parameter α.

To verify the error estimates in Section 2.1 we see that for given solutions $\varphi \in V$ to (38) and $\bar{\varphi} \in \bar{V}$ to (37) the error in the value functions is by (24) - (27)

$$E = \bar{H}_\delta(\bar{\varphi}, \bar{\varphi}) - H(\varphi, \varphi). \tag{56}$$

Section 2.1 and Theorem 2.1 estimate such errors in terms of the L^2 projection error $|P\varphi - \varphi|$ and the difference between the Hamiltonians H and $\bar{H}$ along the same path. Now we apply this using the Hamiltonian $\bar{H}_\delta$ defined in (35). The Legendre transform can be used as in Section 2.3 to obtain from $\bar{H}_\delta$ a flux $\bar{f}$ and a running cost $\bar{h}$ defined on $\bar{V}$. By (5) this defines a Hamiltonian $\bar{H} : V \times \bar{V} \to \mathbb{R}$, which is used in the analysis in Section 2.1. Definition (5) and the fact that $\bar{H}$ and $\bar{H}_\delta$ coincide on $\bar{V} \times \bar{V}$ show that

$$\bar{H}(\lambda, \bar{\varphi}) = \bar{H}(P\lambda, \bar{\varphi}) = \bar{H}_\delta(P\lambda, \bar{\varphi}). \tag{57}$$

We expect $\lambda = \partial u$ and $\bar{\lambda} = \partial \bar{u}$ in (15) and (17). Replacing ∂u by λ and $\partial \bar{u}$ by $\bar{\lambda}$ would give an upper and a lower bound

$$\hat{E}_+ := \bar{H}_\delta(\bar{\lambda}, P\varphi) - H(\bar{\lambda}, \varphi), \qquad \hat{E}_- := (\bar{H}_\delta - H)(\lambda, \bar{\varphi}),$$

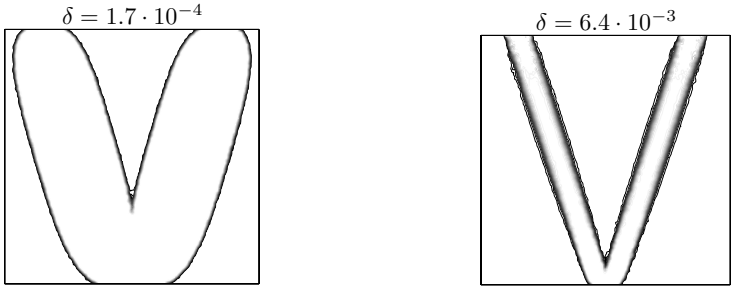

FIGURE 6. Electric conduction: Contour plots of $\mathfrak{h}'_\delta$ for different values of η. Left: Data as in Figure 5 but with $\eta = 0.1$. Right: Data as in Figure 5 but with $\eta = 1.5$. The left example has reached $\delta \approx 10^{-4}$ in 23 reductions of δ starting with $\delta = 10$, while the right example was stopped after 30 reductions of δ.

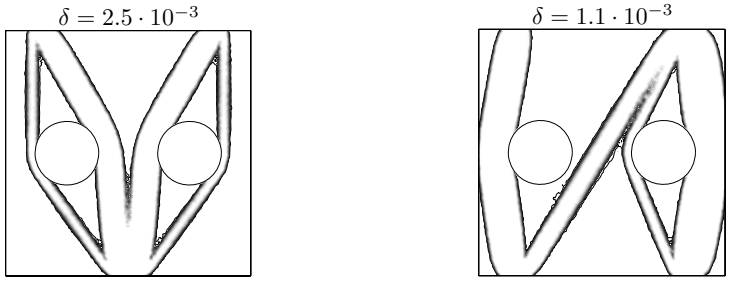

FIGURE 7. Electric conduction: Contour plots of $\mathfrak{h}'_\delta$ for different geometries and boundary currents q. Left: Data as in Figure 5 but with two holes cut out. Right: Data as in Figure 5 but with four contacts of width 0.1 and currents $q = -1$ and $q = -2$ on the top contacts and $q = 1.5$ on the bottom contacts.

of the error. The symmetry $\lambda = \varphi$, $\bar{\lambda} = \bar{\varphi}$ and (57) imply $\hat{E}_+ = \hat{E}_- = \hat{E}$, where

$$\begin{aligned} \hat{E} &:= \bar{H}_\delta(\bar{\varphi}, P\varphi) - H(\bar{\varphi}, \varphi) \\ &= \int_\Omega \mathfrak{h}_\delta(\underbrace{\eta - \nabla\bar{\varphi}\cdot\nabla P\varphi}_{\bar{v}}) - \mathfrak{h}(\underbrace{\eta - \nabla\bar{\varphi}\cdot\nabla\varphi}_{v})\,\mathrm{d}x + \int_{\partial\Omega} q(P\varphi - \varphi)\,\mathrm{d}s, \end{aligned} \tag{58}$$

and from (58) we get the error bound

$$
\begin{aligned}
|\hat{E}| &= \left| \int_\Omega \mathfrak{h}_\delta(\bar{v}) - \mathfrak{h}(v)\ \mathrm{d}x + \int_{\partial\Omega} q(P\varphi - \varphi)\ \mathrm{d}s \right| \\
&= \left| \int_\Omega \mathfrak{h}_\delta(\bar{v}) - \mathfrak{h}_\delta(v) + \mathfrak{h}_\delta(v) - \mathfrak{h}(v)\ \mathrm{d}x + \int_{\partial\Omega} q(P\varphi - \varphi)\ \mathrm{d}s \right| \\
&\leq C_0\delta + \left| \int_\Omega \mathfrak{h}_\delta(\bar{v}) - \mathfrak{h}_\delta(v)\ \mathrm{d}x + \int_{\partial\Omega} q(P\varphi - \varphi)\ \mathrm{d}s \right| \\
&= C_0\delta + \left| \int_\Omega \int_0^1 \mathfrak{h}'_\delta\Big(t\bar{v} + (1-t)v\Big)(\bar{v} - v)\ \mathrm{d}t\ \mathrm{d}x + \int_{\partial\Omega} q(P\varphi - \varphi)\ \mathrm{d}s \right| \\
&\leq C_0\delta + \underbrace{\int_\Omega \sigma_+ \Big|\nabla\bar{\varphi}\cdot\nabla(\varphi - P\varphi)\Big|\ \mathrm{d}x + \left| \int_{\partial\Omega} q(P\varphi - \varphi)\ \mathrm{d}s \right|}_{E_3},
\end{aligned}
\tag{59}
$$

which can be estimated by

$$
|\hat{E}| \leq C_0\delta + \underbrace{C_1 h_{max}\|\bar{\varphi}\|_{W^{1,\infty}(\Omega)}\|\varphi\|_{W^{2,1}(\Omega)} + C_2 h_{max}\|q\|_{\mathrm{L}^\infty(\partial\Omega)}\|\varphi\|_{W^{2,1}(\Omega)}}_{E_4}. \tag{60}
$$

This estimate follows from stability of the L^2 projection onto V, *cf.* [17], combined with a standard interpolation error estimate [6]. The regularized function $\mathfrak{h}_\delta$ in (59) is chosen such that $C_0 \approx 0.05$ independently of δ.

To numerically verify the different estimates (56), (58), (59) and (60), we let $\bar{\varphi} \in \bar{V}$ and $\varphi \in V$ be finite element solutions to (37) and (38) with Hamiltonians $\bar{H}_\delta$ and $H = \bar{H}_{\delta_0}$ where $\delta_0 \approx 0$. Estimate (56) then becomes

$$
\begin{aligned}
E_1 &:= \bar{H}_\delta(\bar{\varphi}, \bar{\varphi}) - H_{\delta_0}(\varphi, \varphi) \\
&= \int_\Omega \mathfrak{h}_\delta(\eta - |\nabla\bar{\varphi}|^2) - \mathfrak{h}_{\delta_0}(\eta - |\nabla\varphi|^2)\ \mathrm{d}x + 2\int_{\partial\Omega} q(\bar{\varphi} - \varphi)\ \mathrm{d}s,
\end{aligned}
\tag{61}
$$

and (58) becomes

$$
\begin{aligned}
E_2 &:= \bar{H}_\delta(\bar{\varphi}, P\varphi) - H_{\delta_0}(\bar{\varphi}, \varphi) \\
&= \int_\Omega \mathfrak{h}_\delta(\eta - \nabla\bar{\varphi}\cdot\nabla P\varphi) - \mathfrak{h}_{\delta_0}(\eta - \nabla\bar{\varphi}\cdot\nabla\varphi)\ \mathrm{d}x + \int_{\partial\Omega} q(P\varphi - \varphi)\ \mathrm{d}s.
\end{aligned}
\tag{62}
$$

Figure 8 shows the approximation error by comparing the different estimates E_1, E_2, E_3 and E_4 when φ is computed on a finite element mesh considerably finer than the one for $\bar{\varphi}$, and $\delta = \delta_0 \approx 0$. We see that E_2 and E_3 are accurate approximations of the true error $E_1 \approx E$, while E_4 overestimates the error although it has the correct rate. Note that the interpolation constants satisfy $C_1 \approx C_2 \approx 1$. In Figure 9 the regularization error is shown by using the same mesh to compute φ and $\bar{\varphi}$ for different regularizations δ and a fixed $\delta_0 \approx 0$. We see that E_2 again is an accurate approximation of E_1 while E_4 overestimates the error although it has the correct rate; it does not vary with δ. Note that E_3 is not presented in Figure 9 since it has the order of machine precision. We conclude that the approximation of the error estimate (58) in Theorem 2.1 is accurate.

4.2. **Elastic Domain.** For the problem of maximizing the torsional rigidity of an elastic bar (41), we let the cross section Ω of the bar be the unit square. The inverse shear moduli and the multiplier is, as in [1], chosen to be $\sigma_- = 1$, $\sigma_+ = 2$ and $\eta = 0.0165.$, respectively. We also let $\bar{V}$ be the linear finite element subspace of $V \equiv \mathrm{H}_0^1(\Omega)$ with maximum triangle diameter $h_{max} = 0.01$ and choose a regularization as in Section 4.1.

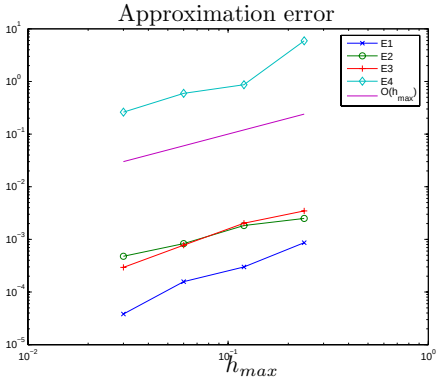

FIGURE 8. Electric conduction: Error estimates for different meshes. Both $\bar{\varphi}$ and φ are solutions to the regularized problem with $\delta \approx 10^{-5}$. The solution φ is computed on a mesh with $h_{max} = 0.015$ and the mesh for $\bar{\varphi}$ is varying.

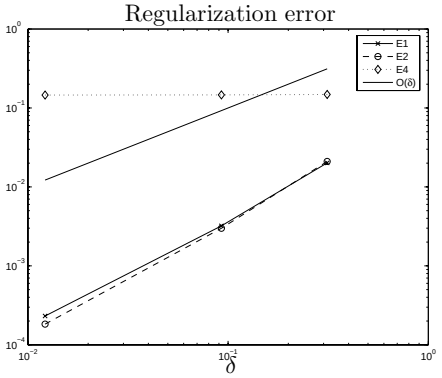

FIGURE 9. Electric conduction: Error estimates for different regularizations. Both $\bar{\varphi}$ and φ are solutions to regularized problems with $h_{max} = 0.015$. The regularization for φ is $\delta_0 \approx 10^{-3}$ and the regularization for $\bar{\varphi}$ is varying. E_3 disappears and E_4 remains constant since no approximation error is present in this case.

The maximization problem (41) has a Hamiltonian (43) which for small regularizations lacks upper semicontinuity, and thus there may not exist any solutions to the corresponding non linear partial differential equation (42). We solve (42) using the Newton method and a simple scheme to reduce the regularization, as in the previous section. As expected, the Newton method works well for sufficiently large regularizations, but does not converge for small regularizations, see Figure 10.

In Section 3.2 we concavify the unregularized Hamiltonian, which not only gurarantees existence of at least one solution, but also gives a maximum that coincides with the supremum of the unregularized Hamiltonian. Figure 10 compares the result from solving the regularized problem (42) with the solution of the concavified problem. The regularized problem was solved by succesively reducing the regularization 30 times, starting with $\delta = 2$.

In Figure 11 we see how the value of the regularized Hamiltonian approaches the value of the concavified Hamiltonian as the regularization decreases. We can also see that the Newton iterations fail when δ becomes too small.

Since the goal is to find an optimal design with a discrete control $\sigma \in \{\sigma_-, \sigma_+\}$ a few additional elementwise iterations with the Discrete Pontryagin method in (39)–(40) is done for postprocessing. These iterations are allowed as long as the value function does not increase substantially. In general, the discrete iterations does not converge and we may need to control the amount of material allowed to change in each iteration; for the non-concave problem this appears however not necessary. The right plot in Figure 10 shows the solutions after a few discrete iterations with initial data from the middle figure.

The Discrete Pontryagin method much resembles the method in [12], which uses topological shape derivatives and starts from a domain with $\sigma = \sigma_+$ and sucessively replaces volume fractions with σ_-. This method is appealing since it is simple and gives interesting designs, but it may not converge to the true optimal design if it is possible to remove too much material, which never can be added again.

Finally, in Figure 12, we show the results from solving the concavified and regularized problem with a different multiplier $\eta = 0.025$.

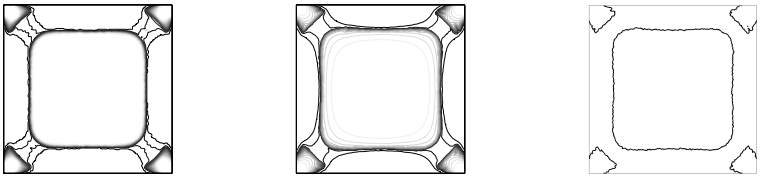

FIGURE 10. Elastic Domain: Left: Contour plot of $\mathfrak{h}'_c$ for the concavified solution with $\eta = 0.0165$. The value of the Hamiltonian is 0.0555. Middle: Contour plot of $\mathfrak{h}'_\delta$ with $\delta = 0.08$ and $\eta = 0.0165$. The value of the Hamiltonian is 0.0570. Right: Five discrete iterations with (39)–(40) using initial data from the middle figure. The value of the Hamiltonian has converged to 0.0554.

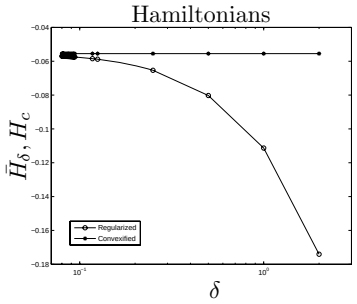

FIGURE 11. Elastic Domain: Plot of the regularized and concavified Hamiltonians for the solutions in Figure 10 with respect to regularization. Only regularizations for which the Newton method has converged are plotted. The regularized Hamiltonian approches the concavified Hamiltonian as $\delta \to 0$, and the relative error for the smallest regularization, $\delta = 0.08$, is 2.7%.

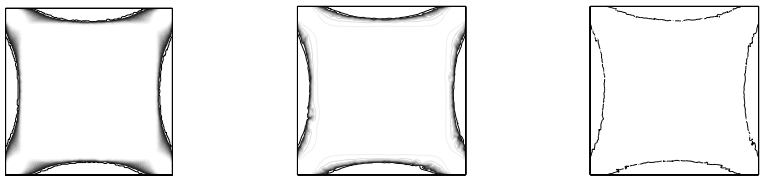

FIGURE 12. Elastic Domain: Left: Contour plot of $\mathfrak{h}'_c$ for the concavified solution with $\eta = 0.025$. The value of the Hamiltonian is 0.0695. Middle: Contour plot of $\mathfrak{h}'_\delta$ with $\delta = 0.1$ and $\eta = 0.025$. The value of the Hamiltonian is 0.0715. Right: Five discrete iterations with (39)–(40) using initial data from the middle figure. The value of the Hamiltonian has converged to 0.0695, with a relative error of 0.9%.

4.3. **Impedance Tomography.** When solving the impedance tomography problem (52) one major issue affecting the reconstruction of the interior conductivity is the choice of input currents $q_1, \ldots, q_N$. Consider applying a surface current q on two different conductivity distributions σ and σ^* and measuring the resulting potentials $\varphi = \Lambda_\sigma q$ and $\varphi^* = \Lambda_{\sigma^*} q$. Due to the nonlinearity of the inverse map $\Lambda_\sigma \to \sigma$, the different conductivities σ and σ^* may produce similar surface potentials φ and φ^* when subjected to a certain input current q, thus causing redundancy in the coupled equations (54). To prevent this we choose, following [13], the input current q to be optimal in the sense that it best distinguishes one conductivity distribution from another, i.e

$$\max_q \Big\{ \|\Lambda_\sigma q - \Lambda_{\sigma^*} q\|_{\mathrm{L}^2(\partial\Omega)} \;\Big|\; \|q\|_{\mathrm{L}^2(\partial\Omega)} = 1, \quad \int_{\partial\Omega} q \, \mathrm{d}s = 0 \Big\}, \tag{63}$$

which from self-adjointness of the Neumann-to-Dirichlet map Λ_σ is maximized by the eigenfunction corresponding to the largest eigenvalue of $\Lambda_\sigma - \Lambda_{\sigma^*}$. For multiple experiments we choose $q_1 \ldots, q_N$ to be the eigenfunctions corresponding to the N largest eigenvalues.

In the numerical experiments we have calculated the input currents using $\sigma = 1.5$ and a true conductivity profile with $\sigma^* = 1$ inside the region marked by a dashed line in Figure 14, and $\sigma^* = 2$ outside. Note, that to calculate an optimal discretized boundary current q iteratively, *e.g.* by the power method, only measurements from the corresponding boundary potentials $\Lambda_\sigma q$ and $\Lambda_{\sigma^*} q$ are needed in each iteration. In Figure 13 the currents corresponding to the eigenfunctions of the four largest eigenvalues are shown. The boundary currents and potentials were calculated using a maximum element diameter of $h_{max} = 0.01$.

The results from solving the coupled non-linear partial differential equations (54) using piecewise linear elements with $h_{max} = 0.03$ can be seen in Figure 14 and 15. Here, the regularization parameter δ must not be too small since different grids are used for measurements and solutions in Figure 14, and 10% white noise is added to the measurements in Figure 15. This means that the discrete solution φ is disturbed componentwise by independent standard normal distributed stochastic variables ξ_i according to $\varphi(x_i)(1 + 0.1\xi_i)$, with nodal points x_i.

How to choose a good value of the regularization parameter, δ, in a real problem may be difficult, at least a separate problem. Here we test how our regularization works by choosing the best possible regularization parameter value, using the

"unknown" solution σ^* to find the parameter value, but nothing else. In the calculations we thus start with an initial regularization $\delta = 1$, reduce δ at most 30 times and stop if $\delta \leq 10^{-4}$ or if there is no decrease in the $\mathrm{L}^2(\Omega)$-norm of $\mathfrak{h}'_\delta - \sigma^*$.

From Figure 14 it is evident that increasing the number of experiments has a significant effect on the reconstruction. The impedance tomography problem seems here to behave as the concave problem in Section 4.1. However in our experience there are cases, such as large differences between σ^*_- and σ^*_+ ,where (54) is harder to solve.

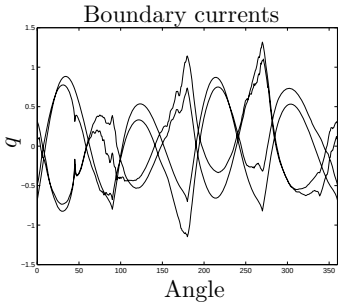

FIGURE 13. Boundary currents used for the impedance tomography problem plotted as a function of the angle variable in polar coordinates starting at the lower left corner of Ω.

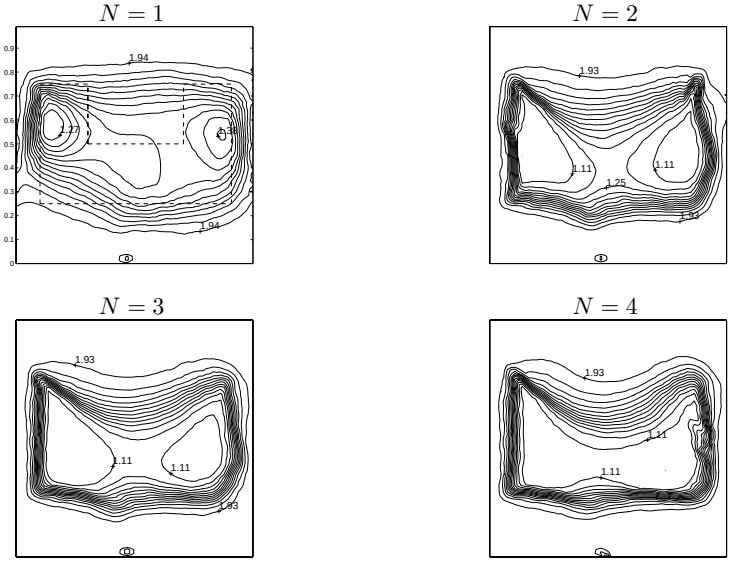

FIGURE 14. Impedance tomography: Plots of $\mathfrak{h}'_\delta$ for different number of experiments with $h_{max} = 0.03$. The measured data was generated from solving the forward problem with $h_{max} = 0.01$ using the conductivity profile marked with a dashed line in the upper left figure. The true conductivity is $\sigma^* = 1$ inside and $\sigma^* = 2$ outside the marked region.

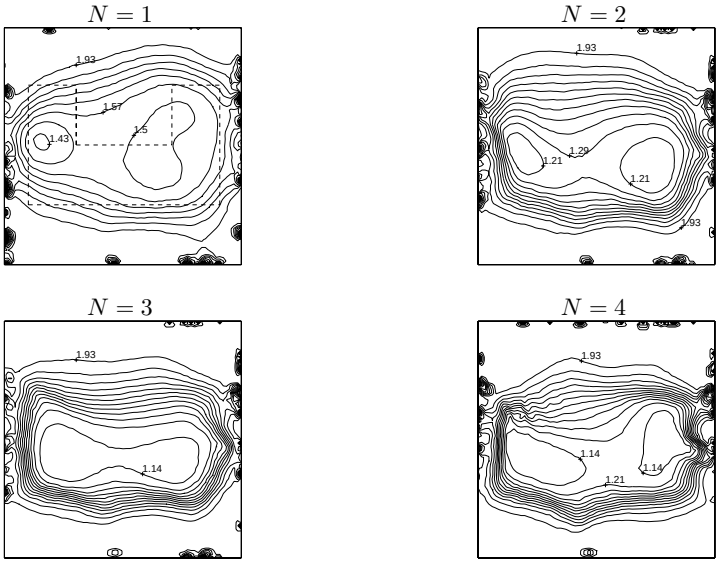

FIGURE 15. Impedance tomography: Plots of $\mathfrak{h}'_\delta$ for different number of experiments. Data as in Figure 14 but with 10% noise added to the measurements.

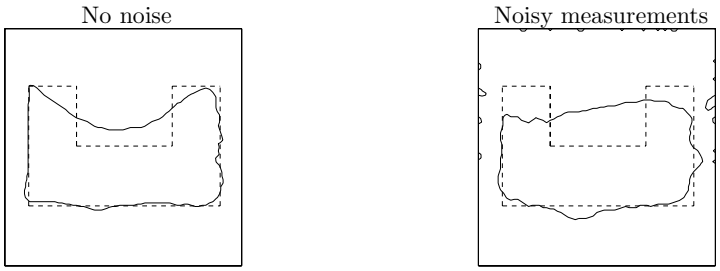

FIGURE 16. Impedance tomography: Plots of $\mathfrak{h}'_0$ after one discrete iteration ($N = 4$). Left: Initial data taken from the lower right plot in Figure 14. Right: Initial data taken from the lower right plot in Figure 15.

References

[1] Grégoire Allaire. *Shape optimization by the homogenization method*, volume 146 of *Applied Mathematical Sciences*. Springer-Verlag, Nw York, 2002.

[2] Martino Bardi and Italo Capuzzo-Dolcetta. *Optimal control and viscosity solutions of Hamilton-Jacobi-Bellman equations*. Systems & Control: Foundations & Applications. Birkhäuser Boston Inc., Boston, MA, 1997. With appendices by Maurizio Falcone and Pierpaolo Soravia.

[3] Guy Barles. *Solutions de viscosité des équations de Hamilton-Jacobi*, volume 17 of *Mathématiques & Applications (Berlin) [Mathematics & Applications]*. Springer-Verlag, Paris, 1994.

[4] M. P. Bendsøe and O. Sigmund. *Topology optimization*. Springer-Verlag, Berlin, 2003. Theory, methods and applications.

[5] Liliana Borcea. Electrical impedance tomography. *Inverse Problems*, 18(6):R99–R136, 2002.

[6] Susanne C. Brenner and L. Ridgway Scott. *The mathematical theory of finite element methods*, volume 15 of *Texts in Applied Mathematics*. Springer-Verlag, New York, 1994.

[7] P. Cannarsa and H. Frankowska. Value function and optimality condition for semilinear control problems. II. Parabolic case. *Appl. Math. Optim.*, 33(1):1–33, 1996.

[8] Piermarco Cannarsa and Halina Frankowska. Some characterizations of optimal trajectories in control theory. *SIAM J. Control Optim.*, 29(6):1322–1347, 1991.

[9] Piermarco Cannarsa and Halina Frankowska. Value function and optimality conditions for semilinear control problems. *Appl. Math. Optim.*, 26(2):139–169, 1992.

[10] Piermarco Cannarsa and Carlo Sinestrari. *Semiconcave functions, Hamilton-Jacobi equations, and optimal control*. Progress in Nonlinear Differential Equations and their Applications, 58. Birkhäuser Boston Inc., Boston, MA, 2004.

[11] Jesper Carlsson. Symplectic reconstruction of data for heat and wave equations. *preprint*, 2008.

[12] Jean Céa, Stéphane Garreau, Philippe Guillaume, and Mohamed Masmoudi. The shape and topological optimizations connection. *Comput. Methods Appl. Mech. Engrg.*, 188(4):713–726, 2000. IV WCCM, Part II (Buenos Aires, 1998).

[13] M. Cheney and D. Isaacson. Distinguishability in impedance imaging. *IEEE Transactions on Biomedical Engineering*, 39(8):852–860, 1992.

[14] Frank H. Clarke. *Optimization and Nonsmooth Analysis*. Canadian Mathematical Society series in mathematics. John Wiley and Sons, Inc., 1983.

[15] M. G. Crandall, L. C. Evans, and P.-L. Lions. Some properties of viscosity solutions of Hamilton-Jacobi equations. *Trans. Amer. Math. Soc.*, 282(2):487–502, 1984.

[16] Michael G. Crandall, Hitoshi Ishii, and Pierre-Louis Lions. User's guide to viscosity solutions of second order partial differential equations. *Bull. Amer. Math. Soc. (N.S.)*, 27(1):1–67, 1992.

[17] M. Crouzeix and V. Thomée. The stability in L_p and W_p^1 of the L_2-projection onto finite element function spaces. *Math. Comp.*, 48(178):521–532, 1987.

[18] Bernard Dacorogna. *Direct methods in the calculus of variations*, volume 78 of *Applied Mathematical Sciences*. Springer-Verlag, Berlin, 1989.

[19] Heinz W. Engl, Martin Hanke, and Andreas Neubauer. *Regularization of inverse problems*, volume 375 of *Mathematics and its Applications*. Kluwer Academic Publishers Group, Dordrecht, 1996.

[20] Lawrence C. Evans. *Partial differential equations*, volume 19 of *Graduate Studies in Mathematics*. American Mathematical Society, Providence, RI, 1998.

[21] Halina Frankowska. Contingent cones to reachable sets of control systems. *SIAM J. Control Optim.*, 27(1):170–198, 1989.

[22] Jonathan Goodman, Robert V. Kohn, and Luis Reyna. Numerical study of a relaxed variational problem from optimal design. *Comput. Methods Appl. Mech. Engrg.*, 57(1):107–127, 1986.

[23] Ernst Hairer, Christian Lubich, and Gerhard Wanner. *Geometric numerical integration*, volume 31 of *Springer Series in Computational Mathematics*. Springer-Verlag, Berlin, 2002. Structure-preserving algorithms for ordinary differential equations.

[24] Bernhard Kawohl, Jana Stará, and Gabriel Wittum. Analysis and numerical studies of a problem of shape design. *Arch. Rational Mech. Anal.*, 114(4):349–363, 1991.

[25] Robert V. Kohn and Alan McKenney. Numerical implementation of a variational method for electrical impedance tomography. *Inverse Problems*, 6(3):389–414, 1990.

[26] Robert V. Kohn and Gilbert Strang. Optimal design and relaxation of variational problems. I. *Comm. Pure Appl. Math.*, 39(1):113–137, 1986.

[27] Robert V. Kohn and Gilbert Strang. Optimal design and relaxation of variational problems. II. *Comm. Pure Appl. Math.*, 39(2):139–182, 1986.
[28] Robert V. Kohn and Gilbert Strang. Optimal design and relaxation of variational problems. III. *Comm. Pure Appl. Math.*, 39(3):353–377, 1986.
[29] F. Natterer. *The mathematics of computerized tomography*, volume 32 of *Classics in Applied Mathematics*. Society for Industrial and Applied Mathematics (SIAM), Philadelphia, PA, 2001. Reprint of the 1986 original.
[30] Olivier Pironneau. *Optimal shape design for elliptic systems*. Springer Series in Computational Physics. Springer-Verlag, New York, 1984.
[31] R. Tyrrell Rockafellar. *Convex analysis*. Princeton Mathematical Series, No. 28. Princeton University Press, Princeton, N.J., 1970.
[32] M. Sandberg and A. Szepessy. Convergence rates of symplectic Pontryagin approximations in optimal control theory. *M2AN*, 40(1), 2006.
[33] Mattias Sandberg. Convergence rates for numerical approximations of an optimally controlled Ginzburg-Landau equation. *preprint*, 2006.
[34] Daniel Tataru. Viscosity solutions for Hamilton-Jacobi equations with unbounded nonlinear term: a simplified approach. *J. Differential Equations*, 111(1):123–146, 1994.
[35] Andrey N. Tikhonov and Vasiliy Y. Arsenin. *Solutions of ill-posed problems*. V. H. Winston & Sons, Washington, D.C.: John Wiley & Sons, New York, 1977. Translated from the Russian, Preface by translation editor Fritz John, Scripta Series in Mathematics.
[36] Curtis R. Vogel. *Computational methods for inverse problems*, volume 23 of *Frontiers in Applied Mathematics*. Society for Industrial and Applied Mathematics (SIAM), Philadelphia, PA, 2002. With a foreword by H. T. Banks.
[37] A. Wexler, B. Fry, and M.R. Neuman. Impedance-computed tomography algorithm and system. *Applied Optics*, 24(23):3985–3992, 1985.

Department of Numerical Analysis, Kungl. Tekniska Högskolan, 100 44 Stockholm, Sweden
E-mail address: jesperc@kth.se

CMA, University of Oslo, P.O. Box 1053 Blindern, NO-0316 Oslo, Norway
E-mail address: mattias.sandberg@cma.uio.no

Department of Mathematics, Kungl. Tekniska Högskolan, 100 44 Stockholm, Sweden
E-mail address: szepessy@kth.se

Paper 2

PONTRYAGIN APPROXIMATIONS FOR OPTIMAL DESIGN OF ELASTIC STRUCTURES

JESPER CARLSSON

ABSTRACT. This article presents a numerical method for approximation of some optimal control problems for partial differential equations. The method uses regularization derived from consistency with the corresponding Hamilton-Jacobi-Bellman equations in infinite dimension. In particular, optimal designs of elastic structures such as distributing a limited amount of material to minimize its compliance, or to detect interior material distributions from surface measurements, are computed. The derived Pontryagin based method presented here is simple to use with standard PDE-software using Newton iterations with a sparse Hessian.

CONTENTS

1. THE OPTIMAL DESIGN PROBLEM

Optimal design can be described as the particular inverse problem of controlling a partial differential equation to meet some design criteria in an optimal way. The control typically consists of changing the computational domain (shape optimization) or distributing a coefficient in the partial differential equation (parameter design). It is well known that these inverse problems often are ill posed, *e.g.* small perturbations of data lead to large changes in the solution, and need to be regularized to obtain good approximations, *cf.* [6, 13]. The goal of this article is to investigate a numerical method, based on a regularization derived from consistency with the corresponding Hamilton-Jacobi-Bellman equation in infinite dimension, for the particular problem of optimally controlling the partial differential equations of linear elasticity. This extends the work in [11], for control of ordinary differential equations, and [3], for control of scalar partial differential equations.

This article focuses on two types of inverse problems in elasticity: to optimally design an elastic structure and to optimally reconstruct an unknown elastic structure from boundary measurements. The first is a typical problem in optimal design where the objective is to place a given amount of elastic material, submitted to

2000 *Mathematics Subject Classification.* Primary: 65N21; Secondary: 49L25.

Key words and phrases. Topology Optimization, Inverse Problems, Hamilton-Jacobi, Regularization.

Support by the Swedish Research Council grants 2002-6285 and 2002-4961, and the European network HYKE, funded by the EC as contract HPRN-CT-2002-00282, is acknowledged.

static equilibrium and prescribed volume and surface forces, in a given domain $\Omega \in \mathbb{R}^d$, in order to maximize its stiffness. An alternative similar problem is to minimize the compliance

$$l(u) \equiv \int_\Omega f_b \cdot u \, \mathrm{d}x + \int_{\Gamma_N} f_s \cdot u \, \mathrm{d}s, \tag{1}$$

where $u : \Omega \to \mathbb{R}^d$ denotes the displacements at static equilibrium when applying given volume forces $f_b : \Omega \to \mathbb{R}^d$ and surface forces $f_s : \Gamma_N \to \mathbb{R}^d$, $\Gamma_N \subset \partial\Omega$. For convenience it is here assumed that a part of the boundary is fixed, *i.e.* $u_{\Gamma_D} = 0$ where $\Gamma_D = \partial\Omega \setminus \Gamma_N \neq \emptyset$.

For a linearly elastic material, the work done by a virtual displacement v at static equilibrium, can described by the bilinear energy functional

$$a_\rho(u, v) \equiv \int_\Omega \rho\varepsilon_{ij}(u) E_{ijkl} \varepsilon_{kl}(v) \, \mathrm{d}x, \quad i, j, k, l = 1, \ldots, d, \tag{2}$$

with a relative material density ρ, linearized strains $\varepsilon_{ij}(u) = \frac{1}{2}(\frac{\partial u_i}{\partial x_j} + \frac{\partial u_j}{\partial x_i})$ and an elasticity tensor E_{ijkl}. We here use the Einstein summation convention for summation over indices occurring more than once in an expression. The elasticity tensor relates linearized strains to linearized stresses by Hooke's law $\sigma_{ij} = E_{ijkl}\varepsilon_{kl}$, which for an isotropic material can be written as

$$\sigma_{ij} = \lambda\delta_{ij}\varepsilon_{kk} + 2\mu\varepsilon_{ij} \tag{3}$$

where λ and μ are the Lamé coefficients, and δ_{ij} denote the Kronecker delta. From the principle of virtual work, the displacement $u \in V = \{v \in H^1(\Omega)^d | v_{\Gamma_D} = 0\}$ at equilibrium, must then satisfy the variational equation

$$a_\rho(u, v) = l(v), \quad \forall v \in V. \tag{4}$$

To indicate void or material an ideal relative material density would be to let $\rho : \Omega \to \{0, 1\}$, but in order for (4) to be well defined we restrict the density to $\rho : \Omega \to \{\rho_-, 1\}$ with some small $\rho_- > 0$.

In summary, the problem to optimally design a structure with minimal compliance, for some fixed volume C, can be formulated as the minimization problem

$$\inf_{\rho:\Omega\to\{\rho_-,1\}} \left\{ l(u) \;\middle|\; a_\rho(u, v) = l(v), \ \forall v \in V, \ \int_\Omega \rho \, \mathrm{d}x = C \right\}. \tag{5}$$

Since the volume constraint in (5) is difficult to handle, we here use an alternative formulation, were the volume constraint is relaxed by introducing a corresponding Lagrange multiplier $\eta \in \mathbb{R}$. This gives the simpler problem

$$\inf_{\rho:\Omega\to\{\rho_-,1\}} \left\{ l(u) + \eta \int_\Omega \rho \, \mathrm{d}x \;\middle|\; a_\rho(u, v) = l(v), \ \forall v \in V \right\}. \tag{6}$$

In a real application, η of course needs to be determined to meet the desired volume C, but as a preliminary step we consider (6) with some a priori value of η. In practice, the multiplier could be determined by solving (6) in an inner loop and iteratively changing η in an outer loop, but to come up with an effective procedure for this is a difficult task not dealt with here. Observe that (5) and (6) are not truly equivalent, since even though every choice of volume in (5) corresponds to a unique multiplier η, the converse is not necessarily true.

It is well known that (5) and (6) are ill-posed minimization problems in the sense that existence of a minimizer cannot be guaranteed [1]. In fact, a minimizing sequence $\{\rho_n\}$ would oscillate more wildly as $n \to \infty$ and the limit would not even belong to the discrete set $\{\rho_-, 1\}$ anymore. The general cure of ill-posedness of this optimal design problem is to introduce a proper relaxation of the set of admissible designs, thus replacing (6) with a well-posed problem. This can be done by adding

a penalty on the variation of the control ρ, so called Tikhonov regularization, or in this particular case by allowing intermediate densities $\rho : \Omega \to [\rho_-, 1]$, the so called plate thickness problem [2]. Another approach is to minimize (6) over the class $\mathcal{E}_\mathcal{C}$ of elasticity tensors for certain composites of materials, *i.e.*

$$\min_{\rho\in[\rho_-,1],E\in\mathcal{E}_\mathcal{C}} \left\{ l(u) + \eta \int_\Omega \rho \, \mathrm{d}x \;\middle|\; a_{\rho,E}(u,v) = l(v),\ \forall v \in V \right\}, \tag{7}$$

where $a_{\rho,E}(u,v) \equiv a_\rho(u,v)$ to indicate the dependence of E. Here, the tensor E now describes the micro-structure of the material, and for the right choice of $\mathcal{E}_\mathcal{C}$, *e.g.* sequential laminated composites, the minimization problem (7) is well posed, and the solution corresponds to a homogenized optimal design, *cf.* [1]. Homogenization in optimal design is closely connected to the concept of quasi-convexity, which in the standard theory of variational calculus is a necessary condition for the existence of a minimizer [5]. In fact, homogenization or quasi-convexification gives truly optimal designs in the sense that the minimum of (7) coincides with the infimum of (6). Ill-posed problems related to optimal design has been studied extensively in the context of relaxation by quasi-convexification and homogenization in for example [1, 7, 8] and [9].

In Section 2, we derive an alternative regularization which can be compared to a Tikhonov type penalty. The regularization is based on the Hamilton-Jacobi-Bellman equation corresponding to the optimal control problem (6) and the existence of a minimizer essentially depends on the quasi-convexity of the Hamiltonian. Numerical examples for the particular problem (6) are studied in Section 4.

Another inverse problem studied in Section 4 is the reconstruction of an unknown density from boundary measurements: apply given forces $f_s : \Gamma_N \to \mathbb{R}^d$ and reconstruct the interior density $\rho : \Omega \to \{\rho_-, 1\}$ from the resulting boundary displacements u_{meas} on Γ_N by minimizing

$$\inf_{\rho:\Omega\to\{\rho_-,1\}} \left\{ \int_{\Gamma_N} |u - u_{meas}|^2 \, \mathrm{d}s \;\middle|\; a_\rho(u,v) = l(v),\ \forall v \in V \right\}. \tag{8}$$

The problem to determine ρ is in general ill-posed due to non-continuous dependence on measured data. For this problem Tikhonov type regularization methods therefore seem standard, since to introduce intermediate values $\rho : \Omega \to [\rho-, 1]$ is not sufficient. Note, that the measurements u_{meas} may be restricted to a subset of Γ_N and can also be contaminated by noise, which makes (8) even harder to solve without proper regularization. Also note that the above optimal control problems (6) and (8) are single-load problems which easily can be extended to the multi-load case. In Section 4 we present some numerical results for the reconstruction problem (8) using multiple loads.

2. Pontryagin Approximations for Optimal Control

It is well known that inverse problems need to be regularized to obtain good approximations [6], and regularization may also be necessary to assure the mere existence of a solution. In the following section we present a Pontryagin method for optimal control of partial differential equations using a regularization derived from consistency with the corresponding Hamilton-Jacobi-Bellman equations in infinite dimension. To make the presentation clear and concise we first describe the method for controlling a system of ordinary differential equations, and then apply the methodology to control of partial differential equations, following [3].

Consider the optimal control problem for a controlled ordinary differential equation

$$\inf_{\alpha\in\mathcal{A}} \left\{ g(X(T)) + \int_0^T h(X(s),\alpha(s)) \, \mathrm{d}s \;\middle|\; X'(t) = f(X(t),\alpha(t)),\ X(0) = X_0 \right\}, \tag{9}$$

with given data $g : \mathbb{R}^n \to \mathbb{R}$, $h : \mathbb{R}^n \times B \to \mathbb{R}$, $f : \mathbb{R}^n \times B \to \mathbb{R}^n$, $X_0 \in \mathbb{R}^n$, the state variable $X : [0,T] \to \mathbb{R}^n$ and a set of controls $\mathcal{A} = \{\alpha : [0,T] \to B \subset \mathbb{R}^m\}$. Optimal control problems like (9) can be solved by dynamic programming or by the Lagrange principle. Defining the value function

$$u(x,t) \equiv \inf_{X(t)=x, \alpha \in \mathcal{A}} \left\{ g\big(X(T)\big) + \int_t^T h\big(X(s), \alpha(s)\big)\ \mathrm{d}s \right\},$$

the dynamic programming approach gives that $u : \mathbb{R}^n \times [0,T] \to \mathbb{R}$ is the bounded uniformly continuous viscosity solution of the nonlinear Hamilton-Jacobi-Bellman partial differential equation

$$\begin{aligned} \partial_t u(x,t) + H\big(\partial_x u(x,t), x\big) &= 0, \qquad (x,t) \in \mathbb{R}^n \times (0,T), \\ u(x,T) &= g(x), \qquad x \in \mathbb{R}^n, \end{aligned} \tag{10}$$

where the Hamiltonian function $H : \mathbb{R}^n \times \mathbb{R}^n \to \mathbb{R}$ is defined by

$$H(\lambda, x) \equiv \min_{\alpha \in B} \big\{ \lambda \cdot f(x,\alpha) + h(x,\alpha) \big\}.$$

The Hamilton-Jacobi partial differential equation approach has the advantage that a global minimum is found, but cannot be used computationally for high dimensional problems where $n \gg 1$, and gives no direct information on the optimal path $X(t)$ and control $\alpha(t)$. On the other hand, assuming that H, f, g, h are differentiable, the Lagrange principle gives that an optimal path $X(t)$ satisfies the Hamiltonian boundary value system

$$\begin{aligned} X'(t) &= \partial_\lambda H\big(\lambda(t), X(t)\big), \quad X(0) = X_0, \\ -\lambda'(t) &= \partial_x H\big(\lambda(t), X(t)\big), \quad \lambda(T) = g'(X(T)), \end{aligned} \tag{11}$$

Solving (11) is actually the method of characteristics for the Hamilton-Jacobi equation (10) provided $\lambda(t) \equiv \partial_x u(X(t), t)$ exists. Also note that equation (11) is equal to

$$\begin{aligned} X'(t) &= f\big(X(t), \alpha(t)\big), \\ X(0) &= X_0, \\ -\lambda_i'(t) &= \partial_{x_i} f\big(X(t), \alpha(t)\big) \cdot \lambda(t) + h_{x_i}\big(X(t), \alpha(t)\big), \\ \lambda(T) &= g'\big(X(T)\big). \end{aligned}$$

with the control α determined by the Pontryagin principle

$$\alpha(t) \in \mathrm{argmin}_{a \in B} \ \big\{ \lambda(t) \cdot f(X(t), a) + h(X(t), a) \big\}, \tag{12}$$

The Lagrange principle has the advantage that high dimensional problems, $n \gg 1$ can be solved computationally and the drawback is that in practice only local minima can be found computationally. Also, when using (11) to solve the minimization problem (9) it is assumed that the Hamiltonian is explicitly known and differentiable. In general, Hamiltonians are only Lipschitz continuous for smooth f, g and h. As we will see in Section 4, explicit Hamiltonians do exist for many interesting applications, and they can be approximated by differentiable ones. To emphasize the connection with the optimal control we refer to solving (11) as the *Pontryagin method*.

Many optimal control problems lead to non-smooth optimal controls, *e.g.* bang-bang controls, which occur by two reasons: the Hamiltonian is in general only Lipschitz continuous, even though f, g, h are smooth, and backward optimal paths $X(t)$ may collide. The theory of viscosity solutions to Hamilton-Jacobi equations elegantly handles non-smooth solutions, but to be able to use the computational advantage of solving the Hamiltonian boundary value system (11) we introduce a regularized problem with a $\mathcal{C}^2(\mathbb{R}^n \times \mathbb{R}^n)$ λ-concave approximation H_δ of the

Hamiltonian H. This approximation not only gives meaning to (11), but is well defined in the sense that the corresponding approximated value function u_δ is close to the original value function u. In [11], error analysis yields the estimate

$$\|u_\delta - u\|_{L^\infty(\mathbb{R}^d \times \mathbb{R}_+)} = \mathcal{O}(\delta), \tag{13}$$

for the real and approximate value functions u and u_δ, and with a regularization parameter δ, such that $\|H_\delta - H\|_{L^\infty(\mathbb{R}^n \times \mathbb{R}^n)} = \mathcal{O}(\delta)$. This error estimate is not explicitly dependent on the dimension n and is thus suitable for optimal control of discretized partial differential equations. Observe that $\|u_\delta - u\|_{L^\infty(\mathbb{R}^n \times \mathbb{R}_+)} \to 0$ does not necessarily imply convergence of the optimal paths $X(t)$ or the controls $\alpha(t)$.

Now, consider the above analysis extended to control of a time dependent partial differential equation, as in [3],

$$\begin{aligned} \partial_t \varphi(x,t) &= f\big(\varphi(x,t), \alpha(x,t)\big), \quad (x,t) \in \Omega \times (0,T) \\ \varphi(x,0) &= \varphi_0, \qquad\qquad\qquad\quad x \in \Omega \end{aligned}$$

where f is a partial differential operator, $\Omega \subset \mathbb{R}^n$, and $\varphi(\cdot,t)$ belongs to some Hilbert space V on Ω. The minimization problem corresponding to (9) then becomes

$$\begin{aligned} \inf_{\alpha:\Omega\times[0,T]\to B} \Big\{ g\big(\varphi(\cdot,T)\big) + \int_0^T h\big(\varphi(\cdot,t), \alpha(\cdot,t)\big)\ \mathrm{d}t \ \Big| \\ \partial_t \varphi = f\big(\varphi(\cdot,t), \alpha(\cdot,t)\big),\ \varphi(\cdot,0) = \varphi_0 \Big\}, \end{aligned} \tag{14}$$

The Hamiltonian $H : V \times V \to \mathbb{R}$ is defined as

$$H(\lambda, \varphi) \equiv \min_{\alpha:\Omega\to B} \{\langle \lambda, f(\varphi,\alpha)\rangle + h(\varphi,\alpha)\}, \tag{15}$$

and the value function $u : V \times [0,T] \to \mathbb{R}$,

$$\begin{aligned} u(\phi,\tau) \equiv \inf_{\alpha:\Omega\times[0,T]\to B} \Big\{ g\big(\varphi(\cdot,T)\big) + \int_\tau^T h\big(\varphi(\cdot,t), \alpha(\cdot,t)\big)\ \mathrm{d}t \ \Big| \\ \partial_t \varphi = f\big(\varphi(\cdot,t), \alpha(\cdot,t)\big),\ \varphi(\cdot,\tau) = \phi \in V \Big\} \end{aligned}$$

solves the Hamilton-Jacobi-Bellman equation

$$\partial_t u(\phi,t) + H\big(\partial_\phi u(\phi,t), \phi\big) = 0, \quad u(\cdot,T) = g. \tag{16}$$

Here, ∂ now denotes Gâteaux derivatives (except for ∂_t), and $\langle v, w\rangle$ is the duality pairing on V, which reduces to the $L^2(\Omega)$ inner product if $v, w \in L^2(\Omega)$. From the Lagrange principle we get the Hamiltonian system

$$\begin{aligned} \partial_t \varphi &= \partial_\lambda H(\lambda,\varphi), \qquad \varphi(\cdot,0) = \phi \\ \partial_t \lambda &= -\partial_\varphi H(\lambda,\varphi), \quad \lambda(\cdot,T) = \partial_\varphi g\big(\varphi(\cdot,T)\big). \end{aligned} \tag{17}$$

To solve (17), consider a finite element subspace $\bar{V} \subset V$ and a corresponding $\mathcal{C}^2$ regularized approximate Hamiltonian $\bar{H}_\delta : V \times \bar{V} \to \mathbb{R}$,

$$\bar{H}_\delta(\lambda, \bar{\varphi}) \equiv \min_{\alpha:\Omega\to B} \{\langle \lambda, f_\delta(\bar{\varphi},\alpha)\rangle + h_\delta(\bar{\varphi},\alpha)\},$$

with approximations f_δ and h_δ. For $\varphi, \lambda \in \bar{V}$, the problem has now been transformed into the control of a system of ordinary differential equations, so the estimate (13) still holds for the value functions $\bar{u}_\delta$ and $\bar{u}$ solving (16) using $\bar{H}_\delta$ and the unregularized Hamiltonian $\bar{H} : V \times \bar{V} \to \mathbb{R}$ respectively, see [3, 11]. An error estimate for the difference between the true value function u and the regularized approximate value function $\bar{u}_\delta$ is however harder to derive, since it seems to require knowledge of the difference between true optimal paths (φ, λ) and approximated

optimal paths $(\bar{\varphi}_\delta, \bar{\lambda}_\delta)$. As noted earlier these paths does in general not converge for a non-differentiable Hamiltonian, since the control becomes discontinuous. In [3], an estimate of $u - \bar{u}_\delta$, using only the difference of H and $\bar{H}_\delta$ along the same path, is derived. This estimate gives an error estimate which in practice can be bounded in terms of the regularization parameter δ and the finite element mesh size, such that the value functions converge even though the optimal paths do not. For more on this issue, see [3, 12].

In the following sections the Pontryagin method is used for solving time independent optimal design problems with only Lipschitz continuous Hamiltonians. All examples presented give Lipschitz continuous Hamiltonians which need to be regularized.

3. Concave Maximization

To apply the methodology of time dependent optimal control from Section 2 to the time independent optimal design problem in Section 1, we first concentrate on a simpler scalar problem of electric conductivity [10]: to place a given amount of conducting material in a given domain $\Omega \subset \mathbb{R}^d$ in order to minimize the power loss for a given surface current q, satisfying $\int_{\partial\Omega} q \, \mathrm{d}s = 0$. Let, as in Section 1, $\eta \in \mathbb{R}$ be a given constant, associated to the given amount of material, and find an optimal conduction distribution $\sigma : \Omega \to \{\sigma_-, \sigma_+\}$, where $\sigma_\pm > 0$, such that

$$\inf_\sigma \left\{ \int_{\partial\Omega} q\varphi \;\; \mathrm{d}s + \eta \int_\Omega \sigma \;\; \mathrm{d}x \;\middle|\; \mathrm{div}(\sigma\nabla\varphi)\Big|_\Omega = 0, \; \sigma\frac{\partial\varphi}{\partial n}\Big|_{\partial\Omega} = q \right\}, \tag{18}$$

here $\partial/\partial n$ denotes the normal derivative, $\mathrm{d}s$ is the surface measure on $\partial\Omega$ and $\varphi \in V \equiv \{v \in H^1(\Omega) : \int_\Omega v \, \mathrm{d}x = 0\}$ is the electric potential.

Now, consider the parabolic variant of the constraint in (18), with $\sigma : \Omega\times[0,T] \to \{\sigma_-, \sigma_+\}$, $\varphi : \Omega \times [0,T] \to \mathbb{R}$ and initial data $\varphi_0 \in V$:

$$\begin{aligned} \partial_t\varphi &= \mathrm{div}\big(\sigma\nabla\varphi\big), && (x,t) \in \Omega \times (0,T) \\ \sigma\frac{\partial\varphi}{\partial n} &= q(x), && (x,t) \in \partial\Omega \times (0,T) \\ \varphi(x,0) &= \varphi_0, && x \in \Omega, \end{aligned}$$

and the time dependent minimization problem

$$\begin{aligned} \inf_\sigma \Big\{ \int_0^T \int_{\partial\Omega} q\varphi \;\; \mathrm{d}s + \eta \int_\Omega \sigma \;\; \mathrm{d}x \;\; \mathrm{d}t \;\Big| \\ \partial_t\varphi = \mathrm{div}(\sigma\nabla\varphi), \; \sigma\frac{\partial\varphi}{\partial n}\Big|_{\partial\Omega} = q, \; \varphi(\cdot,0) = \varphi_0 \Big\}. \end{aligned} \tag{19}$$

The Lagrangian takes the form

$$\mathcal{L}(\sigma,\lambda,\varphi) := \int_0^T \int_{\partial\Omega} q(\varphi+\lambda) \;\; \mathrm{d}s \;\; \mathrm{d}t + \int_0^T \int_\Omega \sigma \underbrace{(\eta - \nabla\varphi\cdot\nabla\lambda)}_{\mathfrak{v}} - \partial_t\varphi\lambda \;\; \mathrm{d}x \;\; \mathrm{d}t,$$

with $\lambda = \lambda(x,t)$ and the Hamiltonian corresponding to (15) becomes

$$\begin{aligned} H(\lambda,\varphi) &= \min_{\sigma:\Omega\to\{\sigma_\pm\}} \left\{ \int_\Omega \sigma\mathfrak{v} \;\; \mathrm{d}x + \int_{\partial\Omega} q(\varphi+\lambda) \;\; \mathrm{d}s \right\} \\ &= \int_\Omega \underbrace{\min_{\sigma\in\{\sigma_-,\sigma_+\}} \{\sigma\mathfrak{v}\}}_{\mathfrak{h}(\mathfrak{v})} \;\; \mathrm{d}x + \int_{\partial\Omega} q(\varphi+\lambda) \;\; \mathrm{d}s. \end{aligned} \tag{20}$$

As in Section 2, the value function

$$u(\phi,\tau) = \inf_{\sigma} \Big\{ \int_\tau^T \int_{\partial\Omega} q\varphi \ \mathrm{d}s + \eta \int_\Omega \sigma \ \mathrm{d}x \ \mathrm{d}t \ \Big| \ \partial_t\varphi = \mathrm{div}(\sigma\nabla\varphi),\ \sigma\frac{\partial\varphi}{\partial n}\Big|_{\partial\Omega} = q,\ \varphi_\tau = \phi \Big\}$$

satisfies the infinite dimensional Hamilton-Jacobi equation

$$\partial_t u(\phi,t) + H(\partial_\phi u(\phi,t),\phi) = 0 \quad t < T, \quad u(\cdot,T) = 0,$$

using the Gâteaux derivative $\partial_\phi u(\phi,t)$ of the functional $u(\phi,t)$ in $L^2(\Omega)$. The corresponding Hamiltonian system is the parabolic system

$$\begin{aligned} \int_\Omega \partial_t\varphi w + \mathfrak{h}'(\eta - \nabla\varphi\cdot\nabla\lambda)\nabla\varphi\cdot\nabla w \ \mathrm{d}x &= \int_{\partial\Omega} qw \ \mathrm{d}s, \quad \varphi(\cdot,0) = \varphi_0, \\ \int_\Omega -\partial_t\lambda v + \mathfrak{h}'(\eta - \nabla\varphi\cdot\nabla\lambda)\nabla\lambda\cdot\nabla v \ \mathrm{d}x &= \int_{\partial\Omega} qv \ \mathrm{d}s, \quad \lambda(\cdot,T) = 0, \end{aligned} \tag{21}$$

for all test functions $v, w \in V \equiv \{v \in H^1(\Omega) : \int_\Omega v \ \mathrm{d}x = 0\}$.

From (20) it is evident that the control becomes undefined and the Hamiltonian non-differentiable when $\mathfrak{v} \equiv \eta - \nabla\varphi\cdot\nabla\lambda = 0$. We thus replace H with the concave regularization H_δ depending on a smooth approximation, $\mathfrak{h}_\delta \in \mathcal{C}^2(\mathbb{R})$, of the Lipschitz continuous and monotonically increasing function $\mathfrak{h}$, see left part of Figure 1. In this case the regularization H^δ is therefore similar to a Tikhonov reg-

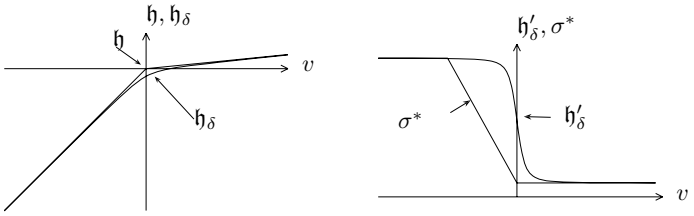

FIGURE 1. Left: The function $\mathfrak{h}$ and its regularization $\mathfrak{h}_\delta$ with respect to $\mathfrak{v}$. Right: The approximation $\mathfrak{h}'_\delta$ compared to a control σ^* obtained from adding a Tikhonov type penalty $\delta\int_\Omega \sigma^2 \ \mathrm{d}x$ to (20) with $\sigma : \Omega \to [\sigma_-, \sigma_+]$.

ularization with penalty on the L^2 norm of σ, see right part of Figure 1. Note that $\sigma : \Omega \to [\sigma_-, \sigma_+]$ in (20) will lead to the same Hamiltonian as $\sigma : \Omega \to \{\sigma_-, \sigma_+\}$.

To connect the optimal design problem (18) with the artificial time-dependent problem (19) we assume that

$$\lim_{T\to\infty} \frac{u(\cdot,0)}{T} = \inf_\sigma \Big\{ \int_{\partial\Omega} q\varphi \ \mathrm{d}s + \eta\int_\Omega \sigma \ \mathrm{d}x \ \Big| \ \mathrm{div}(\sigma\nabla\varphi)\Big|_\Omega = 0,\ \sigma\frac{\partial\varphi}{\partial n}\Big|_{\partial\Omega} = q \Big\},$$

which can be achieved by assuming $\partial_t\varphi = \partial_t\lambda = 0$ in the Hamiltonian system (21). Time independent solutions to (21) exhibits symmetry $\varphi = \lambda$ and solves the nonlinear elliptic partial differential equation

$$\begin{aligned} \mathrm{div}\big(\mathfrak{h}'_\delta(\eta - |\nabla\varphi|^2)\nabla\varphi\big) &= 0, \quad x \in \Omega \\ \mathfrak{h}'_\delta\frac{\partial\varphi}{\partial n} &= q, \quad x \in \partial\Omega \end{aligned} \tag{22}$$

which can be formulated as the concave maximization problem: $\varphi \in V$ is the unique maximizer of

$$H_\delta(\varphi,\varphi) = \int_\Omega \mathfrak{h}_\delta(\eta - |\nabla\varphi(x)|^2)\ \mathrm{d}x + 2\int_{\partial\Omega} q\varphi\ \mathrm{d}s.$$

An advantage with the Pontryagin approach (22) is that the Hessian of H_δ can be determined explicitly and is sparse, so that the Newton method can be used for iterative solution of (22). Note that the opposite problem of maximizing power loss, *i.e.* replacing the 'inf' in (18) with a 'sup', would in general not give a concave regularized Hamiltonian H_δ. The existence of a maximizer φ depends on the weak upper semi-continuity of H_δ, which in this particular case can be guaranteed if $\mathfrak{h}_\delta$ is concave with respect to $|\nabla\varphi|$, see [5]. In Figure 2, $\mathfrak{h}$ and $\mathfrak{h}_\delta$ are shown as functions of $|\nabla\varphi|$ for both minimizing and maximizing power loss. The function $\mathfrak{h}_\delta$ for the problem of maximizing power loss is only concave for sufficiently large regularizations.

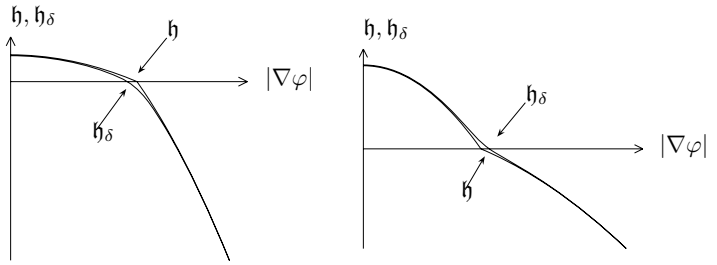

FIGURE 2. The function $\mathfrak{h}$ and its regularization $\mathfrak{h}_\delta$ with respect to $|\nabla\varphi|$ when minimizing power loss (left) and maximizing power loss (right).

4. Numerical Examples

To numerically solve the optimal design problems (6) and (8) in Section 1, we consider the planar stress case, $\sigma_{3l} = \sigma_{l3} = 0$, $l = 1, 2, 3$, for a thin plate located in the xy-plane. The plate can be described by the two dimensional domain $\Omega \subset \mathbb{R}^2$, and the material density ρ can be interpreted as the thickness of the plate. For planar forces $f_b : \Omega \to \mathbb{R}^2$ and $f_s : \Gamma_N \to \mathbb{R}^2$, $\Gamma_N \subset \partial\Omega$, the planar displacements $u : \Omega \to \mathbb{R}^2$ can be separated from the anti-planar displacement, and satisfy the variational equation (4), for $d = 2$. The Lamé coefficients in Hooke's law (3) takes the form

$$\mu = \frac{E}{2(1+\nu)}, \quad \lambda = \frac{E\nu}{1-\nu^2},$$

with a Young's modulus E and a Poisson ratio ν. In all examples we assume $E = 100$, $\nu = 0.3$, and that no volume forces are present, *i.e.* $f_b = 0$.

4.1. **Compliance Optimization.** Recall the compliance minimization problem (6), *i.e.*

$$\inf_\rho \left\{ l(u) + \eta \int_\Omega \rho\ \mathrm{d}x \;\middle|\; a_\rho(u,v) = l(v),\ \forall v \in V \right\}.$$

with relative material density $\rho : \Omega \to \{\rho_-, 1\}$, displacement $u : \Omega \to \mathbb{R}^2$, compliance functional $l(u)$ and bilinear energy functional $a_\rho(u,v)$. Similarly to Section 3,

we note that the Lagrangian takes the form

$$\mathcal{L}(u,\lambda,\rho) = l(u) + l(\lambda) + \int_\Omega \rho\Big(\underbrace{\eta - \sum_{ijkl} \varepsilon_{ij}(u)E_{ijkl}\varepsilon_{kl}(\lambda)}_{\mathfrak{v}}\Big)\ \mathrm{d}x,$$

and the Hamiltonian is

$$H(u,\lambda) = l(u) + l(\lambda) + \int_\Omega \underbrace{\min_{\rho\in\{\rho_-,1\}}\{\rho\mathfrak{v}\}}_{\mathfrak{h}(\mathfrak{v})}\ \mathrm{d}x.$$

Regularizing $\mathfrak{h}$ with $\mathfrak{h}_\delta$, and consequently H with H^δ, gives a Hamiltonian system which by symmetry, $u = \lambda$, can be reduced to the variational equation

$$\int_\Omega \mathfrak{h}'_\delta\Big(\eta - \sum_{mnop} \varepsilon_{mn}(u)E_{mnop}\varepsilon_{op}(u)\Big)\varepsilon_{ij}(u)E_{ijkl}\varepsilon_{kl}(v)\ \mathrm{d}x = l(v) \tag{23}$$

for all admissible displacements $v \in V = \{H^1(\Omega)^d, v_{\Gamma_D} = 0\}$, which is the Euler-Lagrange equation of the problem to find the unique maximizer $u \in V$ of the functional

$$H^\delta = 2l(u) + \int_\Omega \mathfrak{h}_\delta\Big(\eta - \sum_{ijkl} \varepsilon_{ij}(u)E_{ijkl}\varepsilon_{kl}(u)\Big)\ \mathrm{d}x. \tag{24}$$

In all numerical tests for the compliance minimization problem we let Ω be the rectangular domain defined by $(x,y) \in (0,2)\times(0,1)$, and solve (23) on the finite element subspace consisting of nine-node quadrilateral elements on a uniform mesh. The left boundary is fixed and a downward force, $f_s(2,y) = -10$, $y \in [0.45, 55]$, is applied to the middle of the right boundary. The lower bound on the material density is $\rho_- = 10^{-3}$, and the regularized function $\mathfrak{h}_\delta$ is chosen such that

$$\mathfrak{h}'_\delta(\mathfrak{v}) = \frac{1}{2}\left(\rho_- + 1 + (\rho_- - 1)\tanh\left(\frac{\mathfrak{v}\ \tanh^{-1}(0.99)}{\delta}\right)\right),$$

see Figure 1. The resulting discrete system is solved with Newton's method and for successively smaller regularizations according to the scheme:

- if the Newton method for δ_{old} converged choose

$$\delta_{new} = \alpha_{old}\delta_{old}, \quad \alpha_{new} = \alpha_{old},$$

- otherwise let

$$\delta_{new} = \frac{1}{2}\delta_{old}(1 + \frac{1}{\alpha_{old}}), \quad \alpha_{new} = \frac{2\alpha_{old}}{\alpha_{old}+1}.$$

This means that if the Newton method fails to converge for some regularization δ, the new regularization will be the average of δ and the last successful regularization. Also, the parameter α is constructed such that if this new averaged regularization works, we will once again try the regularization where the method previously failed. Here, $\alpha_{old} = 0.5$ is used as initial step-size.

In the left part of Figure 3 to Figure 7, the variational equation (23) is solved using FEMLAB and the Newton method for successively smaller values of δ. As δ is reduced the density will not achieve purely discrete values, but rather remain at intermediate values in large regions. This agrees with results from other regularizations, such as the plate thickness approach [2] or the homogenization method [1]. The smooth density is consistent with the fact that a minimizing sequence for the original formulation (6) will oscillate in these areas, and the regularized solution will behave approximately as an average of these oscillations.

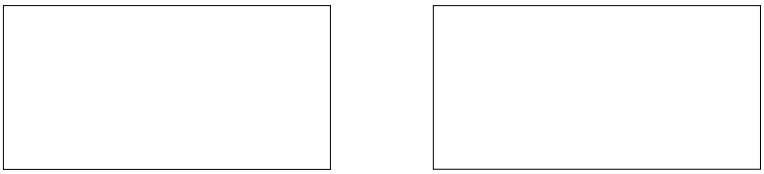

FIGURE 3. Plot of $\mathfrak{h}'_\delta$ as an approximation of the relative material density when minimizing compliance of an elastic plate with a fixed right side and an external load $f_s(2, y) = -10$, $y \in [0.45, 55]$. A uniform mesh with 80×40 nine-node quadrilateral finite elements and a multiplier $\eta = 5 \cdot 10^{-3}$ was used. In the left figure, (4) was solved with the Newton method and by successively reducing the regularization δ until $\delta \approx 3.5 \cdot 10^{-4}$. The right figure shows the density after 100 iterations using (25) with $\delta = 0$ and with the solution from the left part taken as initial guess.

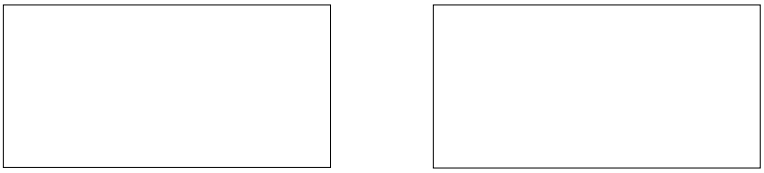

FIGURE 4. Plot of $\mathfrak{h}'_\delta$ calculated with data as in Figure 3 but using a 240×120 mesh. Note that the unregularized design on the right is mesh dependent. The discrete designs are also sensitive to the initial data and the fraction of elements allowed to change in each iteration. Although the discrete design here differs a lot from the one in Figure 3, the compliance only differs by less than 0.1 percent.

Since ρ can be determined explicitly by the Pontryagin method an alternative approach to solving (23) with the Newton method is to iterate separately over ρ and u according to the scheme

$$\rho_{m+1} = \mathfrak{h}'_\delta\left(\eta - \sum_{ijkl} \varepsilon_{ij}(u_m) E_{ijkl} \varepsilon_{kl}(u_m)\right) \tag{25}$$

where u_m solves (23) with $\rho = \rho_m$. This scheme, which essentially is the Jacobi method, is highly unstable since information from the Hessian is lost. It is, however, still possible to use this method, with $\delta = 0$, as post-processing to eliminate areas of intermediate density generated by the Newton method. In general, such discrete

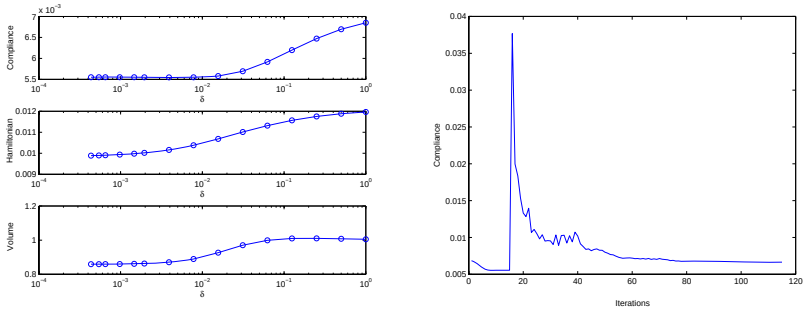

FIGURE 5. Convergence plots corresponding to Figure 4. Left: Convergence of the compliance, the Hamiltonian, and the volume with respect to the regularization. Right: Plot of the compliance for the discrete iterations corresponding to the right plot in Figure 4. The values from the left plot is included in the first iterations for comparison. Note that although the compliance for the discrete iterations decreases it will never reach the compliance for the regularized problem.

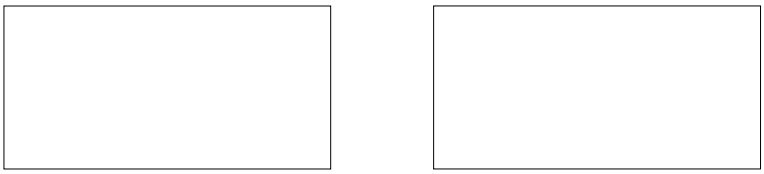

FIGURE 6. Plot of $\mathfrak{h}'_\delta$ with $\eta = 2 \cdot 10^{-2}$ and a 80×40 mesh. The regularization in the left figure is $\delta \approx 1.5 \cdot 10^{-3}$.

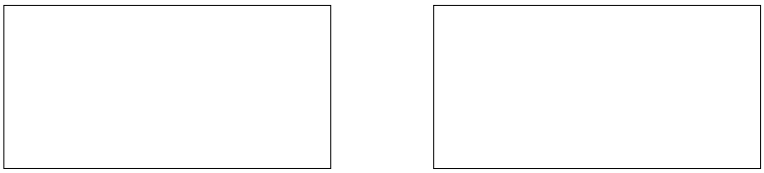

FIGURE 7. Plot of $\mathfrak{h}'_\delta$ with data as in Figure 6 but with a 240×120 mesh. The compliance of the discrete design is here $1.6 \cdot 10^{-2}$ compared with $3.6 \cdot 10^{-2}$ for the discrete design in Figure 6, and $9.7 \cdot 10^{-3}$ for the regularized designs.

iterations do not converge and we may need to restrict the amount of material allowed to change in each iteration. The right part of Figure 3 to Figure 7 shows the density after 100 iterations using a variant of (25) with $\delta = 0$ and with solutions from the left part of the figures taken as initial guesses. Here, ρ is updated elementwise and only a fraction of elements, corresponding to the smallest and largest values of v, is allowed to change, such that the volume remains constant. In all experiments, the compliance initially drops but eventually starts to oscillate, and at this point the control ρ will start to form checkerboard structures in large areas. To prevent the formation of such structures we here reduce the fraction of elements allowed to change as soon as the compliance starts to oscillate.

FIGURE 8. The relative material density when material has been iteratively removed from a completely filled domain by sorting $\varepsilon_{ij}(u)E_{ijkl}\varepsilon_{kl}(u)$ and removing the material corresponding to the largest values. In each iteration the volume to be removed is adjusted to follow a geometric sequence of volumes such that the final volume is the same as in Figure 4. The final compliance after 70 iterations has converged to $6.78 \cdot 10^{-3}$ compared to $6.65 \cdot 10^{-3}$ for the discrete iterations in Figure 4 and 5.

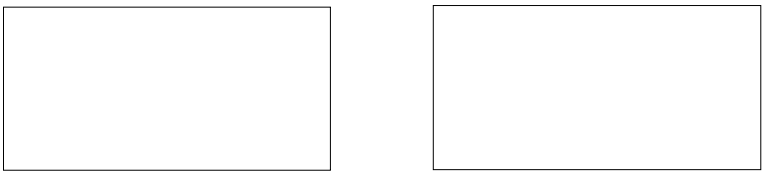

FIGURE 9. Plot of $\mathfrak{h}'_\delta$ as an approximation of the relative material density when maximizing compliance. A uniform mesh with 240×120 nine-node quadrilateral finite elements, a lower relative density $\rho_- = 0.5$, and a multiplier $\eta = 2 \cdot 10^{-3}$, was used. The discrete iterations give no further information in this case.

It can also be noted that the expression $\mathfrak{v} \equiv \eta - \varepsilon_{ij}(u)E_{ijkl}\varepsilon_{kl}(u)$ resembles the the topological gradient used in the topological shape method [4]. The topological

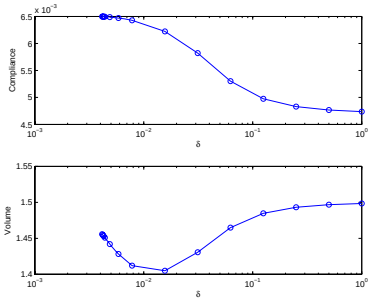

FIGURE 10. Convergence history for the compliance maximization problem. Although the volume does not converge as the regularization decreases, the compliance here seems to increase and level out. For comparison the compliance for a intuitive guess, with ρ_- close to the left and right boundary, ρ_+ in the middle, and the same volume, gives a compliance of $5.7 \cdot 10^{-3}$ compared with $6.4 \cdot 10^{-3}$ in the figure. Also, note that the Newton iterations fail to converge for small regularizations.

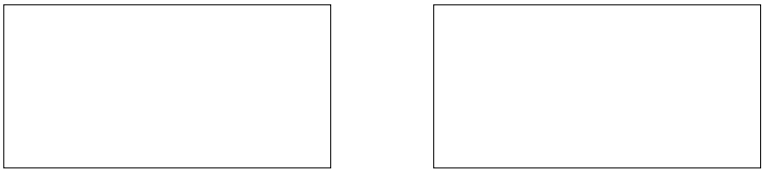

FIGURE 11. The compliance minimization problem for a downward force $f_s(x, 0) = -10$, $x \in [0.95, 1.05]$, and with supports located at $x \in [0.2, 0.25]$ and $x \in [1.75, 1.8]$. Both supports are fixed in both the x- and y-direction. A uniform mesh with 240×120 elements and a multiplier $\eta = 5 \cdot 10^{-3}$ was used. In the left plot the regularization is $\delta \approx 10^{-3}$ and the compliance is $1.3 \cdot 10^{-3}$. The compliance after 100 discrete iterations, shown in the right plot, is $1.5 \cdot 10^{-3}$.

shape method starts from a completely filled domain and successively removes material according to the sign of the topological derivative. This method is appealing since it is simple and gives interesting designs, but it may not converge to the true optimal design if it is possible to remove too much material, which never can be added again. In Figure 8, material has been iteratively removed from a completely filled domain by sorting $\varepsilon_{ij}(u)E_{ijkl}\varepsilon_{kl}(u)$ and removing the material corresponding to the largest values. In each iteration the volume to be removed is adjusted to follow a geometric sequence such that the final volume is approximately the same as the one in Figures 3 and 4.

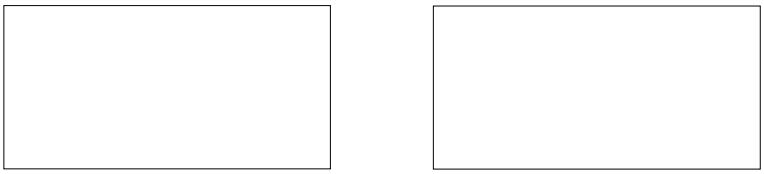

FIGURE 12. The compliance minimization problem with data as in Figure 11 but with both supports fixed in the y-direction and free to move in the x-direction. The smallest regularization was $\delta \approx 10^{-3}$ with a compliance of $1.5 \cdot 10^{-3}$. The compliance after 100 discrete iterations was $2.8 \cdot 10^{-3}$.

As a comparison with the concave maximization problem of minimizing compliance, it is interesting to see what happens for the problem of maximizing compliance. Replacing the 'inf' in (24) with a 'sup' gives, similarly to Section 3, a regularized Hamiltonian which only has a unique minimizer for sufficiently large regularizations. In Figure 9, the Pontryagin method is used to maximize compliance by placing two materials with $\rho \in \{0.5, 1\}$. The reason to not have $\rho_- = 10^{-3}$, is that maximizing compliance here seems to lead to a structure not connected to the part of the boundary where the external force is applied, thus making the problem harder to solve. It is also not clear that the solution for a small value of ρ_- is a good approximation of the solution for $\rho_- = 0$ in this example. The solution to the regularized Hamiltonian system gives, in Figure 9, a design which has the interesting shape of a turning fork. In Figure 10, we see that the Newton iterations do not converge for small regularizations, which indicates that there does not longer exist any minimizer to the regularized Hamiltonian. Also, discrete iterations with (25) does not give any additional information.

Finally, in Figures 11 and 12 the compliance minimization problem is solved for a slightly different example where a downward force is applied to the middle of the lower side, $f_s(x, 0) = -10$, $x \in [0.95, 1.05]$, and supports are located at $x \in [0.2, 0.25]$ and $x \in [1.75, 1.8]$. In Figure 11 the supports are fixed in both the x- and y-direction whereas they are only fixed in the y-direction in Figure 12.

4.2. **Interior Reconstruction.** For the compliance optimization problem (6) symmetry, $u = \lambda$, reduced the Hamiltonian system to the variational equation (23). Symmetry is common in many optimization problems connected to minimization of energy, but there are important exceptions such as inverse problems related to reconstruction from measurements. For example, consider the multi-experiment case of the reconstruction problem (8) stated in Section 1: reconstruct an unknown density $\rho : \Omega \to \{\rho_-, 1\}$ from M different boundary measurements $u_{meas,i}$, $i = 1, \dots, M$ on Γ_N resulting from applying given forces $f_{s,i}, f_{b,i} : \Gamma_N \to \mathbb{R}^d$, $i = 1, \dots, M$. One strategy is then to find the density ρ such that

$$\inf_{\rho:\Omega\to\{\rho_-,1\}} \Big\{ \sum_{m=1}^{M} \int_{\Gamma_N} |u_m - u_{meas,m}|^2 \, \mathrm{d}s \;\Big|\; a_\rho(u_m, v) = l_m(v),\ \forall v \in V,\ m = 1, \dots, M \Big\}, \tag{26}$$

where $a_\rho(u,v)$ is given by (2) and the compliance is given by

$$l_m(u) \equiv \int_\Omega f_{b,m} \cdot u \, \mathrm{d}x + \int_{\Gamma_N} f_{s,m} \cdot u \, \mathrm{d}s.$$

The Lagrangian is then

$$\begin{aligned}\mathcal{L}(u_1,\dots,u_M,\lambda_1,\dots,\lambda_M,\rho) = \sum_{m=1}^{M} \int_{\Gamma_N} |u_m - u_{meas,m}|^2 \, \mathrm{d}s + l_m(\lambda_m) \\ + \int_\Omega \underbrace{-\rho \sum_{m=1}^{M} \varepsilon_{ij}(u_m) E_{ijkl} \varepsilon_{kl}(\lambda_m)}_{\mathfrak{v}} \, \mathrm{d}x,\end{aligned}$$

and the Hamiltonian is

$$H = \sum_{m=1}^{M} \int_{\Gamma_N} |u_m - u_{meas,m}|^2 \, \mathrm{d}s + l_m(\lambda_m) + \int_\Omega \underbrace{\min_{\rho \in \{\rho_-,1\}} \{\rho \mathfrak{v}\}}_{\mathfrak{h}(\mathfrak{v})} \, \mathrm{d}x. \tag{27}$$

In this case no symmetry is present and the regularized Hamiltonian system becomes

$$\begin{aligned} a_{\mathfrak{h}'_\delta}(u_m, v_m) \, \mathrm{d}x &= l_m(v_m), \\ a_{\mathfrak{h}'_\delta}(u_m, w_m) \, \mathrm{d}x &= 2 \int_{\Gamma_N} (u_m - u_{meas,m}) \cdot w_m \, \mathrm{d}s, \end{aligned} \tag{28}$$

for all test functions $v_m, w_m \in V$, $m = 1,\dots,M$. Note, that replacing $\rho : \Omega \to \{\rho_-, 1\}$, in the original formulation (26), with $\rho : \Omega \to [\rho_-, 1]$, gives the same Hamiltonian (27).

FIGURE 13. Material densities to be reconstructed. The density is 0.5 in the white region, and 1 elsewhere.

In Figures 14 and 17 the system (28) is solved, for $M = 1, 2$, using the finite element method on a quadrilateral 40×40 mesh with nine-node elements, and Newton iterations. In all examples we use the computational domain $\Omega = (-1,1) \times (-1,1)$, with a fixed right boundary, and external boundary forces applied to the lower and left boundaries. Two sets of measurements were simulated by solving (4) on a quasi-uniform triangular mesh with 28000 quadratic Lagrange elements, for a given material density, with applied boundary forces $f_{s,1} = (10\cos(\pi y/2), 0)$ on the left boundary and $f_{s,2} = (0, 10\cos(\pi x/2))$ on the lower boundary. No external force is applied to the top boundary and no volume forces are present. In all examples we use $\rho : \Omega \to \{0.5, 1\}$ and seek to reconstruct two cases of material distributions:

FIGURE 14. Approximated material density, $\mathfrak{h}'_\delta$, from reconstruction of the amoeba shaped density. Left: Measurements from one experiment. Right: Measurements from two experiments. Using measurements from two different experiments here sharpens the edges and better resolves the region close to the fixed boundary.

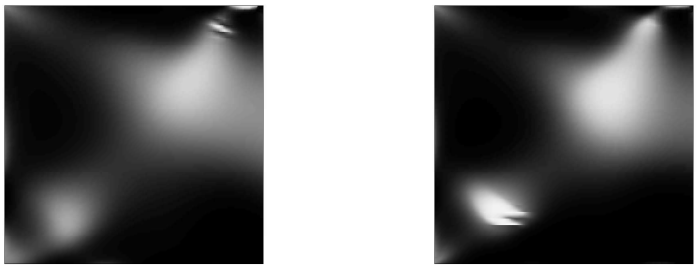

FIGURE 15. Material density reconstructed from experiment with an amoeba and a circle. Left: Data from one experiment is used. Right: Data from two experiments is used. In this example the reconstructed density does not gain much from using multiple measurements. Choosing different boundary forces could here potentially give an improvement of the finest details of the amoeba shape.

First we use a material with a density distribution in the form of an amoeba (see left part of Figure 13),

$$\rho = \begin{cases} 1, & x^2 + (y-0.1)^2 \geq 0.2 + 0.1e^{1.4\cos(3\theta-2)+0.4\sin^2\theta} \\ 0.5, & x^2 + (y-0.1)^2 < 0.2 + 0.1e^{1.4\cos(3\theta-2)+0.4\sin^2\theta} \end{cases}$$

with $\theta = \arctan(x/(y-0.1))$. Then, we combine the amoeba shape with a circle of radius 0.2, see right part of Figure 13.

In figure 14 and 15, we see how using multiple experiments increases the quality of the recovered material distribution, and in Figure 16 we see how the quality decreases after adding Gaussian random values to the measured data. The added noise is here scaled to correspond to 5% of the measured data. Note that despite the bad reconstructions in Figure 16, the $L^2(\partial\Omega)$ error between u and the noisy measurements u_{meas} levels out, so we can in this case therefore not hope for a better

reconstruction, even if we continue to reduce the regularization. This is known as the discrepancy principle, see [6] and [13].

As in section 4.1, discrete iterations in ρ and u can be done as post-processing to remove intermediate values of ρ. Such iterations does not, however, seem to give any additional information in this example. Also, using a small value for ρ_- to mimic void, makes the problem too ill-posed to solve with such accuracy in the reconstructed density as in the examples shown here. From our experience, solving the system (28) for a small ρ_- only seems possible for reconstruction of small circular inclusions close to the boundaries.

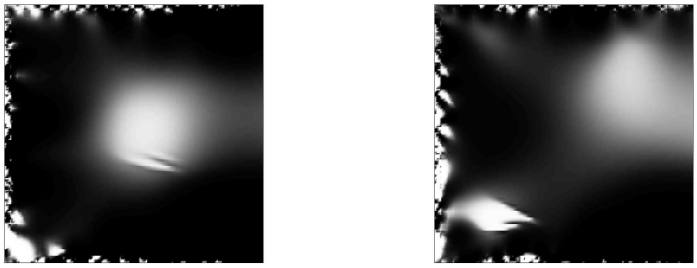

FIGURE 16. Material density reconstructed from noisy data, using two experiments and adding 5% white noise to the measured data. Although, artifacts are here introduced near the forced boundaries, and the resolution of the shapes is lost, the positions of the regions are still visible.

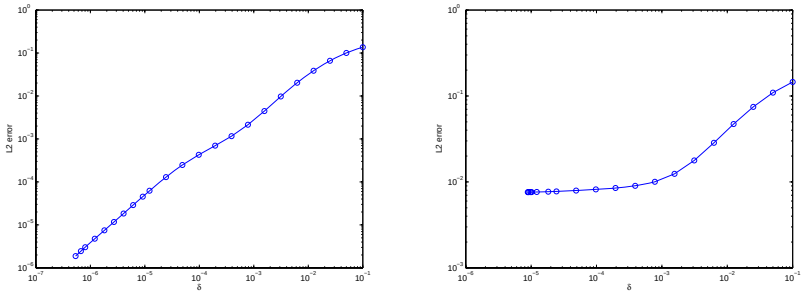

FIGURE 17. Plot of the $L^2(\partial\Omega)$ norm of $u - u_{meas}$ with respect to the regularization. Left: Error history corresponding to the single experiment case in Figure 14. Right: Error history corresponding to the single experiment case in Figure 15. The error in the right figure reaches its minimum value, and no better reconstruction can here be expected without additional post-processing of the measurements.

References

[1] Grégoire Allaire. *Shape optimization by the homogenization method*, volume 146 of *Applied Mathematical Sciences*. Springer-Verlag, Nw York, 2002.

[2] M. P. Bendsøe and O. Sigmund. *Topology optimization*. Springer-Verlag, Berlin, 2003. Theory, methods and applications.

[3] Jesper Carlsson, Mattias Sandberg, and Anders Szepessy. Symplectic Pontryagin approximations for optimal design. *preprint*, 2006.

[4] Jean Céa, Stéphane Garreau, Philippe Guillaume, and Mohamed Masmoudi. The shape and topological optimizations connection. *Comput. Methods Appl. Mech. Engrg.*, 188(4):713–726, 2000. IV WCCM, Part II (Buenos Aires, 1998).

[5] Bernard Dacorogna. *Direct methods in the calculus of variations*, volume 78 of *Applied Mathematical Sciences*. Springer-Verlag, Berlin, 1989.

[6] Heinz W. Engl, Martin Hanke, and Andreas Neubauer. *Regularization of inverse problems*, volume 375 of *Mathematics and its Applications*. Kluwer Academic Publishers Group, Dordrecht, 1996.

[7] Robert V. Kohn and Gilbert Strang. Optimal design and relaxation of variational problems. I. *Comm. Pure Appl. Math.*, 39(1):113–137, 1986.

[8] Robert V. Kohn and Gilbert Strang. Optimal design and relaxation of variational problems. II. *Comm. Pure Appl. Math.*, 39(2):139–182, 1986.

[9] Robert V. Kohn and Gilbert Strang. Optimal design and relaxation of variational problems. III. *Comm. Pure Appl. Math.*, 39(3):353–377, 1986.

[10] Olivier Pironneau. *Optimal shape design for elliptic systems*. Springer Series in Computational Physics. Springer-Verlag, New York, 1984.

[11] M. Sandberg and A. Szepessy. Convergence rates of symplectic Pontryagin approximations in optimal control theory. *M2AN*, 40(1), 2006.

[12] Mattias Sandberg. Convergence rates for numerical approximations of an optimally controlled Ginzburg-Landau equation. *preprint*, 2006.

[13] Curtis R. Vogel. *Computational methods for inverse problems*, volume 23 of *Frontiers in Applied Mathematics*. Society for Industrial and Applied Mathematics (SIAM), Philadelphia, PA, 2002. With a foreword by H. T. Banks.

Department of Numerical Analysis, Royal Institute of Technology, 100 44, Sweden
E-mail address: jesperc@nada.kth.se
URL: nada.kth.se/~jesperc

Paper 3

SYMPLECTIC RECONSTRUCTION OF DATA FOR HEAT AND WAVE EQUATIONS

JESPER CARLSSON

Abstract. This report concerns the inverse problem of estimating a spacially dependent coefficient of a partial differential equation from observations of the solution at the boundary. Such a problem can be formulated as an optimal control problem with the coefficient as the control variable and the solution as state variable. The heat or the wave equation is here considered as state equation. It is well known that such inverse problems are ill-posed and need to be regularized. The powerful Hamilton-Jacobi theory is used to construct a simple and general method where the first step is to analytically regularize the Hamiltonian; next its Hamiltonian system, a system of nonlinear partial differential equations, is solved with the Newton method and a sparse Jacobian.

Contents

1. Introduction

In this paper we study the inverse problem to determine a spacially dependent coefficient σ of a partial differential equation from partial knowledge of the forward solution u. In particular, we seek the diffusion coefficient in the heat equation and the wave speed coefficient in the wave equation. Inverse problems arise in many applications such as inverse scattering, impedance tomography and topology optimization, see *e.g.* [1, 3, 6, 14], and share the property that they are ill posed *i.e.* given data u there may not exist a corresponding coefficient σ, and if it exists it may not be unique nor depend continuously on u. To be able to determine σ

2000 *Mathematics Subject Classification.* Primary: 65M32; Secondary: 49L25.

Key words and phrases. Inverse Problems, Parameter Reconstruction, Hamilton-Jacobi, Regularization.

Support by the Swedish Research Council grants 2002-6285 and 2002-4961, and the European network HYKE, funded by the EC as contract HPRN-CT-2002-00282, is acknowledged.

the problem thus needs to be regularized such that it becomes well posed. The method used here to regularize and to solve the inverse problem is based on the work [7, 8, 15, 16] where the inverse problem is formulated as an optimal control problem and the corresponding Hamilton-Jacobi equation is used to construct a regularization, to obtain convergence results, and to finally solve the regularized problem by using the method of characteristics, *i.e.* to solve the corresponding Hamiltonian system.

The paper is stuctured as follows: In Section 2 the general theory of optimal control of partial differential equations and Hamilton-Jacobi-Bellman is presented. In Section 3 the idea of how to optimally control the heat equation is discussed together with numerical examples, and in Section 4 the control of the wave equation is treated.

2. Optimal Control and Dynamic Programming

Consider a differential equation constrained minimization problem with solution $\varphi : \Omega \times [0,T] \to \mathbb{R}$, $\varphi(\cdot,t) \in V$ and control $\sigma : \Omega \times [0,T] \to B$, $\sigma(\cdot,t) \in W$ for an open domain Ω, some Hilbert spaces V and W on Ω, and a closed bounded set $B \subset \mathbb{R}$:

$$\begin{aligned} &\min_{\sigma:\Omega\times[0,T]\to B} \int_0^T h(\varphi,\sigma)\ \mathrm{d}t + g(\varphi^T), \\ &\varphi_t = f(\varphi,\sigma), \end{aligned} \tag{1}$$

with $\varphi^T := \varphi(\cdot,T)$ and given initial value $\varphi^0 = \varphi(\cdot,0)$. Here, φ_t denotes the partial derivative with respect to time, $f : V \times W \to V$ is the flux, and $h : V \times W \to \mathbb{R}$, $g : V \to \mathbb{R}$ are given functions.

This optimal control problem can be solved either directly using constrained minimization or by dynamic programming. The Lagrangian becomes

$$L(\varphi,\lambda,\sigma) := \int_0^T \langle \lambda, f(\varphi,\sigma) - \varphi_t \rangle + h(\varphi,\sigma)\ \mathrm{d}t,$$

with Lagrange multiplier $\lambda : \Omega \times [0,T] \to \mathbb{R}$, $\lambda(\cdot,t) \in V$, and the constrained minimization method is based on the Pontryagin method

$$\begin{aligned} \varphi_t &= f(\varphi,\sigma), \\ \lambda_t &= -\langle \lambda, f_\varphi(\varphi,\sigma)\rangle + h_\varphi(\varphi,\sigma), \\ \sigma(\cdot,t) &\in \operatorname*{argmin}_{a:\Omega\to B} \{\langle \lambda, f(\varphi,a)\rangle + h(\varphi,a)\}. \end{aligned} \tag{2}$$

with given initial value φ^0, final value $\lambda^T := \lambda(\cdot,T) = g_\varphi(\varphi^T)$, and where f_φ, h_φ denotes the Gateaux derivatives with respect to φ and $\langle v,w\rangle$ is the duality pairing on V, which reduces to the $L^2(\Omega)$ inner product if $v,w \in L^2(\Omega)$. For a differentiable Lagrangian that is convex in σ the Pontryagin principle coincides with the Lagrangian formulation for a constrained interior minimum

$$\begin{aligned} \varphi_t &= f(\varphi,\sigma), \\ \lambda_t &= -\langle \lambda, f_\varphi(\varphi,\sigma)\rangle + h_\varphi(\varphi,\sigma) \\ 0 &= \langle \lambda, f_\sigma(\varphi,\sigma)\rangle + h_\sigma(\varphi,\sigma), \\ \sigma &\in B, \end{aligned} \tag{3}$$

but in general (2) and (3) may have different solutions φ,λ,σ although both describe necessary conditions for a minimizer to (1). If an explicit minimizer in (2) can be found the Pontryagin principle gives additional information about the control.

Pontryagin's minimum principle can also be written as a Hamiltonian system, see [2],

$$\begin{aligned} \varphi_t &= H_\lambda(\varphi, \lambda) \\ \lambda_t &= -H_\varphi(\varphi, \lambda) \end{aligned} \tag{4}$$

with φ^0 given, $\lambda^T = g_\varphi(\varphi^T)$, and the Hamiltonian $H : V \times V \to \mathbb{R}$ defined as

$$H(\lambda, \varphi) \quad := \min_{a:\Omega \to B} \{\langle \lambda, f(\varphi, a)\rangle + h(\varphi, a)\}. \tag{5}$$

The alternative dynamic programming method is based on the value function $U : V \times [0, T] \to \mathbb{R}$,

$$U(\phi, \tau) := \inf_{\sigma:\Omega\times[\tau,T]\to B} \left\{ \int_\tau^T h(\varphi, \sigma)\ \mathrm{d}t + g(\varphi^T) \;\middle|\; \varphi_t = f(\varphi, \sigma),\ \varphi(\cdot, \tau) = \phi \in V \right\}$$

which solves the nonlinear Hamilton-Jacobi-Bellman equation

$$\partial_t U(\phi, t) + H\big(U_\phi(\phi, t), \phi\big) = 0, \quad U(\phi, T) = g(\phi), \tag{6}$$

with Hamiltonian defined as in (5). Note that solving the Hamiltonian system (4) is the method of characteristics for the Hamilton-Jacobi equation (6), with $\lambda(x, t) = U_\varphi(\varphi(x, t), t)$. In general, the value function is however not everywhere differentiable and the multiplier λ becomes ill defined in a classical sense.

The Hamilton-Jacobi formulation (6) has the advantages that there is a complete well-posedness theory for Hamilton-Jacobi equations, based on non-differential viscosity solutions, see [9], and it finds a global minimum. However, (6) is not computationally feasible for problems in high dimension, such as the case where φ is an approximation of a solution to a partial differential equation. The Hamiltonian form (4) has the advantage that it is computationally feasible but the drawbacks are that it only focuses on local minima and that the Hamiltonian (5) in general only is Lipschitz continuous, even if f, g and h are smooth, which means that the optimal control depends discontinuously on (λ, φ) and (4) becomes undefined where the Hamiltonian is not differentiable.

In the following sections we will use a regularized version of (4) to iteratively solve the nonlinear constrained optimization problem (1).

3. Parameter Reconstruction for the Heat Equation

A distributed parameter reconstuction problem for the heat equation is to find a heat conductivity (the control) *e.g.* $\sigma : \bar{\Omega} \times [0, T] \to [\sigma_-, \sigma_+]$, $\sigma(\cdot, t) \in W$, $0 < \sigma_- < \sigma_+$, and a temperature distribution (the state) $u : \bar{\Omega} \times [0, T] \to \mathbb{R}$, $u(\cdot, t) \in V$ that satifies the heat equation

$$\begin{aligned} u_t &= \operatorname{div}(\sigma \nabla u), && \text{in } \Omega \times (0, T], \\ \sigma \nabla u \cdot \mathbf{n} &= j, && \text{on } \partial\Omega \times (0, T], \\ u &= 0, && \text{on } \bar{\Omega} \times \{t = 0\}, \end{aligned} \tag{7}$$

such that the error functional

$$\int_0^T \int_{\partial\Omega} (u - u^*)^2\ \mathrm{d}s\ \mathrm{d}t, \tag{8}$$

is minimized. The function $u^* = u^*(x, t)$ often represents physical measurements contaminated by some noise, *e.g.* $u^*(x, t) = u_{true}(x, t) + w(x, t)$ where w is a noise term and u_{true} satisfies the above heat equation for some unknown parameter σ_{true}, and in practice the control is only spacially dependent, $\sigma_{true} = \sigma_{true}(x)$. The primary goal is thus to determine the unknown diffusion coefficient σ_{true} and the method to do so is to minimize the objective functional (8).

Inverse problems like (7), (8) are in general ill-posed due to one or more of the following reasons:

(1) There exists no minimizer (u, σ), something that may occur with noisy data. Given unperturbed data u^* corresponding to σ_{true}, it is evident that there exists a minimizer to (7), (8).
(2) The minimizer is not unique, *e.g.* although it may be possible to find an optimal state that minimizes (8), u and σ may not be unique in Ω.
(3) The solution (u, σ), and particularly the control σ, depends discontinuously on data u^*.

A simple and common way to impose well-posedness to many inverse problems is to add a Tikhonov regularization of the form $\epsilon\|\sigma\|^2_{L^2(\Omega\times(0,T))}$ for $\epsilon > 0$, to the objective functional (8), see [1, 10, 14, 17]. Using the Pontryagin principle presented in the previous section we will in Section 3.2 regularize the inverse problem (7), (8) in a way that is comparable to a Tikhonov regularization.

Formulated as an optimal control problem the most natural assumption on the control σ is that it is dependent on both time and space but as we will see in Section 3.3 it is also possible to let $\sigma = \sigma(x)$, $\sigma = \sigma(t)$, or even let σ be constant in time and space.

3.1. **The Hamiltonian System.** Following Section 2 the Hamiltonian associated to the optimal control problem (7) and (8) is

$$\begin{aligned} H(u,q,t) &:= \min_{\sigma:\Omega\to[\sigma_-,\sigma_+]} \int_{\partial\Omega} (u-u^*)^2 \,\mathrm{d}s + \int_\Omega \operatorname{div}(\sigma\nabla u) q \,\mathrm{d}x \\ &= \int_{\partial\Omega} (u-u^*)^2 + jq \,\mathrm{d}s + \min_{\sigma:\Omega\to[\sigma_-,\sigma_+]} \int_\Omega -\sigma\nabla u\cdot\nabla q \,\mathrm{d}x \\ &= \int_{\partial\Omega} (u-u^*)^2 + jq \,\mathrm{d}s - \int_\Omega \underbrace{\max_{\sigma\in[\sigma_-,\sigma_+]} \{\sigma\nabla u\cdot\nabla q\}}_{\mathfrak{h}(\nabla u\cdot\nabla q)} \,\mathrm{d}x. \end{aligned} \tag{9}$$

and the Hamiltonian system, in strong form, then becomes

$$\begin{aligned} u_t &= \operatorname{div}\big(\tilde\sigma\nabla u\big), && \text{in } \Omega\times(0,T], \\ \tilde\sigma\nabla u\cdot\mathbf{n} &= j, && \text{on } \partial\Omega\times(0,T], \\ u &= 0, && \text{on } \bar\Omega\times\{t=0\}, \\ -q_t &= \operatorname{div}\big(\tilde\sigma\nabla q\big), && \text{in } \Omega\times(0,T], \\ \tilde\sigma\nabla q\cdot\mathbf{n} &= 2(u-u^*), && \text{on } \partial\Omega\times(0,T], \\ q &= 0, && \text{on } \Omega\times\{t=T\}, \end{aligned} \tag{10}$$

with

$$\tilde\sigma := \mathfrak{h}'(\nabla u\cdot\nabla q). \tag{11}$$

It is here evident that the Hamiltonian only is Lipschitz continuous and the control $\tilde\sigma$ is a bang-bang type control which depends discontinuously on the solutions (u, q), see Figure 1. From the optimality conditions (3) an optimal solution has to satisfy $\nabla u\cdot\nabla q = 0$ and (10) is thus undefined since $\mathfrak{h}'(0)$ is set valued, which calls for a regularization.

3.2. **Regularization.** A simple regularization of the Hamiltonian system (10), and consequently of the Hamiltonian (9), is to approximate $\mathfrak{h}'$ with the parabolic function

$$\mathfrak{h}'_\delta(\nabla u \cdot \nabla q) := \underbrace{\frac{\sigma_+ + \sigma_-}{2}}_{\bar{\sigma}} + \underbrace{\frac{\sigma_+ - \sigma_-}{2}}_{\hat{\sigma}} \tanh(\frac{1}{\delta}\nabla u \cdot \nabla q), \tag{12}$$

for some small $\delta > 0$, see Figure 1. This regularization can be compared with a classic Tikhonov regularization where a small L^2-penalty of the control is added to the objective function (8), *i.e.* to minimize

$$\int_0^T \int_{\partial\Omega} (u - u^*)^2 \, \mathrm{d}s \, \mathrm{d}t + \delta \int_0^T \int_\Omega \sigma^2 \, \mathrm{d}x \, \mathrm{d}t. \tag{13}$$

Minimizing (13) under the constraint (7) will lead to a C^2-Hamiltonian with

$$H(u,q,t) = \int_{\partial\Omega} (u - u^*)^2 + jq \, \mathrm{d}s - \int_\Omega \underbrace{\max_{\sigma\in[\sigma_-,\sigma_+]} \{\sigma(\nabla u \cdot \nabla q - \delta\sigma)\}}_{\mathfrak{h}_{Tikhonov}(\nabla u \cdot \nabla q)} \, \mathrm{d}x,$$

which can be seen in Figure 1.

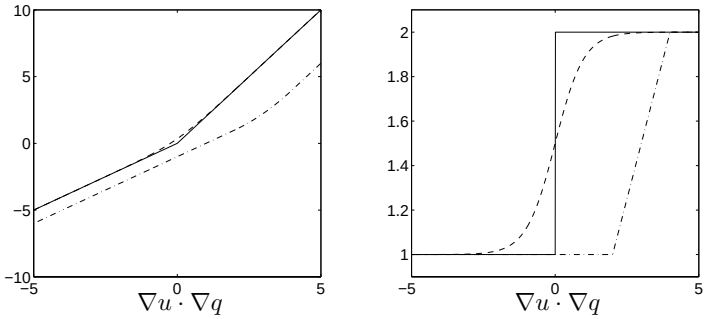

FIGURE 1. The functions $\mathfrak{h}$ (solid line), $\mathfrak{h}_\delta$ (dashed line), $\mathfrak{h}_{Tikhonov}$ (dash-dotted line) to the left and their derivatives to the right.

Another way to describe the simple regularization (12) is to see what kind of penalty on the objective function it corresponds to. We note that the regularized Hamiltionian system can be written as

$$\int_\Omega -u_t v - \mathfrak{h}'_\delta(\nabla u \cdot \nabla q)\nabla u \cdot \nabla v \, \mathrm{d}x + \int_{\partial\Omega} jv \, \mathrm{d}s = 0, \quad \forall v \in V,$$
$$\int_\Omega q_t v - \mathfrak{h}'_\delta(\nabla u \cdot \nabla q)\nabla q \cdot \nabla v \, \mathrm{d}x + \int_{\partial\Omega} 2(u - u^*)v \, \mathrm{d}s = 0, \quad \forall v \in V,$$

or by a redefinition of σ

$$\begin{aligned} \int_\Omega -u_t v - \sigma\nabla u \cdot \nabla v \, \mathrm{d}x + \int_{\partial\Omega} jv \, \mathrm{d}s = 0, \quad & \forall v \in V, \\ \int_\Omega q_t v - \sigma\nabla q \cdot \nabla v \, \mathrm{d}x + \int_{\partial\Omega} 2(u - u^*)v \, \mathrm{d}s = 0, \quad & \forall v \in V, \\ \int_\Omega \Big(\sigma - \mathfrak{h}'_\delta(\nabla u \cdot \nabla q)\Big)v \, \mathrm{d}x = 0, \quad & \forall v \in W. \end{aligned} \tag{14}$$

Let $\mathfrak{H}$ be the primitive function of the inverse function of $\mathfrak{h}'_\delta$ *i.e.*

$$\mathfrak{H}(\sigma) := \frac{\delta}{2\hat{\sigma}}\bigg((\sigma-\sigma_-)\ln\Big(\frac{\sigma-\sigma_-}{\hat{\sigma}}\Big)+(\sigma_+-\sigma)\ln\Big(\frac{\sigma_+-\sigma}{\hat{\sigma}}\Big)\bigg),$$

then it is evident that (14) can be seen as the first order optimality conditions for the problem to minimize

$$\int_0^T\int_{\partial\Omega}(u-u^*)^2\,\mathrm{d}s\,\mathrm{d}t+\int_0^T\int_\Omega\mathfrak{H}(\sigma)\,\mathrm{d}x\,\mathrm{d}t,$$

under the constraint (7). In Figure 2, the function $\mathfrak{H}(\sigma)$ is compared with a Tikhonov regularization of the form $\delta(\sigma-\bar{\sigma})^2$.

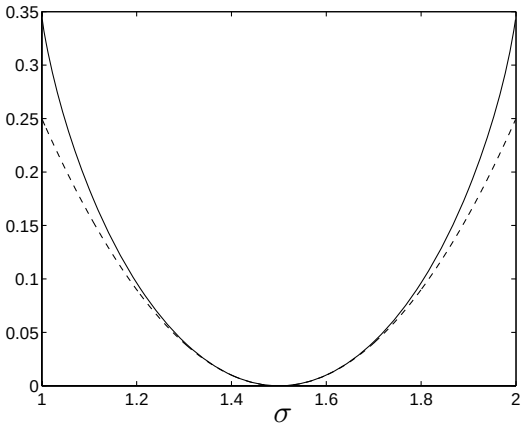

FIGURE 2. The function $\mathfrak{H}(\sigma)$ (solid line) compared to the L^2 penalty function $\delta(\sigma-\bar{\sigma})^2$ (dashed line) for $\delta=1$, $\sigma_-=1$ and $\sigma_+=2$.

It is often beneficial to prevent spacial oscillations of the coefficient by adding a penalty on the L^2-norm of the gradient of the coefficient, *i.e.* $\epsilon\|\nabla\sigma\|^2_{L^2(\Omega\times(0,T))}$, for $\epsilon>0$, to the objective function (8). For such a penalty the minimization in the corresponding Hamiltonian

$$H(u,q,t) := \min_{\sigma:\Omega\to[\sigma_-,\sigma_+]}\int_{\partial\Omega}(u-u^*)^2\,\mathrm{d}s+\int_\Omega \mathrm{div}(\sigma\nabla u)q+\epsilon|\nabla\sigma|^2\,\mathrm{d}x, \tag{15}$$

can not be done explicitly, and instead taking the first variation in σ would give the system

$$\begin{aligned} u_t &= \mathrm{div}\big(\sigma\nabla u\big),\\ -q_t &= \mathrm{div}\big(\sigma\nabla q\big),\\ 2\epsilon\Delta\sigma &= -\nabla u\cdot\nabla q,\\ \sigma &\in [\sigma_-,\sigma_+]. \end{aligned}$$

which corresponds to the usual first order optimality conditions for the Lagrangian. How to treat different penalties on the control in an optimal control setting is discussed in Section 3.4.

3.3. **Time Independent Control.** To study the case when the control σ is independent of time we first assume that it not only is independent of time but also depends on an auxilliary variable z, *i.e.* $\sigma : \bar{\Omega} \times [0, \tilde{T}] \to [\sigma_-, \sigma_+]$, $\sigma = \sigma(x, z)$. For a moment we also assume that $u : \bar{\Omega} \times [0, T] \times [0, \tilde{T}] \to \mathbb{R}$, $u = u(x, t, z)$, but with the same measurements as in (8). If we treat z as the time and t as a spacial variable we can define the optimal control problem

$$\min_{\sigma:\bar{\Omega}\times[0,\tilde{T}]\to[\sigma_-,\sigma_+]} \frac{1}{\tilde{T}} \int_0^{\tilde{T}} \int_0^T \int_{\partial\Omega} (u - u^*)^2 \, \mathrm{d}s \, \mathrm{d}t \, \mathrm{d}z, \tag{16}$$

where the state u satisfies the partial differential equation

$$\begin{aligned} u_z &= \frac{1}{\tilde{T}}\Big(\operatorname{div}(\sigma \nabla u) - u_t\Big), && \text{in } \Omega \times (0, T) \times (0, \tilde{T}], \\ \sigma \nabla u \cdot \mathbf{n} &= j, && \text{on } \partial\Omega \times (0, T) \times (0, \tilde{T}], \\ u &= 0, && \text{on } \bar{\Omega} \times \{t = 0\} \times (0, \tilde{T}], \\ u &= u_0, && \text{on } \bar{\Omega} \times (0, T) \times \{z = 0\}. \end{aligned} \tag{17}$$

for some arbitrary initial condition $u(x, t, 0) = u_0$.

The Hamiltonian for (16), (17) is

$$\begin{aligned} H(u, q, z) :=& \min_{\sigma:\Omega\to[\sigma_-,\sigma_+]} \frac{1}{\tilde{T}} \int_0^T \int_{\partial\Omega} (u - u^*)^2 \, \mathrm{d}s \, \mathrm{d}t \\ &+ \frac{1}{\tilde{T}} \int_0^T \int_\Omega \Big(\operatorname{div}(\sigma \nabla u) - u_t\Big) q \, \mathrm{d}x \, \mathrm{d}t \\ =& \frac{1}{\tilde{T}} \int_0^T \int_{\partial\Omega} (u - u^*)^2 + jq \, \mathrm{d}s \, \mathrm{d}t - \frac{1}{\tilde{T}} \int_0^T \int_\Omega u_t q \, \mathrm{d}x \, \mathrm{d}t \\ &- \frac{1}{\tilde{T}} \int_\Omega \underbrace{\max_{\sigma\in[\sigma_-,\sigma_+]} \left\{ \sigma \int_0^T \nabla u \cdot \nabla q \, \mathrm{d}t \right\}}_{\mathfrak{h}\left(\int_0^T \nabla u \cdot \nabla q \, \mathrm{d}t\right)} \mathrm{d}x, \end{aligned} \tag{18}$$

and the Hamiltonian system is given by

$$\begin{aligned} u_z &= \frac{1}{\tilde{T}}\Big(\operatorname{div}(\mathfrak{h}' \nabla u) - u_t\Big), && \text{in } \Omega \times (0, T) \times (0, \tilde{T}], \\ \mathfrak{h}' \nabla u \cdot \mathbf{n} &= j, && \text{on } \partial\Omega \times (0, T) \times (0, \tilde{T}], \\ u &= 0, && \text{on } \bar{\Omega} \times \{t = 0\} \times (0, \tilde{T}], \\ u &= u_0, && \text{on } \bar{\Omega} \times (0, T) \times \{z = 0\}, \\ -q_z &= \frac{1}{\tilde{T}}\Big(\operatorname{div}(\mathfrak{h}' \nabla q) + q_t\Big), && \text{in } \Omega \times (0, T) \times (0, \tilde{T}], \\ \mathfrak{h}' \nabla q \cdot \mathbf{n} &= 2(u - u^*), && \text{on } \partial\Omega \times (0, T) \times (0, \tilde{T}], \\ q &= 0, && \text{on } \bar{\Omega} \times \{t = T\} \times (0, \tilde{T}], \\ q &= 0, && \text{on } \bar{\Omega} \times (0, T) \times \{z = \tilde{T}\}. \end{aligned} \tag{19}$$

Under the assumption that the solutions u and q in (19) are asymptotically stationary as $\tilde{T} \to \infty$, the Hamiltonian system for the problem (7), (8), with a time-independent control, is given by (10) and

$$\tilde{\sigma} := \mathfrak{h}'\Big(\int_0^T \nabla u \cdot \nabla q \, \mathrm{d}t \Big). \tag{20}$$

Similarly, the case of a space independent coefficient $\sigma = \sigma(t)$ will lead to

$$\tilde{\sigma} := \mathfrak{h}'\Big(\frac{1}{|\Omega|}\int_\Omega \nabla u \cdot \nabla q \ \mathrm{d}x\Big),$$

and for the case where σ is constant

$$\tilde{\sigma} := \mathfrak{h}'\Big(\frac{1}{|\Omega|}\int_0^T\int_\Omega \nabla u \cdot \nabla q \ \mathrm{d}x \ \mathrm{d}t\Big).$$

3.4. **Penalty on the Control.** If we want to reconstruct a time independent control it can be beneficial to put a penalty on σ_t, *i.e.* we want to minimize the objective functional

$$F(u,\sigma_t) := \int_0^T\int_{\partial\Omega}(u-u^*)^2 \ \mathrm{d}s \ \mathrm{d}t + \varepsilon\int_0^T\int_\Omega \sigma_t^2 \ \mathrm{d}x \ \mathrm{d}t, \tag{21}$$

under the usual constraint (7). To do this the optimal control problem has to be reformulated such that σ is a state variable and the control is defined as $z := \sigma_t(x,t)$, $z : \bar{\Omega}\times[0,T] \to [z_-, z_+]$. The optimal control problem is thus to find a control z and state variables u and σ such that $F(u,z)$ is minimized and the system

$$\begin{aligned}
u_t &= \operatorname{div}(\sigma\nabla u), && \text{in } \Omega\times(0,T],\\
\sigma_t &= z && \text{in } \Omega\times(0,T],\\
\sigma\nabla u\cdot\mathbf{n} &= j, && \text{on } \partial\Omega\times(0,T],\\
u &= 0, && \text{on } \bar{\Omega}\times\{t=0\},\\
\sigma &= \sigma_0 > 0, && \text{on } \bar{\Omega}\times\{t=0\}.
\end{aligned}$$

is satisfied. The Hamiltonian becomes

$$\begin{aligned}
H(u,q,\sigma,\lambda,t) &:= \min_{z:\Omega\to[z_-,z_+]}\int_{\partial\Omega}(u-u^*)^2 \ \mathrm{d}s + \int_\Omega \operatorname{div}(\sigma\nabla u)q + z\lambda + \varepsilon z^2 \ \mathrm{d}x\\
&= \int_{\partial\Omega}(u-u^*)^2 + jq \ \mathrm{d}s - \int_\Omega \sigma\nabla u\cdot\nabla q \ \mathrm{d}x\\
&\quad + \int_\Omega \underbrace{\min_{z:\Omega\to[z_-,z_+]}\{z(\varepsilon z+\lambda)\}}_{\mathfrak{h}(\lambda)} \ \mathrm{d}x,
\end{aligned}$$

and the corresponding Hamiltonian system is

$$\begin{aligned}
u_t &= \operatorname{div}\big(\sigma\nabla u\big), && \text{in } \Omega\times(0,T],\\
\sigma_t &= \mathfrak{h}'(\lambda) && \text{in } \Omega\times(0,T],\\
\sigma\nabla u\cdot\mathbf{n} &= j, && \text{on } \partial\Omega\times(0,T],\\
u &= 0, && \text{on } \bar{\Omega}\times\{t=0\},\\
\sigma &= \sigma_0 > 0, && \text{on } \bar{\Omega}\times\{t=0\}.\\
-q_t &= \operatorname{div}\big(\sigma\nabla q\big), && \text{in } \Omega\times(0,T],\\
-\lambda_t &= -\nabla u\cdot\nabla q && \text{in } \Omega\times(0,T],\\
\sigma\nabla q\cdot\mathbf{n} &= 2(u-u^*), && \text{on } \partial\Omega\times(0,T],\\
q &= 0, && \text{on } \Omega\times\{t=T\},\\
\lambda &= 0, && \text{on } \Omega\times\{t=T\},
\end{aligned}$$

which is equivalent to (10) with

$$\tilde{\sigma} := \sigma_0 + \int_0^t \mathfrak{h}'\Big(\int_y^T -(\nabla u\cdot\nabla q)(x,z) \ \mathrm{d}z\Big) \ \mathrm{d}y.$$

Note, since we no longer have a constraint $\sigma > 0$, the bound z_- has to be carefully chosen to ensure well-posedness of the forward problem.

In a similar fashion as for penalizing temporal variations of the control it is also possible to penalize spacial variations, as was briefly mentioned in Section 3.2, where the objective was to minimize $F(u, |\nabla\sigma|)$ under the constraint (7), which leads to the Hamiltonian (15). To be able to explicitly find the minimum in the Hamiltonian we once again let σ act as a state variable, introduce the control z and the dynamics

$$\begin{aligned} \sigma_t &= \frac{z - |\nabla\sigma|^2}{\gamma}, \qquad \text{in } \Omega \times (0, T], \\ \sigma &= \sigma_0 > 0, \qquad \text{in } \Omega \times \{t = 0\}, \end{aligned} \tag{22}$$

for $\gamma > 0$. The slightly perturbed control problem is now to minimize the objective function $F(u, z)$ such that (7) and (22) holds, which leads to the Hamiltonian

$$\begin{aligned} H(u, q, \sigma, \lambda, t) &:= \min_{z:\Omega\to[z_-,z_+]} \int_{\partial\Omega} (u - u^*)^2 \, \mathrm{d}s + \int_\Omega \operatorname{div}(\sigma\nabla u)q + \lambda\frac{z - |\nabla\sigma|^2}{\gamma} + \varepsilon z \, \mathrm{d}x \\ &= \int_{\partial\Omega} (u - u^*)^2 + jq \, \mathrm{d}s - \int_\Omega \sigma\nabla u \cdot \nabla q + \lambda\frac{|\nabla\sigma|^2}{\gamma} \, \mathrm{d}x \\ &\quad + \int_\Omega \underbrace{\min_{z:\Omega\to[z_-,z_+]} \{z(\varepsilon + \frac{\lambda}{\gamma})\}}_{\mathfrak{h}(\lambda)} \, \mathrm{d}x, \end{aligned}$$

and the Hamiltonian system

$$\begin{aligned} u_t &= \operatorname{div}\big(\sigma\nabla u\big), \\ \sigma_t &= \mathfrak{h}'(\lambda) - \frac{|\nabla\sigma|^2}{\gamma}, \\ -q_t &= \operatorname{div}\big(\sigma\nabla q\big), \\ -\lambda_t &= \nabla u \cdot \nabla q - 2\lambda\frac{\Delta\sigma}{\gamma}. \end{aligned}$$

3.5. **Numerical Approximation and Symplectic Methods.** Let $\bar{V} \subset V := H^1(\Omega)$ be the finite element subspace of piecewise linear functions defined on a triangulation of Ω, which implies that our optimal control problems in the previous sections are approximated by optimal control problems for ordinary differential equations. We also let the functions $\mathfrak{h}_\delta$,H^δ and h_δ denote the regularized counterparts to $\mathfrak{h}$,H and h. The regularized version of $\mathfrak{h}$ is given by (12) from which the definition of H^δ follows. The regularized function h_δ can be derived from H^δ by $h_\delta := H^\delta - \langle\lambda, H^\delta_\lambda\rangle$ and a regularized version of f can be defined as $f_\delta := H^\delta_\lambda$.

Now, introduce the uniform partition $\{t_i = ki\}_{i=0}^N$, $k = T/N$ of the time interval $[0, T]$, and the corresponding finite element approximations at each time step $\varphi_n := \varphi(t_n), \lambda_n := \lambda(t_n)$. Also define a discrete regularized version $\bar{U} : \bar{V} \times [0, T] \to \mathbb{R}$ of the value function (2),

$$\bar{U}(\phi, t_m) := \min_{\varphi_m = \phi} \left\{ g(\varphi_N) + k \sum_{n=m}^{N-1} h_\delta(\varphi_n, \lambda_{n+1}) \right\},$$

where φ_n and λ_n satisfy a symplectic scheme, *e.g.* the symplectic forward Euler method

$$\begin{aligned} \varphi_{n+1} - \varphi_n &= kH^\delta_\lambda(\varphi_n, \lambda_{n+1}), \quad \text{for } n = m, \dots, N-1 \text{ given } \varphi_m = \phi, \\ \lambda_n - \lambda_{n+1} &= kH^\delta_\varphi(\varphi_n, \lambda_{n+1}), \quad \text{for } n = m, \dots, N-1 \text{ given } \lambda_N = g_\varphi(\varphi_N). \end{aligned} \tag{23}$$

Symplecticity here means that $\bar{U}_\varphi(\varphi_n, t_n) = \lambda_n$, *i.e.* the gradient of the discrete value function coincides with the discrete dual λ_n, and given that $|H - H^\delta| = \mathcal{O}(\delta)$ it can be shown that for symplectic one-step schemes

$$\left| U(\varphi_0, t_0) - g(\varphi_N) - k \sum_{n=m}^{N-1} h_\delta(\varphi_n, \lambda_{n+1}) \right| = \mathcal{O}(k),$$

for $\delta \sim k$, see [15]. It is thus essential to use a symplectic time discretization of the regularized Hamiltonian system

$$\begin{aligned} \varphi_t &= H^\delta_\lambda(\varphi, \lambda), \\ \lambda_t &= -H^\delta_\varphi(\varphi, \lambda), \end{aligned}$$

in order to have convergence in the value function.

Some examples of other symplectic schemes are the the backward Euler method

$$\begin{aligned} \varphi_{n+1} - \varphi_n &= k H^\delta_\lambda(\varphi_{n+1}, \lambda_n), \quad \text{for } n = 0, \dots, N-1 \text{ given } \varphi_0, \\ \lambda_n - \lambda_{n+1} &= k H^\delta_\varphi(\varphi_{n+1}, \lambda_n), \quad \text{for } n = 0, \dots, N-1 \text{ given } \lambda_N, \end{aligned} \tag{24}$$

and the implicit midpoint method

$$\begin{aligned} \varphi_{n+1} - \varphi_n &= k H^\delta_\lambda\left(\frac{\varphi_n + \varphi_{n+1}}{2}, \frac{\lambda_n + \lambda_{n+1}}{2} \right), \quad n = 0, \dots, N-1, \text{ given } \varphi_0, \\ \lambda_n - \lambda_{n+1} &= k H^\delta_\varphi\left(\frac{\varphi_n + \varphi_{n+1}}{2}, \frac{\lambda_n + \lambda_{n+1}}{2} \right), \quad n = 0, \dots, N-1, \text{ given } \lambda_N. \end{aligned} \tag{25}$$

See [12] for a thorough description of symplectic methods.

3.6. **The Newton Method.** To solve the coupled nonlinear symplectic schemes (23)-(25) above, it is tempting to propose fix-point schemes that partly removes the coupling between the forward and bacward equation, *e.g.* by iterating separately in φ and λ. Such methods has the advantage that existing partial differential equation solvers can be used to efficiently solve the forward and backward problems in each iteration, but the disadvantage is that the convergence to an optimal solution tends to be slow, and also dependent on the discretization. A more suitable strategy is to use information of the Hessian of H^δ; *e.g.* Quasi-Newton methods, or since the Hessian in our case can be found explicitly and is sparse, the Newton method itself.

For the Hamiltonian system (10) with $\tilde{\sigma} := \mathfrak{h}'_\delta$ given by (12) the symplectic backward Euler can be written as

$$F_n(w) = 0, \quad G_n(w) = 0, \quad n = 0, \dots, N-1, \quad \forall w \in \bar{V}$$

where

$$\begin{aligned} F_n(w) &:= \int_\Omega (u_{n+1} - u_n) w + k \mathfrak{h}'_\delta(\nabla u_{n+1} \cdot \nabla q_n) \nabla u_{n+1} \cdot \nabla w \, \mathrm{d}x \\ &\quad - \int_{\partial\Omega} k j_{n+1} w \, \mathrm{d}s, \\ G_n(w) &:= \int_\Omega (q_n - q_{n+1}) w + k \mathfrak{h}'_\delta(\nabla u_{n+1} \cdot \nabla q_n) \nabla q_n \cdot \nabla w \, \mathrm{d}x \\ &\quad - \int_{\partial\Omega} 2k(u_{n+1} - u^*_{n+1}) w \, \mathrm{d}s, \end{aligned} \tag{26}$$

and $u_0 = q_N = 0$. Given an initial guess $u[0]$, $q[0]$ the (damped) Newton method yields that

$$\begin{aligned} u[i+1] &= u[i] - \alpha \hat{u}, \\ q[i+1] &= q[i] - \alpha \hat{q}, \end{aligned}$$

where $\alpha \in (0, 1]$ and, for each iteration, the updates $\hat{u}$ and $\hat{q}$ solve a linear system of the form

$$\begin{pmatrix} K_{11} & K_{12} \\ K_{21} & K_{11}^T \end{pmatrix} \begin{pmatrix} \hat{u} \\ \hat{q} \end{pmatrix} = \begin{pmatrix} f \\ g \end{pmatrix}, \tag{27}$$

where

$$\hat{u} = \begin{pmatrix} \hat{u}_1 & \dots & \hat{u}_N \end{pmatrix}^T, \qquad \hat{q} = \begin{pmatrix} \hat{q}_0 & \dots & \hat{q}_{N-1} \end{pmatrix}^T,$$
$$f = \begin{pmatrix} F_0 & \dots & F_{N-1} \end{pmatrix}^T, \quad g = \begin{pmatrix} G_0 & \dots & G_{N-1} \end{pmatrix}^T.$$

The matrix K_{11} is a bi-diagonal block matrix with $M + S_i$ for $i = 0, \dots, N-1$ on the diagonal and $-M$ on the sub-diagonal, where M denotes the mass matrix

$$\int_\Omega w\bar{w} \, \mathrm{d}x,$$

and

$$S_n := \int_\Omega k\mathfrak{h}_\delta''(\nabla u_{n+1} \cdot \nabla q_n)\nabla q_n \cdot \nabla w \; \nabla u_{n+1} \cdot \nabla \bar{w} \, \mathrm{d}x + \int_\Omega k\mathfrak{h}_\delta'(\nabla u_{n+1} \cdot \nabla q_n)\nabla w \cdot \nabla \bar{w} \, \mathrm{d}x.$$

for $w, \bar{w} \in \bar{V}$. The matrices K_{12}, K_{21} are symmetric block-diagonal matrices with

$$\int_\Omega k\mathfrak{h}_\delta''(\nabla u_{n+1} \cdot \nabla q_n)\nabla u_{n+1} \cdot \nabla w \; \nabla u_{n+1} \cdot \nabla \bar{w} \, \mathrm{d}x,$$

and

$$\int_\Omega k\mathfrak{h}_\delta''(\nabla u_{n+1} \cdot \nabla q_n)\nabla q_n \cdot \nabla w \; \nabla q_n \cdot \nabla \bar{w} \, \mathrm{d}x - \int_{\partial\Omega} 2k\bar{w}w \, \mathrm{d}s,$$

for $n = 0, \dots, N-1$ on the the diagonals, respectively.

If we repartition the block 2×2 linear system (27) to

$$\begin{pmatrix} K_{21} & K_{11}^T \\ K_{11} & K_{12} \end{pmatrix} \begin{pmatrix} \hat{u} \\ \hat{q} \end{pmatrix} = \begin{pmatrix} g \\ f \end{pmatrix}, \tag{28}$$

we see that it is a generalized saddle point system [4] with symmetric matrices K_{21}, K_{12}, and $K_{11}^T \neq 0$, $K_{21} \neq 0$. However, unlike saddle point problems arising from *e.g.* the steady-state Navier-Stokes equations or from the Karush-Kuhn-Tucker optimality conditions for equality constrained minimization problems, both K_{12} and K_{21} may here be indefinite and singular.

Since (27) and (28) are increasingly ill-conditioned with respect to reduction in mesh size, step size and regularization, the success of iterative algorithms like Krylov sub-space methods will depend heavily on the choice of preconditioner. Standard algebraic preconditioners like incomplete LU-factorization are often unsuitable for saddle-point problems due to the indefiniteness and lack of diagonal dominance, so the preconditioner must be tailored for the specific problem at hand. One popular approach for PDE-constrained optimization problems is to base the preconditioner on the solution from a reduced approximated problem where the Schur complement is replaced by an approximation *e.g.* by quasi-newton methods, see [5].

In our case we use the GMRES method to solve the non-symmetric system (27) and base our preconditioner on the approximate solution of a simple blockwise Gauss-Seidel method *i.e.* to start with a guess $\hat{q}^0$ and iteratively solve

$$\begin{aligned} K_{11}\hat{u}^{i+1} &= f - K_{12}\hat{q}^i, \\ K_{11}^T\hat{q}^{i+1} &= g - K_{21}\hat{u}^{i+1}, \end{aligned} \tag{29}$$

which works well for large regularizations *i.e.* when $\mathfrak{h}_\delta''$ is small and the diagonal blocks of (27) are dominant. Also, each iteration with this method only requires

one forward and one backward solve in time of a modified heat equation so the computational work for one iteration is concentrated to solving $N-1$ smaller systems with system matrices $(M+S_i)$. In practice, the Gauss-Seidel method will break down for small regularizations but for our problems (and discretizations) only one iteration with (29) turns out to be a fairly good approximation to use as preconditioner. Note that for $\hat{q}^0 = 0$, one Gauss-Seidel iteration is the same as solving (27) with the approximation $K_{12} = 0$.

Another more elaborate idea is to use a preconditioner based on the solution of an approximated Schur complement system

$$\begin{pmatrix} K_{11} & K_{12} \\ 0 & S \end{pmatrix} \begin{pmatrix} \hat{u} \\ \hat{q} \end{pmatrix} = \begin{pmatrix} g \\ f - K_{12}K_{11}^{-1}g \end{pmatrix},$$

where S is an approximation of the Schur complement

$$K_{11}^T - K_{21}K_{11}^{-1}K_{12}.$$

which essentially is to find a good approximation of the lower triangular block matrix K_{11}^{-1}.

Although solution algorithms for saddle point systems on the symmetric form (28) are extensively treated in the litterature, see [4] for an overview, we here favour the non-symmetric form (27), since a Schur complement reduction of (28) means to find an approximation to the Schur complement

$$K_{12} - K_{11}K_{21}^{-1}K_{11}^T,$$

which since K_{21} here can be singular, is unavailable. One way around this obstacle is to rewrite (28) by *e.g.* the augmented Lagrangian method which leads to a symmetric invertible Schur complement but where the physical meaning of the original system, on PDE level, is partially lost.

If a direct solver is used for the Newton system it is appropriate to reorder (27) such that the solution vector and right hand side contains time steps in increasing order, which leads to a banded Jacobian with band-width of the same order as the number of spacial degrees of freedom.

Our computations were implemented MATLAB (for the one dimensional examples), and in DOLFIN [13], the C++/Python interface of the finite element solver environment FEniCS [11] (for the two dimensional examples). Piecewise linear basis functions were used for the finite element subspace $\bar{V}$, and in all examples the solution u, q was first calculated for a large regularization which was succesively reduced such that the solution from the previous regularization served as starting guess for a smaller regularization.

For the two dimensional examples the sadde-point system (27) was solved with the PETSc implementation of GMRES (used by DOLFIN) with preconditioning based on the solution from one iteration of blockwise Gauss-Seidel method. For the one dimensional examples a direct solver was used. The number of iterations for GMRES with the Gauss-Seidel preconditioner seems to be relatively insensitive with respect to temporal and spacial discretization but still highly sensitive to the regularization in our examples.

To give a time independent approximation $\sigma(x)$ of the time dependent control $\sigma(x,t)$, approximated by $\tilde{\sigma} := \mathfrak{h}'_\delta(\nabla u \cdot \nabla q)$ where u, q are solutions to the Hamiltonian system (10), three different types of averaging were tested as post-processing:

(1) Let the time independent control be defined by the Hamiltonian (18), *i.e.*

$$\sigma := \mathfrak{h}'_\delta\Big(\int_0^T \nabla u \cdot \nabla q \, \mathrm{d}t \Big). \tag{30}$$

(2) Let the time independent control be the average of the time dependent control, *i.e.*

$$\sigma := \frac{1}{T}\int_0^T \mathfrak{h}'_\delta(\nabla u \cdot \nabla q)\ \mathrm{d}t. \tag{31}$$

(3) Let the time independent control be the weighted average

$$\sigma := \frac{\int_0^T \mathfrak{h}'_\delta(\nabla u \cdot \nabla q)|\nabla u \cdot \nabla q|\ \mathrm{d}t}{\int_0^T |\nabla u \cdot \nabla q|\ \mathrm{d}t}, \tag{32}$$

of the time dependent control $\mathfrak{h}'_\delta(\nabla u \cdot \nabla q)$.

The weighted average turned out to be the most successful aproximation and can be explained by first extending the Hamiltonian (9) to also depend on the artifical variable z as in Section 3.3

$$\begin{aligned} H(u,q,z) :=& \frac{1}{\bar{T}}\int_0^T \int_{\partial\Omega} (u-u^*)^2 + jq\ \mathrm{d}s\ \mathrm{d}t - \frac{1}{\bar{T}}\int_0^T \int_\Omega u_t q\ \mathrm{d}x\ \mathrm{d}t \\ & - \frac{1}{\bar{T}}\int_\Omega \int_0^T \mathfrak{h}'(\nabla u \cdot \nabla q)\nabla u \cdot \nabla q\ \mathrm{d}t\ \mathrm{d}x, \end{aligned}$$

where $\mathfrak{h}'(\nabla u \cdot \nabla q)\nabla u \cdot \nabla q = \mathfrak{h}(\nabla u \cdot \nabla q)$ by definition. For the problem with a time independent control we now seek an approximation of the Hamiltonian (18) of the form

$$\begin{aligned} \bar{H}(u,q,z) :=& \frac{1}{\bar{T}}\int_0^T \int_{\partial\Omega} (u-u^*)^2 + jq\ \mathrm{d}s\ \mathrm{d}t - \frac{1}{\bar{T}}\int_0^T \int_\Omega u_t q\ \mathrm{d}x\ \mathrm{d}t \\ & - \frac{1}{\bar{T}}\int_\Omega f(\nabla u \cdot \nabla q)\int_0^T \nabla u \cdot \nabla q\ \mathrm{d}t\ \mathrm{d}x, \end{aligned}$$

that best approximates H, *i.e.*

$$f(\nabla u \cdot \nabla q) := \frac{\int_0^T \mathfrak{h}'(\nabla u \cdot \nabla q)\nabla u \cdot \nabla q\ \mathrm{d}t}{\int_0^T \nabla u \cdot \nabla q\ \mathrm{d}t}.$$

In Figure 3, one dimensional reconstructions from three sets of simulated data u^*, generated from a time independent conductivity σ_{true}, are compared:

(1) Data calculated with the same discretization as u and q.
(2) Different discretizations used for data and solutions.
(3) Different discretizations used for data and solutions and with noise in the data u^*.

The last set is the most realistic one since for true experimental data of u^* it is inevitable to have noisy measurements. To simulate noise the discrete solution u^* was multiplied componentwise by independent standard normal distributed stochastic variables ε_{ij} according to $u^*(x_i,t_j)(1+\eta\epsilon_{ij})$, where η denotes the percentage of noise. It is notable that the systematic error from using different meshes can have a much bigger effect on the solutions than additional noise, which can be observed from the dual solution q in Figure 3.

In Figure 4 the time independent post-processing of the time dependent reconstruction can be found. It is here evident that the weighted average (32) performs better than (31), but since the reconstruction is highly dependent on the given boundary condition, see Figure 5 for comparison, there are situations where the different post-processing techniques perform equally well. It would of course be optimal to use the knowledge that σ_{true} is independent of time in the calculations, *i.e.* to use the Newtion system for (10) with time independent-control (20). This would however lead to a dense Jacobian.

Note that in the examples the limits σ_- and σ_+ were chosen to be the biggest and smallest values of σ_{true}. In our experience the Pontryagin method is not well suited for reconstruction of values between σ_- and σ_+, if there is noise or other measurement errors present in data.

Figure 6 shows two-dimensional reconstructions of two different time independent conductivities. Unlike the one-dimensional example the quality of the reconstruction here deteriorates quickly as the distance to the measurement locations is increased.

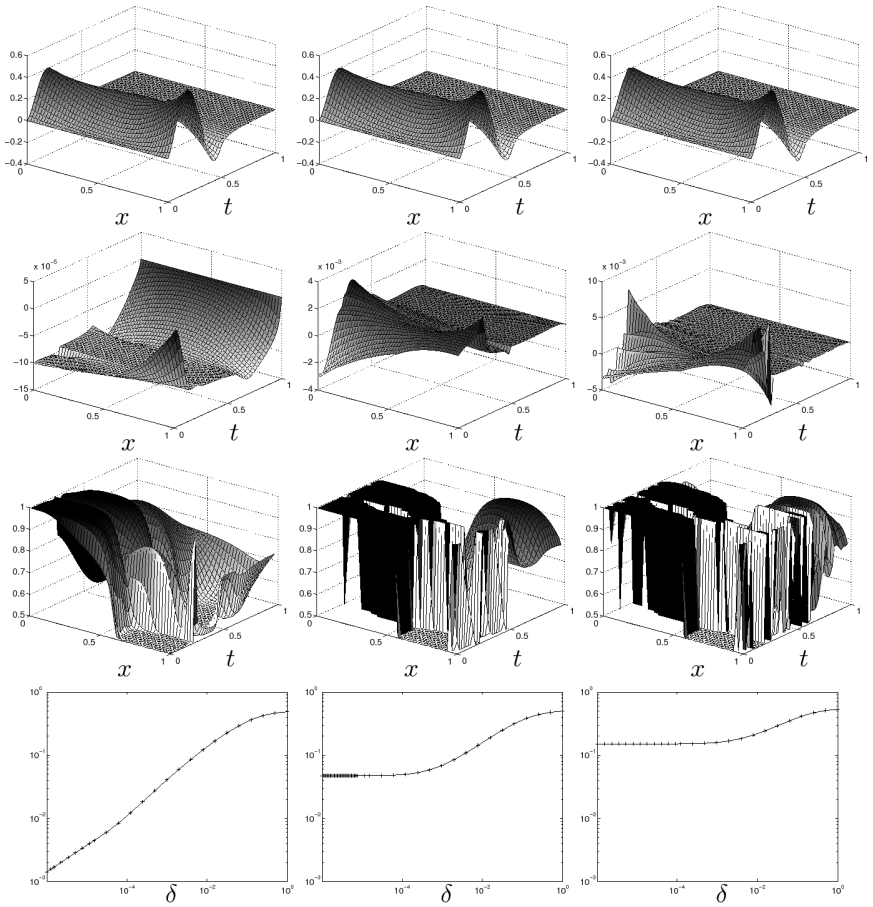

FIGURE 3. 1D reconstruction of $\sigma_{true} = 0.75 - 0.5\tanh(20x - 10)$ for $\delta = 10^{-6}$, $\sigma_- = 0.5$, and $\sigma_+ = 1$. Measurements were collected on both boundaries and the Neumann boundary condition was $\sigma u_x(0,t) = -\sigma u_x(1,t) = \sin(4t)$ for $t < 0.5$ and 0 elsewhere. The plot shows, from top to bottom, u, q, $\mathfrak{h}'_\delta$ and the objective function $\|u - u^*\|_{L^2(\partial\Omega\times[0,T])}$. In all cases u, q was calculated with 50 steps in space and time. In the left column, the data u^* was generated by solving the heat equation for σ_{true} with 50 steps in time and space, while 200 steps in time and space was used in the middle and right columns. In the right column 10% noise was also added to u^*.

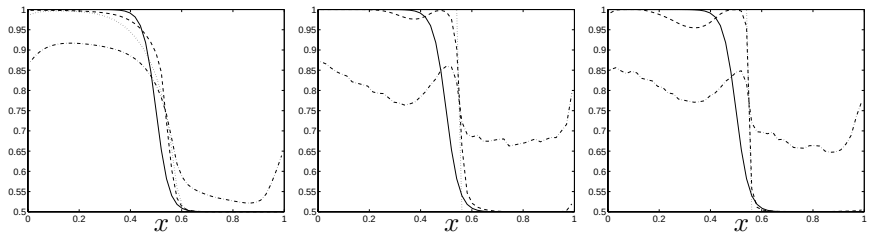

FIGURE 4. The time independent post-processed conductivity for the 1D reconstructions in Figure 3. The true control σ_{true} is indicated by a solid line and the averaged controls (30), (31) and (32) are indicated by dotted, dash-dotted and dashed lines, respectively.

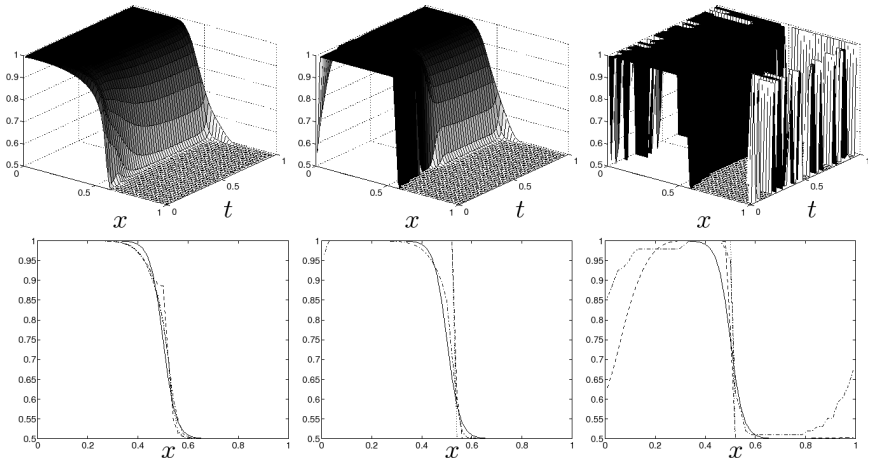

FIGURE 5. 1D reconstruction with data as in Figure 3 and 4 but with Neumann boundary condition $\sigma u_x(0,t) = -\sigma u_x(1,t) = 1$. The top row shows $\mathfrak{h}'_\delta$ and the bottom row the averaged conductivities, as described in Figure 4.

4. Reconstruction from the Wave Equation

In this section the goal is to determine the wave speed for a scalar acoustic wave equation: Given measured data u^*, find the state $u : \bar{\Omega} \times [0,T] \to \mathbb{R}$, $u(\cdot,t) \in V$ and a control $\sigma : \bar{\Omega} \times [0,T] \to [\sigma_-, \sigma_+]$, $\sigma = \sigma(x,t)$ where $0 < \sigma_- < \sigma_+$, that solves the partial differential equation

$$\begin{aligned} u_{tt} &= \operatorname{div}(\sigma \nabla u), && \text{in } \Omega \times (0,T], \\ \sigma \nabla u \cdot \mathbf{n} &= j, && \text{on } \partial\Omega \times (0,T], \\ u &= u_t = 0, && \text{on } \bar{\Omega} \times \{t = 0\}, \end{aligned} \tag{33}$$

such that the error functional

$$\int_0^T \int_{\partial\Omega} (u - u^*)^2 \, \mathrm{d}s \, \mathrm{d}t, \tag{34}$$

is minimized. The control σ is here the square of the wave speed of the medium and u is the pressure deviation.

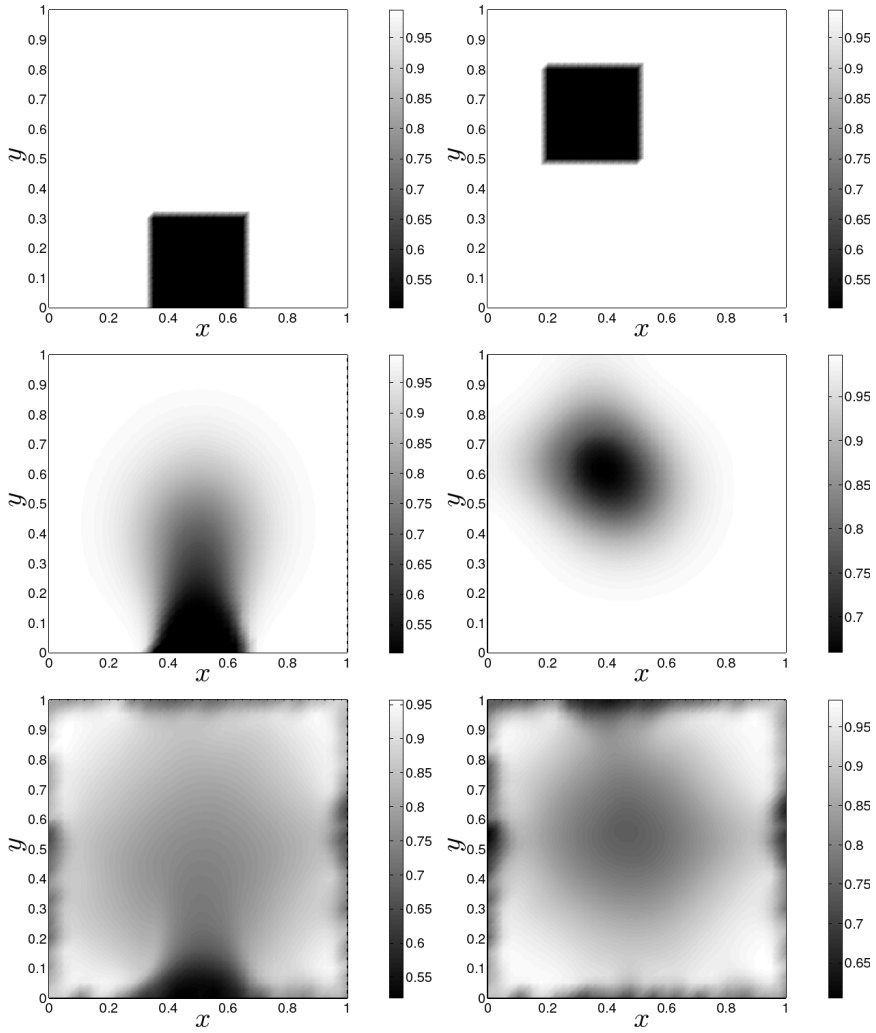

FIGURE 6. 2D reconstruction on the unit square with final time $T = 1$ and Neumann boundary condition $\sigma \frac{\partial u}{\partial n} = 1$ on $\partial\Omega \times [0, T]$. The data u^* was simulated by solving the forward equation on a quasi-uniform mesh with 13000 triangles and 80 time steps while the inverse problem was solved on a uniform mesh with 3200 triangles and 40 time steps. Measurements from the whole boundary were used. Top: True conductivity σ_{true}. Middle: Reconstructed condictivity for $\delta \approx 0.002$ using the weighted average (32). Bottom: As in middle but for $\delta \approx 0.05$ and with 5% noise in the measurements.

To use the framework of the previous section we note that (33) can be written as the first order system

$$
\begin{aligned}
v_t &= \operatorname{div}(\sigma \nabla u), && \text{in } \Omega \times (0, T], \\
u_t &= v, && \text{in } \bar{\Omega} \times (0, T], \\
\sigma \nabla u \cdot \mathbf{n} &= j, && \text{on } \partial\Omega \times (0, T], \\
u &= v = 0, && \text{on } \bar{\Omega} \times \{t = 0\}.
\end{aligned} \tag{35}
$$

4.1. **The Hamiltonian System.** As in Section 3.1 we have a Hamiltonian associated with the optimal control problem (34) and (35) which is defined by

$$\begin{aligned} H &:= \min_{\sigma:\Omega\to[\sigma_-,\sigma_+]} \int_{\partial\Omega} (u-u^*)^2 \,\mathrm{d}s + \int_\Omega \operatorname{div}(\sigma\nabla u)q + vp \,\mathrm{d}x \\ &= \int_{\partial\Omega} (u-u^*)^2 + jq \,\mathrm{d}s + \min_{\sigma:\Omega\to[\sigma_-,\sigma_+]} \int_\Omega -\sigma\nabla u\cdot\nabla q + vp \,\mathrm{d}x \\ &= \int_{\partial\Omega} (u-u^*)^2 + jq \,\mathrm{d}s + \int_\Omega vp - \underbrace{\max_{\sigma\in[\sigma_-,\sigma_+]} \{\sigma\nabla u\cdot\nabla q\}}_{\mathfrak{h}(\nabla u\cdot\nabla q)} \,\mathrm{d}x, \end{aligned} \tag{36}$$

and the Hamiltonian system becomes

$$\begin{aligned} v_t &= \operatorname{div}\big(\tilde\sigma\nabla u\big), && \text{in } \Omega\times(0,T], \\ u_t &= v, && \text{in } \bar\Omega\times(0,T], \\ \tilde\sigma\nabla u\cdot\mathbf{n} &= j, && \text{on } \partial\Omega\times(0,T], \\ u &= v = 0, && \text{on } \bar\Omega\times\{t=0\}, \\ -p_t &= \operatorname{div}\big(\tilde\sigma\nabla q\big), && \text{in } \Omega\times(0,T], \\ -q_t &= p, && \text{in } \bar\Omega\times(0,T], \\ \tilde\sigma\nabla q\cdot\mathbf{n} &= 2(u-u^*), && \text{on } \partial\Omega\times(0,T], \\ p &= q = 0, && \text{on } \Omega\times\{t=T\}, \end{aligned} \tag{37}$$

or equivalently

$$\begin{aligned} u_{tt} &= \operatorname{div}\big(\tilde\sigma\nabla u\big), && \text{in } \Omega\times(0,T], \\ \tilde\sigma\nabla u\cdot\mathbf{n} &= j, && \text{on } \partial\Omega\times(0,T], \\ u &= u_t = 0, && \text{on } \bar\Omega\times\{t=0\}, \\ q_{tt} &= \operatorname{div}\big(\tilde\sigma\nabla q\big), && \text{in } \Omega\times(0,T], \\ \tilde\sigma\nabla q\cdot\mathbf{n} &= 2(u-u^*), && \text{on } \partial\Omega\times(0,T], \\ q &= q_t = 0, && \text{on } \bar\Omega\times\{t=T\}. \end{aligned} \tag{38}$$

with

$$\tilde\sigma := \mathfrak{h}'(\nabla u\cdot\nabla q).$$

4.2. **Symplecticity for the Wave Equation.** As a natural case the symplectic methods discussed in 3.5, with $\varphi = (u, v)$, $\lambda = (p, q)$, can be used to solve the system (37). It is however also possible to use a time-discretization that is symmetric in time i.e.

$$\begin{aligned} u_{n+1} - 2u_n + u_{n-1} &= k^2\operatorname{div}\big(\tilde\sigma_n\nabla u_n\big), && \text{in } \Omega, \\ \tilde\sigma_n\nabla u_n\cdot\mathbf{n} &= j_n, && \text{on } \partial\Omega, \\ u_0 &= u_1 = 0, && \text{in } \Omega, \\ q_{n+1} - 2q_n + q_{n-1} &= k\operatorname{div}\big(\tilde\sigma_n\nabla q_n\big), && \text{in } \Omega, \\ \tilde\sigma_n\nabla q_n\cdot\mathbf{n} &= 2(u_n - u_n^*), && \text{on } \partial\Omega, \\ q_N &= q_{N-1} = 0, && \text{in } \Omega, \end{aligned} \tag{39}$$

for $\tilde\sigma_n := \mathfrak{h}'(\nabla u_n\cdot\nabla q_n)$ and $n = 1,\dots,N-1$. For a given $\tilde\sigma$, constant in time, this scheme is the symplectic backward Euler method for the forward wave equation for u, which can be written as the Hamiltonian system (35) with Hamiltonian

$$H_{wave}(u,v) := \frac{1}{2}\int_\Omega |\tilde\sigma\nabla u|^2 + v^2 \,\mathrm{d}x,$$

and the symplectic forward Euler method for the backward wave equation for q.

To see that that the scheme (39) is symplectic for $\tilde{\sigma}_n := \mathfrak{h}'(\nabla u_n \cdot \nabla q_n)$ we note that a one-step method $(\varphi_n, \lambda_n) \to (\varphi_{n+1}, \lambda_{n+1})$ is symplectic if there exists a function $H(\varphi_n, \lambda_{n+1})$ such that (23) holds, or equivalently $H(\varphi_{n+1}, \lambda_n)$ such that (24) holds, see Remark 4.8 in [15] or [12] for details. It thus follows that the one-step method

$$\begin{aligned} v_{n+1} - v_n &= k\mathrm{div}\big(\mathfrak{h}'(\nabla u_n \cdot \nabla q_n)\nabla u_n\big), \\ u_{n+1} - u_n &= k v_{n+1}, \\ p_n - p_{n+1} &= k\mathrm{div}\big(\mathfrak{h}'(\nabla u_n \cdot \nabla q_n)\nabla q_n\big), \\ q_n - q_{n+1} &= k p_{n+1}, \end{aligned}$$

corresponds to the symplectic forward Euler method for the Hamiltonian

$$\tilde{H}(\underbrace{u_n, q_n}_{\varphi_n}, \underbrace{v_{n+1}, p_{n+1}}_{\lambda_{n+1}}) := H(u_n, v_{n+1}, p_{n+1}, q_n) - 2\int_\Omega v_{n+1} p_{n+1}\ \mathrm{d}x,$$

where H is given by (36). Since (39) only is stable for sufficiently small time-steps and still requires to solve a complex saddle point system we will use the symplectic midpoint method in our experiments.

4.3. **Numerical Examples.** Let $\tilde{\sigma} := \mathfrak{h}'_\delta$ where $\mathfrak{h}'_\delta$ is given by (12). The symplectic midpoint method for the regularized Hamiltonian system (37) can then be written as

$$F_n^1(w) = 0, \quad F_n^2(w) = 0, \quad G_n^1(w) = 0, \quad G_n^2(w) = 0,$$

for $n = 0, \dots, N-1$, and $\forall w \in \bar{V}$, where

$$\begin{aligned} F_n^1(w) &:= \int_\Omega (v_{n+1} - v_n)w + k\mathfrak{h}'_\delta\big(\nabla u_{n+\frac{1}{2}} \cdot \nabla q_{n+\frac{1}{2}}\big)\nabla u_{n+\frac{1}{2}} \cdot \nabla w\ \mathrm{d}x \\ &\quad - \int_{\partial\Omega} k j_{n+\frac{1}{2}} w\ \mathrm{d}s, \\ F_n^2(w) &:= \int_\Omega (u_{n+1} - u_n - k v_{n+\frac{1}{2}})w\ \mathrm{d}x, \\ G_n^1(w) &:= \int_\Omega (q_n - q_{n+1} - k p_{n+\frac{1}{2}})w\ \mathrm{d}x. \\ G_n^2(w) &:= \int_\Omega (p_n - p_{n+1})w + k\mathfrak{h}'_\delta(\nabla u_{n+\frac{1}{2}} \cdot \nabla q_{n+\frac{1}{2}})\nabla q_{n+\frac{1}{2}} \cdot \nabla w\ \mathrm{d}x \\ &\quad - \int_{\partial\Omega} 2k(u_{n+\frac{1}{2}} - u^*_{n+\frac{1}{2}})w\ \mathrm{d}s, \end{aligned}$$

and $u_0 = v_0 = p_N = q_N = 0$. The index $n + \frac{1}{2}$ implies the average of the values at n and $n+1$, *i.e.* $u_{n+\frac{1}{2}} := \frac{1}{2}(u_n + u_{n+1})$. Taking the variations with respect to u, v, p, q gives the Newton system

$$\begin{pmatrix} K_{11} & K_{12} & 0 & K_{14} \\ K_{21} & K_{22} & 0 & 0 \\ 0 & 0 & K_{33} & K_{34} \\ K_{41} & 0 & K_{43} & K_{44} \end{pmatrix} \begin{pmatrix} \hat{u} \\ \hat{v} \\ \hat{p} \\ \hat{q} \end{pmatrix} = \begin{pmatrix} f_1 \\ f_2 \\ g_1 \\ g_2 \end{pmatrix}, \tag{40}$$

with increments

$$\begin{aligned} \hat{u} &= \begin{pmatrix} \hat{u}_1 & \dots & \hat{u}_N \end{pmatrix}^T, \qquad \hat{v} = \begin{pmatrix} \hat{v}_1 & \dots & \hat{v}_N \end{pmatrix}^T, \\ \hat{p} &= \begin{pmatrix} \hat{p}_0 & \dots & \hat{p}_{N-1} \end{pmatrix}^T, \quad \hat{q} = \begin{pmatrix} \hat{q}_0 & \dots & \hat{q}_{N-1} \end{pmatrix}^T, \end{aligned}$$

and right hand side

$$f_1 = \begin{pmatrix} F_0^1 & \dots & F_{N-1}^1 \end{pmatrix}^T, \quad f_2 = \begin{pmatrix} F_0^2 & \dots & F_{N-1}^2 \end{pmatrix}^T,$$
$$g_1 = \begin{pmatrix} G_0^1 & \dots & G_{N-1}^1 \end{pmatrix}^T, \quad g_2 = \begin{pmatrix} G_0^2 & \dots & G_{N-1}^2 \end{pmatrix}^T.$$

with submatrices with the following structure:

- K_{11} is lower block bi-diagonal with

$$\begin{aligned} &\frac{1}{2}\int_\Omega k\mathfrak{h}_\delta''(\nabla u_{n+\frac{1}{2}}\cdot\nabla q_{n+\frac{1}{2}})\nabla q_{n+\frac{1}{2}}\cdot\nabla w\ \nabla u_{n+\frac{1}{2}}\cdot\nabla\bar{w}\ \mathrm{d}x \\ &+\frac{1}{2}\int_\Omega k\mathfrak{h}_\delta'(\nabla u_{n+\frac{1}{2}}\cdot\nabla q_{n+\frac{1}{2}})\nabla w\cdot\nabla\bar{w}\ \mathrm{d}x, \end{aligned} \tag{41}$$

  on its main diagonal for $n = 0, \dots, N-1$ and on its sub-diagonal for $n = 1, \dots, N-1$.
- K_{44} is upper block bi-diagonal with (41) on its diagonal for $n = 0, \dots, N-1$ and on its super-diagonal for $n = 0, \dots, N-2$.
- $K_{12} = K_{21} = K_{34}^T = K_{43}^T$ is lower block bi-diagonal with mass matrices M on the main diagonal and $-M$ on the subdiagonal.
- $K_{22} = K_{33}^T$ is lower block bi-diagonal with $-\frac{kM}{2}$ on the diagonal and the sub-diagonal.
- K_{14} is upper block bi-diagonal with

$$\frac{1}{2}\int_\Omega k\mathfrak{h}_\delta''(\nabla u_{n+\frac{1}{2}}\cdot\nabla q_{n+\frac{1}{2}})\nabla u_{n+\frac{1}{2}}\cdot\nabla w\ \nabla u_{n+\frac{1}{2}}\cdot\nabla\bar{w}\ \mathrm{d}x,$$

  on its diagonal for $n = 0, \dots, N-1$ and on its super-diagonal for $n = 0, \dots, N-2$.
- K_{41} is lower block bi-diagonal with

$$\frac{1}{2}\int_\Omega k\mathfrak{h}_\delta''(\nabla u_{n+\frac{1}{2}}\cdot\nabla q_{n+\frac{1}{2}})\nabla q_{n+\frac{1}{2}}\cdot\nabla w\ \nabla q_{n+\frac{1}{2}}\cdot\nabla\bar{w}\ \mathrm{d}x - \int_{\partial\Omega} k\bar{w}w\ \mathrm{d}s,$$

  on its diagonal for $n = 0, \dots, N-1$ and sub-diagonal for $n = 1, \dots, N-1$.

As in the previous section we will solve the Newton system using GMRES and an approximate solution as preconditioner, *e.g.* from the the 2×2 blockwise Gauss-Seidel method

$$\begin{aligned} K_{11}\hat{u}^{i+1} + K_{12}\hat{v}^{i+1} &= f_1 - K_{14}\hat{q}^i, \\ K_{21}\hat{u}^{i+1} + K_{22}\hat{v}^{i+1} &= f_2, \\ K_{33}\hat{p}^{i+1} + K_{34}\hat{q}^{i+1} &= g_1, \\ K_{43}\hat{p}^{i+1} + K_{44}\hat{q}^{i+1} &= g_2 - K_{41}\hat{u}^{i+1}, \end{aligned}$$

which can be written as

$$\begin{aligned} (K_{11} - K_{12}K_{22}^{-1}K_{21})\hat{u}^{i+1} &= f_1 - K_{12}K_{22}^{-1}f_2 - K_{14}\hat{q}^i, \\ (K_{44} - K_{43}K_{33}^{-1}K_{34})\hat{q}^{i+1} &= g_2 - K_{43}K_{33}^{-1}g_1 - K_{41}\hat{u}^{i+1}. \end{aligned} \tag{42}$$

Note that (42) is easily solved since inverting K_{22} and K_{33} only involves the calculation of M^{-1}. In fact, the Schur complements $K_{11} - K_{12}K_{22}^{-1}K_{21}$ and $K_{44} - K_{43}K_{33}^{-1}K_{34}$ becomes lower and upper block trianglar matrices, respectively, and (42) can be solved by one forward substitution in time for $\hat{u}^{i+1}$ and one backward substitution in time for $\hat{q}^{i+1}$. Of course, to save memory the Schur complement system (42) should never be formed explicitly. For large regularizations the Schur complements can be seen as approximations of the operator $-\Delta + \partial_{tt}$. As for the case with the heat equation starting with $\hat{q}^0 = 0$, one iteration with (42) is the same as solving (40) with $K_{14} = 0$.

In Figure 7, a two dimensional example of reconstruction two different speed coefficients is shown. The measured data was here simulated by solving the wave

equation for σ_{true} with the symplectic backward Euler method for (35), which can be written as the second order scheme

$$\int_\Omega (u_{n+1} - 2u_n + u_{n-1})w \, \mathrm{d}x = \int_{\partial\Omega} jw \, \mathrm{d}s - \int_\Omega \sigma \nabla u_n \cdot \nabla w \, \mathrm{d}x, \quad \forall w \in \bar{V}.$$

Since the wave equation is a conservation law and is reversible in time it is tempting to believe that it would be easier to control than the heat equation but there are some computational drawbacks: numerical errors are propagated in time and there seems to be many local minima. From the approximation $\mathfrak{h}'_\delta(\nabla u \cdot \nabla q)$ in Figure 8 it is evident that the time dependent reconstruction varies a lot over time and is not a good approximation of the time independent wave coefficient σ_{true}.

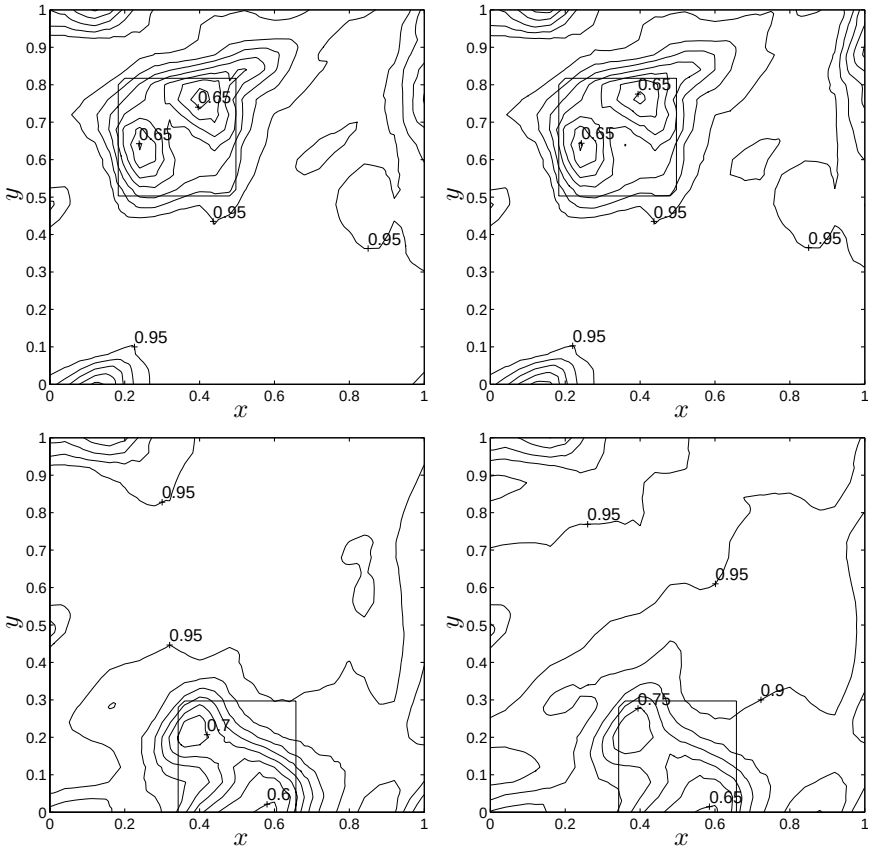

FIGURE 7. 2D reconstruction using the weighted average (32), final time $T = 1.5$ and Neumann boundary condition $2\sin(4\pi t)$ for $(x, y, t) \in \{0\} \times [0.4, 0.6] \times [0, 0.5]$ and 0 elsewhere. The data u^* was simulated by solving the forward equation on a quasi-uniform mesh with 3232 triangles and 328 time steps while the inverse problem was solved on a uniform mesh with 1250 triangles and 30 time steps. Measurements from the whole boundary were used. Top: Reconstruction of $\sigma_{true} = 0.5$ inside the square $[0.2, 0.5] \times [0.5, 0.8]$ and $\sigma_{true} = 1$ elsewhere, with no noise in data (left) and 10% noise in data (right). Bottom: Reconstruction of $\sigma_{true} = 0.5$ inside the square $[0.35, 0.65] \times [0, 0.3]$ and $\sigma_{true} = 1$ elsewhere, with no noise in data (left) and 10% noise in data (right).

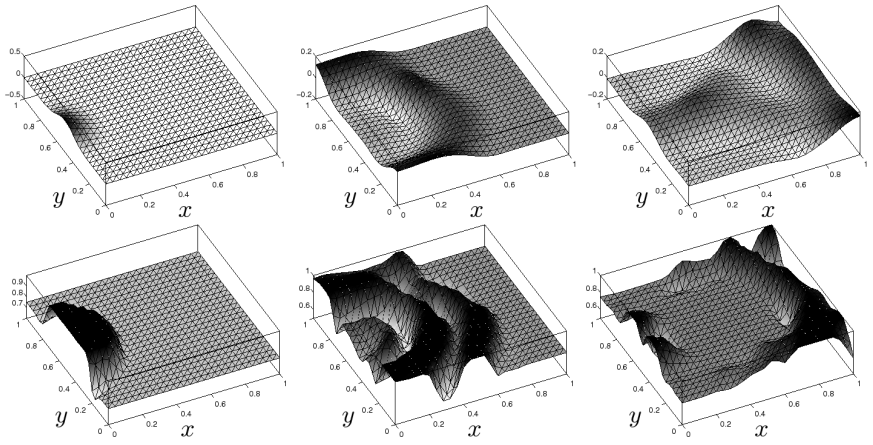

FIGURE 8. Measurements u^* (top) and $\mathfrak{h}'_\delta(\nabla u \cdot \nabla q)$ (bottom) for timesteps 5, 15 and 25. The data here corresponds to the top left plot in Figure 7, and u^* is interpolated onto the mesh used for the calculation of u and q.

References

[1] H. T. Banks and K. Kunisch. *Estimation techniques for distributed parameter systems*, volume 1 of *Systems & Control: Foundations & Applications*. Birkhäuser Boston Inc., Boston, MA, 1989.

[2] Emmanuel Nicholas Barron and Robert Jensen. The Pontryagin maximum principle from dynamic programming and viscosity solutions to first-order partial differential equations. *Trans. Amer. Math. Soc.*, 298(2):635–641, 1986.

[3] M. P. Bendsøe and O. Sigmund. *Topology optimization*. Springer-Verlag, Berlin, 2003. Theory, methods and applications.

[4] Michele Benzi, Gene H. Golub, and Jörg Liesen. Numerical solution of saddle point problems. *Acta Numer.*, 14:1–137, 2005.

[5] George Biros and Omar Ghattas. Parallel Lagrange-Newton-Krylov-Schur methods for PDE-constrained optimization. I. The Krylov-Schur solver. *SIAM J. Sci. Comput.*, 27(2):687–713 (electronic), 2005.

[6] Liliana Borcea. Electrical impedance tomography. *Inverse Problems*, 18(6):R99–R136, 2002.

[7] Jesper Carlsson. Pontryagin approximations for optimal design of elastic structures. *preprint*, 2006.

[8] Jesper Carlsson, Mattias Sandberg, and Anders Szepessy. Symplectic pontryagin approximations for optimal design. *preprint*, 2006.

[9] M. G. Crandall, L. C. Evans, and P.-L. Lions. Some properties of viscosity solutions of Hamilton-Jacobi equations. *Trans. Amer. Math. Soc.*, 282(2):487–502, 1984.

[10] Heinz W. Engl, Martin Hanke, and Andreas Neubauer. *Regularization of inverse problems*, volume 375 of *Mathematics and its Applications*. Kluwer Academic Publishers Group, Dordrecht, 1996.

[11] FEniCS. FEniCS project. URL: urlhttp//www.fenics.org/.

[12] Ernst Hairer, Christian Lubich, and Gerhard Wanner. *Geometric numerical integration*, volume 31 of *Springer Series in Computational Mathematics*. Springer-Verlag, Berlin, second edition, 2006. Structure-preserving algorithms for ordinary differential equations.

[13] J. Hoffman, J. Jansson, A. Logg, and G. N. Wells. DOLFIN. URL: urlhttp//www.fenics.org/dolfin/.

[14] J.-L. Lions. *Optimal control of systems governed by partial differential equations*. Translated from the French by S. K. Mitter. Die Grundlehren der mathematischen Wissenschaften, Band 170. Springer-Verlag, New York, 1971.

[15] M. Sandberg and A. Szepessy. Convergence rates of symplectic Pontryagin approximations in optimal control theory. *M2AN*, 40(1), 2006.

[16] Mattias Sandberg. Convergence rates for numerical approximations of an optimally controlled Ginzburg-Landau equation. *preprint*, 2006.

[17] Curtis R. Vogel. *Computational methods for inverse problems*, volume 23 of *Frontiers in Applied Mathematics*. Society for Industrial and Applied Mathematics (SIAM), Philadelphia, PA, 2002. With a foreword by H. T. Banks.

CSC, Numerical Analysis, Kungl. Tekniska Högskolan, 100 44 Stockholm, Sweden;
E-mail address: jesperc@kth.se

Paper 4

INVERSE RECONSTRUCTION FROM OPTIMAL INPUT DATA

JESPER CARLSSON

Abstract. This report concerns the problem to find optimal input data for an inverse reconstruction problem. In a classical parameter reconstruction problem the goal is to determine a spacially distributed (and optionally time dependent) coefficient of a partial differential equation from observed data. Here, the spacially dependent wave speed coefficient of the acoustic wave equation is sought, given observations of the solution on the boundary. The reconstruction of the coefficient is highly dependent on input data, *e.g.* if Neumann boundary values serve as input data it is in general not possible to determine the coefficient for all possible input data. It is shown that it is possible to formulate meaningful optimality criteria for the input data that enhances quality of the reconstructed coefficient. Both the problem of estimating the coefficient and the problem of finding optimal input data are ill-posed inverse problems and need to be regularized.

Contents

1. Introduction

This paper describes a method to find optimal input data for inverse scattering problems. It is well known that inverse problems are ill-posed and need to be regularized [6]. Much of the research on inverse problems today is focused on how to regularize and to solve them efficiently. A more unusual question is how the choice of input data affects the solution to the inverse problem, and if it is possible to enhance the quality of the solution by simply choosing other input data. This question was asked in [3, 5] for time independent reconstruction problems in impedance tomography, and later for inverse scattering problems [4].

2000 *Mathematics Subject Classification.* 65M32.

Key words and phrases. Inverse Problems, Parameter Reconstruction.

Support by the Swedish Research Council grants 2002-6285 and 2002-4961, and the European network HYKE, funded by the EC as contract HPRN-CT-2002-00282, is acknowledged.

In [4], it was investigated how to best distinguish two different spacially dependent wave coefficients $c(x)$ and $c_0(x)$, for the acoustic wave equation in the half space $x_3 < 0$ in $\mathbb{R}^3$, from each other by using information of the downgoing and upgoing waves at the boundary $x_3 = 0$. As a measure of distinguishability the difference in energy flux between the upgoing fields for c and c_0 was chosen, and it was shown that this difference is maximized by a time-harmonic downgoing wave with frequency depending on the two coefficients. In this paper, a similar approach is used, but with the focus on how the choice of the incoming wave affects the reconstruction for the inverse problem to reconstruct an unknown wave coefficient.

2. Problem Formulation

Consider the acoustic wave equation in an bounded open domain $\Omega \in \mathbb{R}^2$ and for times $t \in [0, T]$:

$$\begin{aligned} \varphi^*_{tt} &= \operatorname{div}(\sigma^* \nabla \varphi^*), && \text{in } \Omega \times (0,T], \\ \sigma^* \nabla \varphi^* \cdot \mathbf{n} &= j, && \text{on } \Gamma_N \times (0,T], \\ \sigma^* \nabla \varphi^* \cdot \mathbf{n} &= 0, && \text{on } \partial\Omega \setminus \Gamma_N \times (0,T], \\ \varphi^* = \varphi^*_t &= 0, && \text{on } \bar{\Omega} \times \{t = 0\}, \end{aligned} \tag{1}$$

where $\varphi^* : \bar{\Omega} \times [0,T] \to \mathbb{R}$ denotes acoustic pressure, $\sigma^* : \bar{\Omega} \to \mathbb{R}$, $\sigma^* > 0$ is the squared wave speed and $\Gamma_N \subseteq \partial\Omega$. To find the acoustic pressure φ^*, for a given coefficient σ^* and boundary data $j : \Gamma_N \times (0,T] \to \mathbb{R}$, is the *forward* problem. Given sufficient regularity of the input data, *e.g.* $\sigma^* \in C^1(\Omega)$ and $j \in L^2(0,T; L^2(\Gamma_N))$, the forward problem is well posed, *i.e.* there exists a unique (weak) solution $\varphi \in L^2(0,T; H^1(\Omega))$ which depends continuously on j and σ^*, see [7]. A typical corresponding *inverse* problem to (1) is to find σ^*, for given input boundary data j and measurements φ^*.

2.1. Inverse Scattering.

Unlike the forward problem above, the inverse problem is ill posed, *i.e.* there may not exist a solution σ^*, and if it exists it may not be unique nor depend continuously on the data j and φ^*. To formulate an inverse problem that has a unique solution, with continuous dependence on data, it is necessary to add some regularization [6].

The *regularized* inverse scattering problem is here: for given Neumann boundary data j and measurements φ^* on $\Gamma_M \subset \partial\Omega$, find the coefficient $\sigma : \bar{\Omega} \to \mathbb{R}$, $\sigma > 0$, and the state $\varphi : \bar{\Omega} \times [0,T] \to \mathbb{R}$, that minimizes the error functional

$$\frac{1}{2} \int_0^T \int_{\Gamma_M} (\varphi - \varphi^*)^2 \, \mathrm{d}s \, \mathrm{d}t + \frac{\delta}{2} \int_\Omega (\sigma^2 + |\nabla \sigma|^2) \, \mathrm{d}x, \tag{2}$$

and satisfies the acoustic wave equation

$$\begin{aligned} \varphi_{tt} &= \operatorname{div}(\sigma \nabla \varphi), && \text{in } \Omega \times (0,T], \\ \sigma \nabla \varphi \cdot \mathbf{n} &= j, && \text{on } \Gamma_N \times (0,T], \\ \sigma \nabla \varphi \cdot \mathbf{n} &= 0, && \text{on } \partial\Omega \setminus \Gamma_N \times (0,T], \\ \varphi = \varphi_t &= 0, && \text{on } \bar{\Omega} \times \{t = 0\}. \end{aligned} \tag{3}$$

The second term in (2) is a Tikhonov regularization, with $\delta > 0$, that ensures that the minimization problem is well posed [7]. Also, it is assumed that the measurements φ^* satisfy (1) for some unknown σ^*.

Note that, for simplicity a pure Neumann boundary condition is here used, but it is possible to use a Dirichlet condition on a subset $\Gamma_D \subset \partial\Omega$, $\Gamma_D \cap \Gamma_M \neq \Gamma_M$, without complication.

2.2. **Optimal Input Data.** The objective of this paper is not only to solve the above minimization problem (2), but also to find the best possible boundary input data j that ensures a good reconstruction of σ^*. For the acoustic wave equation the choice of input data is highly important since a wave may only visit a subset of the region Ω before it is measured, and it can thus only be expected to find an approximation of σ^* in that subset.

One way to define what is meant by the "best" input j is to first define the concept of distinguishability, *i.e.* how to best distinguish two coefficients σ and σ^* from each other. Following [3], let Λ_σ denote the Neumann-to-Dirichlet map

$$\Lambda_\sigma : \sigma \frac{\partial \varphi}{\partial n}\Big|_{\partial\Omega\times(0,T]} \to \varphi|_{\partial\Omega\times(0,T]}$$

which associates the input j with the solution φ on the boundary, and define the distinguishability as

$$d(\sigma,\sigma^*) := \frac{\|(\Lambda_\sigma - \Lambda_{\sigma^*})j\|_{\partial\Omega\times(0,T)}}{\|j\|_{\partial\Omega\times(0,T)}} = \frac{\|\varphi - \varphi^*\|_{\partial\Omega\times(0,T)}}{\|j\|_{\partial\Omega\times(0,T)}},$$

where $\|\cdot\|_A$ denotes the $L^2(A)$ norm with corresponding inner product $(\cdot,\cdot)_A$. Here, the L^2 norm was chosen for simplicity, but it may happen that two coefficients that are not distinguishable in the L^2 norm are still distinguishable in norms that better reflect the regularity of j and φ, see [3].

Given σ and σ^*, the best input j can be defined as the maximizer to $d(\sigma,\sigma^*)$, *i.e.* the eigenfunction that corresponds to the dominating eigenvalue of the difference operator $\Lambda_\sigma - \Lambda_{\sigma^*}$. To find the eigenfunction for the dominating eigenvalue, power iteration can be used, an approach that was used in [2] to find good input currents for impedance tomography.

2.3. **Minimax Problem.** If the Neumann data j is normalized by introducing a new variable $q : \Gamma_N \times (0,T] \to \mathbb{R}$ such that

$$j := \frac{q}{\|q\|_{\Gamma_N\times(0,T)}}, \quad \text{on } \Gamma_N \times (0,T],$$

the problem to find both the coefficient σ^* and an optimal input j can be formulated as the minimax problem

$$\min_\sigma \max_q \|\varphi - \varphi^*\|^2_{\Gamma_M\times(0,T)} + \frac{\delta}{2}\Big(\|\sigma\|^2_\Omega + \|\nabla\sigma\|^2_\Omega\Big), \tag{4}$$

with the constraints (1) and (3). Remember, that since σ^* is unknown Equation (3) cannot be solved, but the measurements φ^* on the boundary are still accessible through experiments.

Similarly to the minimization of (4), the maximization is an inverse problem and can be expected to be ill posed. The normalization of j here acts as a Tikhonov regularization, and ensures that the objective fucnction is bounded, but it is not clear if the maximization admits a solution, or if the solution is unique. Additional regularization may thus be needed. In Section 3.5, it is observed that q and correspondingly φ tends to oscillate in time as the measurement error grows, and to prevent large oscillations the numerical method is interrupted prematurely. An alternative measure would be to add a penalty on the time derivative of q in (4). Physically, it would also be suitable to include a constraint on the energy, as in [4], but this approach is not pursued in this paper.

Since the concavity with respect to q is unclear, the minimization and maximization problems will here be treated as two separate subproblems:

Max: Given σ and σ^*, maximize (4) with respect to j under the constraints (1) and (3).

Min: Given j and φ^*, minimize (4) with respect to σ under the constraint (3).

Even if the min and max in (4) could switch place, there are numerical considerations which leads to two separate subproblems. This will be explained in the following sections.

3. Numerical Solution

3.1. **Discretization.** Let $V \subset H^1(\Omega)$ be the finite element subspace of continuous piecewise linear functions on a triangular finite element mesh on Ω, and divide the interval $[0,T]$ into N intervals of equal length $k = T/N$. An explicit scheme, discretized in time and finite elements in space, for the weak form of Equation (3) is

$$\begin{aligned} (\varphi_{n+1} - 2\varphi_n + \varphi_{n-1}, v)_\Omega &= k^2(j_n, v)_{\Gamma_N} - k^2(\sigma\nabla\varphi_n, \nabla v)_\Omega, \qquad \forall v \in V, \\ \varphi_0 &= \varphi_1 = 0, \end{aligned} \tag{5}$$

for $n = 1, \dots, N-1$. Also, even though Equation (1) is never solved computationally, since φ^* is measured, it is assumed that the measured data uses the same discretization

$$\begin{aligned} (\varphi^*_{n+1} - 2\varphi^*_n + \varphi^*_{n-1}, v)_\Omega &= k^2(j_n, v)_{\Gamma_N} - k^2(\sigma^*\nabla\varphi^*_n, \nabla v)_\Omega, \qquad \forall v \in V, \\ \varphi^*_0 &= \varphi^*_1 = 0, \end{aligned} \tag{6}$$

for $n = 1, \dots, N-1$. Using formulation (4) above, with Neumann boundary data j_n defined by

$$j_n := \frac{q_n}{\sqrt{k\sum_{n=1}^{N-1} \|q_n\|^2_{\Gamma_N}}},$$

the discretized minimax problem is thus to find $\varphi_2, \dots, \varphi_N$, $\varphi^*_2, \dots, \varphi^*_N$, $q_1, \dots, q_{N-1}$ and σ such that

$$\min_\sigma \max_{q_1,\dots,q_{N-1}} \frac{k}{2}\sum_{n=0}^{N} \|\varphi_n - \varphi^*_n\|^2_{\Gamma_M} + \frac{\delta}{2}(\|\sigma\|^2_\Omega + \|\nabla\sigma\|^2_\Omega), \tag{7}$$

under the constraints (5) and (6).

3.2. **Optimality Condition.** To formulate an optimality condition for the discretized problem (7), (5) and (6), the Lagrangian is introduced:

$$\begin{aligned} L := {} & \frac{k}{2}\sum_{n=0}^{N} \|\varphi_n - \varphi^*_n\|^2_{\Gamma_M} + \frac{\delta}{2}(\|\sigma\|^2_\Omega + \|\nabla\sigma\|^2_\Omega) + \\ & + \sum_{n=1}^{N-1} \frac{1}{k}(\varphi_{n+1} - 2\varphi_n + \varphi_{n-1}, \lambda_{n-1})_\Omega - k(j_n, \lambda_{n-1})_{\Gamma_N} + k(\sigma\nabla\varphi_n, \nabla\lambda_{n-1})_\Omega \\ & + \sum_{n=1}^{N-1} \frac{1}{k}(\varphi^*_{n+1} - 2\varphi^*_n + \varphi^*_{n-1}, \lambda^*_{n-1})_\Omega - k(j_n, \lambda^*_{n-1})_{\Gamma_N} + k(\sigma^*\nabla\varphi^*_n, \nabla\lambda^*_{n-1})_\Omega \end{aligned}$$

with multipliers $\lambda_n, \lambda^*_n \in V, n = 0, \dots, N-2$.

An optimal solution to the discretized minimax problem is also stationary point to the Lagrangian, and satisfies

$$\begin{aligned} \partial_{\varphi_{n+1}} L = 0, \quad \partial_{\lambda_{n-1}} L = 0, \\ \partial_{\varphi^*_{n+1}} L = 0, \quad \partial_{\lambda^*_{n-1}} L = 0, \\ \partial_{q_n} L = 0, \qquad \partial_\sigma L = 0, \end{aligned} \tag{8}$$

for $n = 1, \dots, N-1$. The variation with respect to λ_{n-1} and λ^*_{n-1} in (8) becomes Equation (5) and (6), respectively. Variation in φ_{n+1} and φ^*_{n+1} gives the adjoint equations

$$\begin{aligned}(\lambda_{n+1} - 2\lambda_n + \lambda_{n-1}, v)_\Omega =& - k^2(\varphi_{n+1} - \varphi^*_{n+1}, v)_{\Gamma_M} - k^2(\sigma\nabla\lambda_n, \nabla v)_\Omega,\\ \lambda_N = \lambda_{N-1} =& 0,\end{aligned} \tag{9}$$

and

$$\begin{aligned}(\lambda^*_{n+1} - 2\lambda^*_n + \lambda^*_{n-1}, v)_\Omega =& k^2(\varphi_{n+1} - \varphi^*_{n+1}, v)_{\Gamma_M} - k^2(\sigma^*\nabla\lambda^*_n, \nabla v)_\Omega,\\ \lambda^*_N = \lambda^*_{N-1} =& 0,\end{aligned} \tag{10}$$

for all $v \in V$. Stationarity with respect to q_n and σ is given by

$$\frac{k^2(q_n, \lambda_{n-1} + \lambda^*_{n-1})_{\Gamma_N}(q_n, v)_{\Gamma_N}}{\left(k\sum_{n=1}^{N-1}\|q_n\|^2_{\partial\Omega}\right)^{\frac{3}{2}}} - \frac{k(\lambda_{n-1} + \lambda^*_{n-1}, v)_{\Gamma_N}}{\left(k\sum_{n=1}^{N-1}\|q_n\|^2_{\Gamma_N}\right)^{\frac{1}{2}}} = 0, \tag{11}$$

and

$$\delta(\sigma, v)_\Omega + \delta(\nabla\sigma, \nabla v)_\Omega + k\sum_{n=1}^{N-1}(v\nabla\varphi_n, \nabla\lambda_{n-1})_\Omega = 0, \tag{12}$$

respectively, for all $v \in V$. For simplicity, it is here assumed that $\sigma, q_n \in V$.

Expressions (9) and (10) are discretizations of the adjoint equations

$$\begin{aligned}\lambda_{tt} &= \operatorname{div}(\sigma\nabla\lambda), && \text{in } \Omega \times [0,T),\\ \sigma\nabla\lambda\cdot\mathbf{n} &= -(\varphi - \varphi^*), && \text{on } \Gamma_M \times [0,T),\\ \sigma\nabla\lambda\cdot\mathbf{n} &= 0, && \text{on } \partial\Omega\setminus\Gamma_M \times [0,T),\\ \lambda = \lambda_t &= 0, && \text{on } \bar{\Omega}\times\{t = T\},\end{aligned} \tag{13}$$

and

$$\begin{aligned}\lambda^*_{tt} &= \operatorname{div}(\sigma^*\nabla\lambda^*), && \text{in } \Omega \times [0,T),\\ \sigma^*\nabla\lambda^*\cdot\mathbf{n} &= (\varphi - \varphi^*), && \text{on } \Gamma_M \times [0,T),\\ \sigma^*\nabla\lambda^*\cdot\mathbf{n} &= 0, && \text{on } \partial\Omega\setminus\Gamma_M \times [0,T),\\ \lambda^* = \lambda^*_t &= 0, && \text{on } \bar{\Omega}\times\{t = T\},\end{aligned} \tag{14}$$

but compared to the discretization of the forward problem (3) the boundary conditions are evaluated at a different time step. Equation (12) is an approximation to the equation

$$\begin{aligned}\delta(\Delta\sigma - \sigma) &= \int_0^T \nabla\varphi\cdot\nabla\lambda\,\mathrm{d}t, && \text{in } \Omega,\\ \nabla\sigma\cdot\mathbf{n} &= 0, && \text{on } \partial\Omega.\end{aligned} \tag{15}$$

Observe, that since σ^* is unknown neither (1), (14) nor their discretized counterparts (6), (10) can be solved. However, it is possible to experimentally apply the appropriate Neumann boundary conditions and measure the resulting boundary values φ^* and λ^*.

The fact that φ^*, λ^* and σ^* are not acessible in Ω makes it hard to solve the optimality system (8) efficiently since not all of the second variations of the Lagrangian are accessible. Also, as mentioned in Section 2.3, the minimax problem may not be convex-concave, so to simultaneously solve the equations in (8) may not give the same results as treating the minimization and maximization separately. The regularized minimization problem is convex in a neighbourhood of the optimal σ and all second variations are accessible, so Newton's method can be used. However, for the maximization problem none of the second variations are available.

3.3. **Minimization Problem.** Assume that Neumann boundary data j and measurements φ^* are given. The forward equation (5) for φ, the dual equation (9) for λ and the steady state equation (12) for σ can be written as

$$\begin{aligned} f_n :=& \frac{1}{k}(\lambda_{n+1} - 2\lambda_n + \lambda_{n-1}, v)_\Omega + k(\varphi_{n+1} - \varphi^*_{n+1}, v)_{\Gamma_M} + k(\sigma\nabla\lambda_n, \nabla v)_\Omega &= 0 \\ g_n :=& \frac{1}{k}(\varphi_{n+1} - 2\varphi_n + \varphi_{n-1}, v)_\Omega - k(j_n, v)_{\Gamma_N} + k(\sigma\nabla\varphi_n, \nabla v)_\Omega &= 0 \\ h :=& \delta(\sigma, v)_\Omega + \delta(\nabla\sigma, \nabla v)_\Omega + k\sum_{i=1}^{N-1}(v\nabla\varphi_i, \nabla\lambda_{i-1})_\Omega &= 0 \end{aligned}$$

for $n = 1, \dots, N-1$ and $\forall v \in V$. The Newton method for finding the stationary point to the above system is to, given φ, λ and σ, find the updates $\hat\varphi := (\hat\varphi_2, \dots, \hat\varphi_N)^T$, $\hat\lambda := (\hat\lambda_0, \dots, \hat\lambda_{N-2})^T$ and $\hat\sigma$ that satisfies

$$\begin{aligned} k(\hat\varphi_{n+1}, v)_{\Gamma_M} + \frac{1}{k}(\hat\lambda_{n+1} - 2\hat\lambda_n + \hat\lambda_{n-1}, v)_\Omega + \\ + k(\sigma\nabla\hat\lambda_n + \hat\sigma\nabla\lambda_n, \nabla v)_\Omega = -f_n, \quad n = 1, \dots, N-3, \\ k(\hat\varphi_{n+1}, v)_{\Gamma_M} + \frac{1}{k}(-2\hat\lambda_n + \hat\lambda_{n-1}, v)_\Omega + \\ + k(\sigma\nabla\hat\lambda_n + \hat\sigma\nabla\lambda_n, \nabla v)_\Omega = -f_n, \quad n = N-2, \\ k(\hat\varphi_{n+1}, v)_{\Gamma_M} + \frac{1}{k}(\hat\lambda_{n-1}, v)_\Omega + k(\hat\sigma\nabla\lambda_n, \nabla v)_\Omega = -f_n, \quad n = N-1, \\ \frac{1}{k}(\hat\varphi_{n+1}, v)_\Omega + k(\hat\sigma\nabla\varphi_n, \nabla v)_\Omega = -g_n, \quad n = 1, \\ \frac{1}{k}(\hat\varphi_{n+1} - 2\hat\varphi_n, v)_\Omega + k(\sigma\nabla\hat\varphi_n + \hat\sigma\nabla\varphi_n, \nabla v)_\Omega = -g_n, \quad n = 2, \\ \frac{1}{k}(\hat\varphi_{n+1} - 2\hat\varphi_n + \hat\varphi_{n-1}, v)_\Omega + k(\sigma\nabla\hat\varphi_n + \hat\sigma\nabla\varphi_n, \nabla v)_\Omega = -g_n, \quad n = 3, \dots, N-1, \end{aligned}$$

and

$$k\sum_{n=2}^{N-1}(v\nabla\hat\varphi_n, \nabla\lambda_{n-1})_\Omega + k\sum_{n=1}^{N-1}(v\nabla\varphi_n, \nabla\hat\lambda_{n-1})_\Omega + \delta(\hat\sigma, v)_\Omega + \delta(\nabla\hat\sigma, \nabla v)_\Omega = -h,$$

for all $v \in V$, or in matrix notation

$$\begin{pmatrix} K_{11} & K_{12} & K_{13} \\ K_{12}^T & 0 & K_{23} \\ K_{13}^T & K_{23}^T & K_{33} \end{pmatrix} \begin{pmatrix} \hat\varphi \\ \hat\lambda \\ \hat\sigma \end{pmatrix} = - \begin{pmatrix} f \\ g \\ h \end{pmatrix}. \tag{16}$$

where $f := (f_1, \dots, f_{N-1})^T$ and $g := (g_1, \dots, g_{N-1})^T$.

Let M, $\bar M$, $S(\sigma)$ and $P(\varphi)$ be matrices with the elements

$$\begin{aligned} M_{ij} &= (v_i, v_j)_\Omega, & \bar M_{ij} &= (v_i, v_j)_{\partial\Omega}, \\ S_{ij}(\sigma) &= (\sigma\nabla v_i, \nabla v_j)_\Omega, & P_{ij}(\varphi) &= (v_j\nabla\varphi, \nabla v_i)_\Omega, \end{aligned}$$

where v_i denotes the basis functions of the finite element space V, then the submatrices in the Newton system (16) are of the form (for $N = 4$)

$$K_{11} = k\begin{pmatrix} \bar M & & \\ & \bar M & \\ & & \bar M \end{pmatrix}, \quad K_{12} = \frac{1}{k}\begin{pmatrix} M & k^2S(\sigma) - 2M & \\ & M & k^2S(\sigma) - 2M \\ & & M \end{pmatrix},$$

and

$$K_{13} = k\begin{pmatrix} P(\lambda_1) \\ P(\lambda_2) \\ P(\lambda_3) \end{pmatrix}, \quad K_{23} = k\begin{pmatrix} P(\varphi_1) \\ P(\varphi_2) \\ P(\varphi_3) \end{pmatrix}, \quad K_{33} = \delta\big(M + S(1)\big).$$

To solve the Newton system (16) with a direct solver is very demanding for large problems and in practice it must be done iteratively. For the examples in this report, the GMRES method with a simple preconditioner, was used. The preconditioner is based on solving the system approximately, for an arbitrary right hand side (f, g, h), with the Gauss-Seidel method, *i.e.* given $(\hat{\varphi}^i, \hat{\lambda}^i, \hat{\sigma}^i)$ an approximate solution is given by iterating according to the scheme

$$\begin{aligned} K_{12}^T \hat{\varphi}^{i+1} &= g - K_{23}\hat{\sigma}^i, \\ K_{11}\hat{\varphi}^{i+1} + K_{12}\hat{\lambda}^{i+1} &= f - K_{13}\hat{\sigma}^i, \\ K_{13}^T\hat{\varphi}^{i+1} + K_{23}^T\hat{\lambda}^{i+1} + K_{33}\hat{\sigma}^{i+1} &= h. \end{aligned}$$

For the examples in Section 3.5, it turned out that one single iteration with the Gauss-Seidel method provided a sufficiently good preconditioner to achieve acceptable convergence with the GMRES method. This could not be done with any of the standard algebraic preconditioners like Jacobi, ILU or SOR, which worked poorly due to the block structure of the Newton system.

To achieve reasonable convergence for larger problems a more clever approach is needed. One idea is to use the approximate Gauss-Newton system

$$\begin{pmatrix} K_{11} & K_{12} & 0 \\ K_{12}^T & 0 & K_{23} \\ 0 & K_{23}^T & K_{33} \end{pmatrix} \begin{pmatrix} \hat{\varphi} \\ \hat{\lambda} \\ \hat{\sigma} \end{pmatrix} = - \begin{pmatrix} f \\ g \\ h \end{pmatrix}. \tag{17}$$

which arises from the observation that $\lambda \approx 0$ close to an optimum. A preconditioner can be derived from (17) by noting that eliminating $\hat{\varphi}$ and $\hat{\lambda}$ from (17) leads to the reduced system

$$\underbrace{(K_{33} + K_{23}^T K_{12}^{-1} K_{11} K_{12}^{-T} K_{23})}_{H_r} \hat{\sigma} = K_{23}^T K_{12}^{-1}(f - K_{11}K_{12}^{-T}g) - h. \tag{18}$$

with a symmetric positive definite reduced Hessian H_r which then can be approximated by *e.g.* a quasi-Newton method, see [1].

3.4. **Maximization Problem.** Given σ, the maximization problem is solved by the gradient method:

a. Start with an initial guess q^i.
b. Solve the forward equation (5) and the dual equation (9) to get φ and λ.
c. Apply the Neumann boundary values j (given by q^i) and $-\varphi + \varphi^*$ to the physical system (1) with unknown coefficient σ^*, and *measure* the resulting boundary values φ^* and λ^*, respectively.
d. Take a step in the gradient direction in q *i.e.*

$$q_n^{i+1} = q_n^i + \alpha \partial_{q_n} L,$$

for $n = 1, \ldots, N-1$, $\alpha \in (0, 1]$, and with $\partial_{q_n} L$ given by the left hand side of (11).
e. Goto step (a) unless tolerance is achieved or oscillations in q become too large.

3.5. **Results.** In the following examples a slightly different objective function

$$\max_q \frac{\|\varphi - \varphi^*\|^2_{\Gamma_M \times (0,T)}}{\|\varphi\|^2_{\Gamma_M \times (0,T)}}. \tag{19}$$

is used for the maximization problem but not for the minimization problem. Even though φ is bounded in the L^2 norm on $\Gamma_M \times (0, T)$ it may be a good idea restrict φ even more. This does however not change the generality of the prevoius sections other than changing the boundary values $\sigma \nabla\lambda \cdot \mathbf{n}$ and $\sigma^* \nabla\lambda^* \cdot \mathbf{n}$ on $\Gamma_M \times [0, T)$

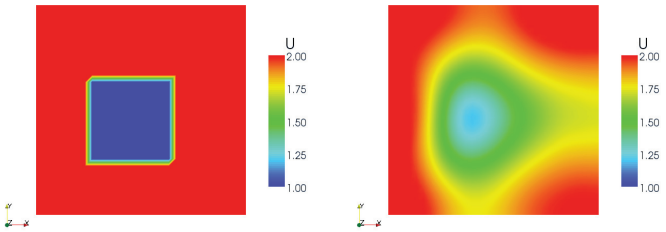

FIGURE 1. Left: The sought coefficient σ^*. Right: σ after first minimization. Boundary data: $q = \sin(2\pi t)\sin(\pi y)$ at $x = 0$.

when performing the maximization. Also, the results do not differ much from using the original objective function (4).

In Figure 1 to 6, three different examples are shown. In all examples a wave coefficient σ^* is reconstructed in the unit square by sending in a wave at $\Gamma_N \times (0,T] := \{x = 0\} \times (0,1]$ and measuring the acoustic pressure φ^* at $\Gamma_M \times (0,T] := \{x = 0\} \times (0,1] \cup \{x = 1\} \times (0,1]$. First, the minimization problem is solved for a small regularization $\delta = 10^{-5}$, then the calculated σ is used to maximize (19) with respect to q. Before the maximization the incoming wave is modelled by $q = \sin(2\pi t)\sin(\pi y)$, in Figures 1 and 3, and $q = \sin(\pi t)\sin(\pi y)$ in Figure 5. Finally, the minimization problem is solved again but with Neumann data j given by the new q. Of course, this can be done repeatedly and it is not necessary to start by solving the minimization problem, but instead start with some qualified guess for σ.

The Newton method for the minimization problem is solved such that the absolute residual error is less than 10^{-13} and the gradient method for the maximization problem is terminated when the L^2 norm of j_t gets to big. The calculations were done on a uniform triangular mesh with 1800 triangles and 125 time steps, and the measurements were simulated by using the same mesh.

The left part of Figure 1, 3 and 5 show the unknown coefficient σ^*, and the right part of the figures show σ after the first minimization. Figure 2, 4 and 6 show σ after the second minimization. In Figure 7 the simulated solution φ^* is shown before and after the maximization in q.

ACKNOWLEDGMENT

I am grateful to Anders Szepessy for his insightful ideas and helpful comments on this work.

REFERENCES

[1] George Biros and Omar Ghattas. Parallel Lagrange-Newton-Krylov-Schur methods for PDE-constrained optimization. I. The Krylov-Schur solver. *SIAM J. Sci. Comput.*, 27(2):687–713 (electronic), 2005.

[2] Jesper Carlsson, Mattias Sandberg, and Anders Szepessy. Symplectic pontryagin approximations for optimal design. Preprint.

[3] Margaret Cheney and David. Isaacson. Distinguishability in impedance imaging. *IEEE Trans. Biomed. Eng.*, 39(8):852–860, 1992.

[4] Margaret Cheney, David Isaacson, and Matti Lassas. Optimal acoustic measurements. *SIAM J. Appl. Math.*, 61(5):1628–1647 (electronic), 2001.

[5] Margaret Cheney, David Isaacson, and Jonathan C. Newell. Electrical impedance tomography. *SIAM Rev.*, 41(1):85–101 (electronic), 1999.

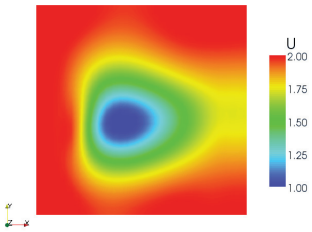

FIGURE 2. The coefficient σ after the second minimization. In the maximization of q, the value function increased 600% and the L^2 norm of q_t increased 100%. The decrease in the $L^2(\Omega)$ norm of $\sigma - \sigma^*$ between the first and second minimization was 30%.

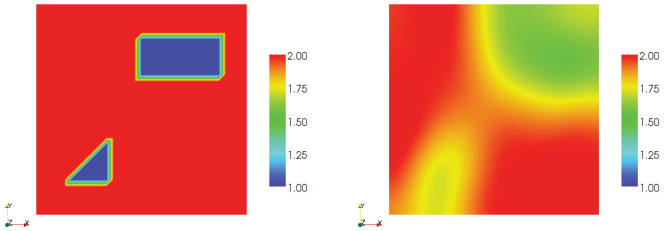

FIGURE 3. Left: The sought coefficient σ^*. Right: σ after first minimization. Boundary data: $q = \sin(2\pi t)\sin(\pi y)$ at $x = 0$.

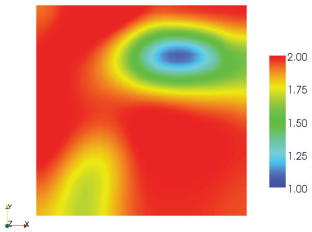

FIGURE 4. The coefficient σ after the second minimization. In the maximization of q, the value function increased 1200% and the L^2 norm of q_t increased 100%. The decrease in the $L^2(\Omega)$ norm of $\sigma - \sigma^*$ between the first and second minimization was 32%.

[6] Heinz W. Engl, Martin Hanke, and Andreas Neubauer. *Regularization of inverse problems*, volume 375 of *Mathematics and its Applications*. Kluwer Academic Publishers Group, Dordrecht, 1996.

[7] J.-L. Lions. *Optimal control of systems governed by partial differential equations*. Translated from the French by S. K. Mitter. Die Grundlehren der mathematischen Wissenschaften, Band 170. Springer-Verlag, New York, 1971.

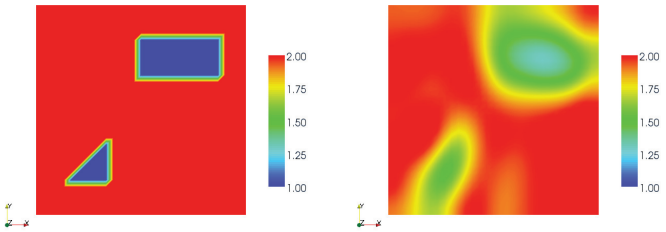

FIGURE 5. Left: The sought coefficient σ^*. Right: σ after first minimization. Boundary data: $q = \sin(\pi t)\sin(\pi y)$ at $x = 0$.

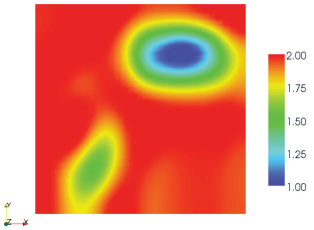

FIGURE 6. The coefficient σ after the second minimization. In the maximization of q, the value function increased 400% and the L^2 norm of q_t increased 50%. The decrease in the $L^2(\Omega)$ norm of $\sigma - \sigma^*$ between the first and second minimization was 40%.

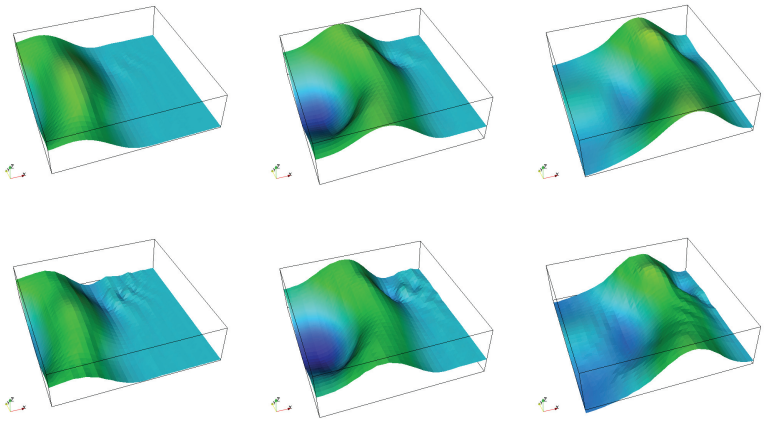

FIGURE 7. The measured solution φ^* before (top) and after (bottom) the maximization in q, for three different timesteps. The oscillations in q after the maximization are clearly visible in φ^*.

CSC, Numerical Analysis, Kungl. Tekniska Högskolan, 100 44 Stockholm, Sweden;
E-mail address: jesperc@kth.se